T-4403

Optical Second Harmonic Generation from Silver Crystals

by

Lin J. Simpson

ProQuest LLC.
789 East Eisenhower Parkway
P.O. Box 1346
Ann Arbor, MI 48106 – 1346

T-4403

A thesis submitted to the Faculty and the Board of Trustees of the Colorado School of Mines in partial fulfillment of the requirements for the degree of Doctor of Philosophy (Materials Science).

Golden, Colorado
Date 8/23/93

Signed: Lin Simpson
Lin J. Simpson

Approved: Thomas Furtak
Dr. T. E. Furtak
Professor of Physics
Thesis Advisor

Golden, Colorado
Date 8/23/93

J. J. Moore
Dr. J. J. Moore
Director
Materials Science Program

ABSTRACT

The goal of this thesis was to measure explicitly the spectral and applied potential dependence of specific nonlinear susceptibilities which govern the optical second harmonic generation (SHG) from silver surfaces. With this work, future experiments and analysis involving SHG from Ag crystals may explicitly deal with the SH contribution from these nonlinear susceptibilities without making the usual and often erroneous assumptions. Furthermore, these experiments were designed to generate future theoretical work and aid in the development of these theories. To accomplish these goals, we measured the s- and p-polarized SHG from Ag(001) and Ag(111) as a function of the sample orientation about its surface normal. We used specific incident and SH photon polarizations along with specific geometric and crystal orientation configurations to determine the SH contribution from specific nonlinear susceptibilities. The dc electric field was applied to the sample by establishing it as an electrode in a high purity electrochemical cell. The applied potential constituted a surface modulation which enabled surface effects to be separated from those originating in the bulk. The experiments were performed over a relatively wide incident photon energy range (1.17 eV to 2.3 eV). The experiments performed on the Ag(001) crystal indicated that the bulk anisotropic susceptibility (ζ) was relatively independent of incident photon energy and surface charge. The p-polarized SH response from the Ag(001) crystal indicated that the usual combination $[\gamma + (\epsilon(\Omega)/\epsilon_o)\partial_{zxx}]$ of nonlinear susceptibilities displayed potential dependence but had relatively little spectral dependence. ∂_{zxx} is a second order surface susceptibility and γ is the isotropic bulk susceptibility. The susceptibility ratio $[(\gamma + (\epsilon(\Omega)/\epsilon_o)\partial_{zxx})/\zeta]$ was found to have an incident photon independent value between 0.1 and 0.13. The normal incident SH

response from Ag(111) indicated that ∂_{xxx} has a resonant peak at 3.76 eV and is potential dependent. The experimentally measured resonance in ∂_{xxx} will provide the foundation for future theoretical endeavors.

The normal incidence Ag(111) experiment also revealed an anomalous isotropic SH response that was attributed to surface defects. This surface defect-induced SHG had the same characteristics as ∂_{xxx} and differed only in overall magnitude. This prompted further SHG investigations using a vicinal Ag(001) surface at normal incidence. Most of the relatively large defect-induced SH response was attributed to nonlinear surface susceptibilities which become allowed as the surface symmetry is reduced. However, the anomalous Ag(111) data and another anomalous effect from the vicinal Ag(001) surface cannot be explained through surface symmetry arguments and instead, are attributed to surface polarizabilities which have field gradients parallel to the surface. These contributions have never before been included in the SHG effective surface polarizability.

We also report on results which compared the present density functional theory for charge modulation on Ag(111) to experimental results. It was found that the theory was in qualitatively agreement with positively charged surfaces and incident photon energies below the interband transition energy of Ag. However, for SH energies above the interband transition energy, and for negatively charged surfaces, the theory and experimental results deviated greatly. In this same experiment, it was found that the anisotropic SH contribution behaved in a way consistent with a potential-induced surface reconstruction from C_{3v} to C_3 under conditions of positive surface charge and resonant enhancement around 3.75 eV. It is not clear at this time whether the defect induced SHG and this surface reconstruction is connected. This ion-induced reconstruction has been recently verified for the Ag(111) surface.

TABLE OF CONTENTS

LIST OF FIGURES

LIST OF TABLES

ACKNOWLEDGMENTS

I would like to acknowledge all those people who made my formal education possible. These include my parents, Jack and Yonlene Simpson, and my brothers Hal and Harry, for their tremendous support throughout the entire ordeal. To all my fellow peers through all the formative years including, Bill Austin, Brad Melnick, Lisa Wagner, Dean Volk, Stephen Buamer, Tom Casper, Carl Fredrickson, Mike Leskovar, Louis Ogden, Steve Roach, John DiGregorio, Walter Strohmeyer, Li Wang, and a host of others, I owe my deepest appreciation and gratitude. I would especially like to thank my previous office mates Carl and John for putting up with me all those years. My greatest appreciation for my academic survival, belongs to my long time mentors and friends, Dr. Frank Kawalski, Dr. Peter Braunlich, and Dr. Thomas Furtak. This thesis is dedicated to Susan.

Chapter 1

INTRODUCTION

Since the inception of the regular arrangement of matter in solids, science has profited greatly from the inherent symmetries associated with condensed matter. Elementary theoretical efforts even assumed perfect symmetry and order [1]. But in order to gain a more realistic understanding, defects and non-uniformities must be considered. Surfaces and interfaces are among the most influential effects that must be incorporated in any realistic analysis. At the very least, boundary conditions affect the interpretation of information obtained from the bulk. Since interfaces are present in any experiment, knowledge of interfacial effects is required for any complete understanding of real systems [2].

The problem then becomes how to study interfaces and quantify their effects [3, 4]. Crystallographic surface structure information is being provided by several methods, including various scanning probe microscopies and some x-ray scattering techniques [5, 6]. Electronic characterization of a material may be done with various optical methods, however, most techniques are not particularly surface sensitive. The fundamental problem still remains separating the bulk and surface contributions. If we consider the second harmonic generation (SHG) from a centrosymmetric material, where the bulk SHG second order dipole response is zero [7], any second order dipole response measured comes exclusively from the interface. These SHG second order processes are allowed because of the loss of inversion symmetry associated with an interface [8].

SHG is a phenomenon in which light of frequency ω interacts with a medium

to produce light at twice the frequency ($\Omega = 2\omega$). This is intrinsically sensitive to the material's electronic structure. The tensor character of SHG also makes the technique sensitive to crystallographic structure. Furthermore, SHG is experimentally simple to implement. As an optical technique, it is applicable to *in situ* studies of the material. Also, when monochromatic incident light is used, the detected light is also at a single well defined frequency, not requiring detailed spectral analysis of the detected light, which is associated with many optical methods. This may also be a limitation as well, since a spectral characterization of a material using SHG will require scanning the frequency of the incident light. The end result, however, is that SHG is a relatively simple interfacial probe that is intrinsically sensitive to the electronic and crystallographic structure of a material.

The SH response at the interface will be dominated by local electric dipole-allowed processes. However, non-local higher order electric quadrupole and magnetic dipole processes, which are normally weaker effects, may accumulate over the light's penetration depth in the material and result in a SH response comparable to that of the interface [8]. Appropriate theories have not been developed to accurately predict how the magnitude of these higher order bulk effects and the second order surface contributions compare for a real material where band structure is important. Thus, direct measurement by an experiment designed to distinguish between bulk and surface effects is required. Such an experiment requires perturbation of the interface. In ultrahigh vacuum, adsorbates are often added to cover the surface and thus modulate the SHG. If the SH response changes, then the extent of that change qualitatively indicates the contribution from the interface. A far more reproducible source of perturbation is to apply a dc electric field (E^{dc}) to the sample. If the material is a metal, then the applied field will be isolated to the atomic layers at the

surface and may result in fields on the order of 10^7 V/cm [9]. The application of E^{dc} to the sample interface is easily done in an electrochemical cell.

The addition of an electrochemical cell requires the use of a corrosion-resistant metal. Some suitable choices are gold, silver, platinum, copper, rhodium, mercury, and lead. Gold and silver have been extensively studied and have well characterized linear optical properties. This is important for investigations with relatively new techniques, in order to understand any new phenomena. Silver was our first choice to do these initial experiments due to our extensive experience with silver, the linear optical properties being relatively uniform for energies below 3.5 eV [14], and the well established surface preparation techniques [14]. Gold and platinum are also excellent materials and are being investigated heavily elsewhere [10, 11].

A fundamental knowledge of the specific susceptibility contributions to SHG is required in order to use it as an interfacial diagnostic tool. Presently, this fundamental knowledge is inadequate [10]. Our program systematically studied the SH response from Ag interfaces to determine the specific contributions from the bulk and interface as a function of interfacial potential and incident photon energy. We utilized specific geometric arrangements and crystal symmetries to further isolate and determine the contributions from specific nonlinear susceptibilities. Our goal was to determine information about the more prevalent and important ones. While we did all of our experimentation on Ag, the results we obtained should be generalizable to similar materials like Au, given the proper considerations for material property differences. This information is required for correctly interpreting SH data in general and is essential for developing the microscopic theories which govern the specific susceptibilities.

SHG is still inherently a surface or interfacial technique in the dipole approx-

imation and is extremely sensitive to the conditions at the interface. Thus, if the dipole processes at the surface dominate the SH response (through resonances or other enhancement effects) or if the dipole contribution in the SH response can be separated from the higher order contributions, then specific information about the interface may be obtained directly. Our efforts in this thesis are aimed at furthering the understanding of these higher order contributions to the SH response with the ultimate goal of increasing the viability of SHG as a mainstream diagnostic tool.

Chapter 2

LITERATURE REVIEW

Franken and coworkers [15] first observed SHG experimentally in 1961 from a non-centrosymmetric quartz crystal. Within a year Terhune *et al.* [16] had observed SHG from a centrosymmetric calcite crystal. In the few years that followed, SHG was observed in all types of materials including metals [17, 18, 19, 20], semiconductors [18, 21], insulators [22] and liquids [24]. SHG from non-centrosymmetric materials is governed by bulk electric dipole processes and is fairly well understood [25]. Bloembergen *et al.* [7] developed most of the early theory governing SHG from centrosymmetric materials. These theories considered the SHG from both the higher order non-local bulk contributions and the strongly polarized but thin surface region contributions, and give the phenomenological description of SHG still used today. The SHG contributions from the surface of a centrosymmetric material were first reported by Brown *et al.* using a silver crystal [17].

Rudnick and Stern [23] in 1971 considered the microscopic origins of SHG from a metal surface. Unlike previous theories which only considered the quadrupole-type contributions from the rapidly varying electric field at the surface, they found that surface details from the loss of inversion symmetry would affect the SH response. Later, Sipe *et al.* [26] extended this theory using a more realistic hydrodynamic model of the electron gas. However, the main problem with most of the theoretical approaches to date has been the inability to include the electronic band structure of the material [28]. This has resulted in investigations of materials which exhibit free electron behavior, like metals [27]. But, even in simple metals, the band structure has

been shown to be important [7, 12, 13, 30], and so most theoretical predictions are limited to energy regions where band structure is not important. This is true even with the most recent models which utilize density functional theories. Recent work by Liebsch and coworkers have adequately accounted for some free electron behavior, but still does not accurately predict the SH response from real metal surfaces [43].

In the late 1970's, Simon *et al.* [48] first observed SHG using attenuated total reflection techniques, which probe surface plasmons. They found that the SH response was significantly increased when coupling into the surface plasmons. This, along with nonlinear optical enhancements due to surface roughness (first observed with Raman spectroscopy [50] and later with SHG [55]), stimulated new investigations into SHG. While the initial investigators were interested in SHG for its own sake, the latest wave of investigation is aimed at the development of SHG as a surface analytical tool [10]. SHG has been used to analyze both the crystallographic and the electronic structure of surfaces and interfaces as well as to determine an adsorbate's relative surface density, alignment and bonding structure [3, 4, 10, 54].

2.1 Modern Theory

Richmond *et al.* [10] have written an extensive review of the various SHG applications. SHG has enjoyed remarkable success in its diversity and applicability. This is mainly due to the complex nature of SHG. However, the very complexity which makes SHG so sensitive, also makes a fundamental understanding difficult. By far, the weakest part of the field is the lack of knowledge of the specific susceptibilities at a microscopic level. The main theoretical difficulty is the inability to adequately account for the band structure of real systems. Even back in the early 1960's, Bloembergen and coworkers [29, 28] realized the electronic band structure had to be included in

the models in order to accurately predict experimental results. However, theoretical progress in this area has not been forthcoming.

Rudnick and Stern [23] used the conventional "jellium" approximation, which assumes only plasma effects and neglects periodic lattice structure in the bulk and any form of surface roughness, to do their calculations. They found three sources of SHG from a metal: a perpendicular and a parallel current from the surface and a bulk current. These have become known as the Rudnick and Stern "a_{RS}", "b_{RS}" and γ terms respectively. Explicit forms of these parameters will be given in the Microscopic Theory chapter of this thesis. Their calculations indicated that the surface current parallel to the surface should be the most sensitive to surface modulations and derived explicit forms for the SH response. Their main contribution was to point out the flaw in using a local field approximation in deriving the longitudinal surface current density, and in showing how the non-local response resolved the controversy surrounding a_{RS}. However, their predictions were only appropriate for an isotropic electron gas, *ie.* jellium. Furthermore, Rudnick and Stern still assumed the local field approximations were still appropriate for the other two susceptibilities.

Sipe *et al.* [32] extended Rudnick and Stern's theory using a hydrodynamic model of an electron gas to analyze the surface plasmon experiments by Simon [48]. The hydrodynamic model includes collective electron motions. The hydrodynamic results for a_{RS} and b_{RS} matched Simon's experimental results well, and reconfirmed the Rudnick and Stern values for a_{RS} and b_{RS} (ie. $2 < a_{RS} < -2$, and $b_{RS} = -1$). Further predictions of the hydrodynamic model, especially by Corvi and Schaich [34], suggest some frequency dependence for excitation energies near or below the bulk plasma energy for the longitudinal SH response from the surface. Later in the same year, Sipe [33] showed how the linear optical properties affect the second order results and laid

the foundation for his 1987 paper [8] which provided a complete phenomenological theory and gave explicit details for experimental observation. That paper is the primary work upon which this thesis is based, and provides the foundation for the four wave mixing theory which we have developed. Sipe and coworkers [26] later extended this phenomenological theory to different experimental geometries. However, the 1987 work represents the complete phenomenological theory for experimental SHG in reflection from samples, including the linear optical contributions, the specific crystal symmetries involved, and the specific second order surface and multipole bulk susceptibilities.

The hydrodynamic model, like the free electron model, not only neglects electronic band structure, but also poorly accounts for the detailed behavior of the surface electron density. In order to more adequately describe the surface electron density, the self consistent density functional theory was applied by Liebsch and coworkers [35, 36, 37, 38, 39, 40, 41, 42, 43] to try to determine the SH response from the surface. The density functional theory uses a continuously varying electron density profile, as compared to the "step models" used previously. The calculations by Liebsch *et al.* found that most of the longitudinal SH current was located out in the electron density's exponential tail. This result predicted that the longitudinal SH current should also be surface sensitive. However, the calculated values for a_{RS} were found to be between -7 and -28, which was a significant difference from the hydrodynamic model and Simon's experimental results given above [48]. The only explanation given for this difference was a possible difference between Simon's metal-glass interface, and the density functional's metal-vacuum assumptions. Other theoretical calculations agree with the density functional model [49] and more recently Liebsch and coworkers [43] calculated the SH response to an externally applied electric field for a relatively large

excitation energy range. These results were experimentally tested by our group [13] and will be discussed later.

2.2 Modern Experiments

As mentioned above, a vast number of SH experiments have been performed and a great deal of information has been obtained [25, 10, 26]. This thesis is primarily concerned with investigating SHG from metal surfaces and more specifically that of Ag. Thus we will limit our discussion to experimental SHG results from Ag and other metals, where appropriate. This is not as restrictive as it may first appear, since the first SHG experiment on a centrosymmetric metal surface was performed on Ag [17], three years after Terhune's work [16]. In 1968 Bloembergen *et al.* [29] wrote a comprehensive review of the previous work done in SHG. Since then several other reviews have been published [25, 26, 45], including one in 1988 by Richmond [10]. This latter review article included most of the SHG work done on the solid/liquid interface to that point, and is therefore of direct relevance to this thesis.

The SH response from metals is a relatively weak effect. Thus, the early work was performed under conditions which maximized the SH response. This included enhancement experiments with resonant conditions, or with geometries and experimental conditions that maximized the SH response [10, 26]. Experiments with adsorbates that resulted in a strong SH response have been done extensively since the 1960's [29]. Also, the use of polycrystalline metals or the (111) and (110) faces of a metal crystal at non-normal incident angles, increases the ability to detect the SH signal. Thus, the vast majority of the experiments have been done under these types of conditions.

The advent of powerful pulsed lasers in the early 1980's marked the turning point

in experimental SHG. These powerful lasers allowed investigation of the fundamental processes involved in SHG. SHG may be used as a probe of surface reactions and adsorption/desorption processes. Once the SH response from the plane metal surface is categorized, changes induced by even submonolayer depositions or changes in the metal surface itself may be detected [46, 92]. This type of analysis has been used extensively in the electrochemical environment, in ultra-high vacuum, and ambient air conditions [10].

SHG is a probe which may be used to determine surface symmetry and structure [12], electronic properties [51] and surface bonding information [10]. SHG has been used to detect surface reconstructions in silicon and gold crystals [64, 65, 66], symmetry changes in the adsorbed ions [10], and possible ion induced surface reconstructions [12]. Bulk and surface electronic states, electron gas plasma energies and even vacuum energy levels have been determined by SHG [45]. Adsorbate orientation and bonding have also been characterized by SHG citerichmond1.

Recently, the spectral characterization of the SH response from the metal surface itself has received intense investigation. Plummer *et al.* [51] in 1990 measured the spectral SH reflectivity from Ag(110). Using SH energy arguments along with selection rules for specific geometries, this group observed a SHG resonant enhancement due to a transition between two surface electronic states. Richmond *et al.* [10, 30, 57, 67, 68, 69, 70, 71, 72] have done extensive work with SHG from metal interfaces in the electrochemical environment and some work in the ultra high vacuum environment. Most of this work is listed in the 1988 review paper [10] and involved SHG using only 1.17 eV incident photons.

In 1990 Richmond and coworkers [68] published their initial work involving other incident photon energies from Ag crystals. This work showed the SH response at 1.17

eV and 2.33 eV from Ag(111) and Ag(011) crystals. The authors explained the notable difference between the SH response at the two energies as being due to a "resonance or near resonant coupling of the radiation fields at the higher energies with surface states on the metal which are altered by variation of the large dc electric field at the surface". In a follow up to this initial work, Richmond and coworkers [69] presented the potential dependent behavior alluded to in the previous publication, for incident photon energies of 1.17 eV, 1.93 eV, 2 eV, and 2.33 eV. Once again the authors concluded that the spectral dependence of the SH response was due to the electronic states at the metal surface. In an addendum to the paper, the authors found that the SH response from a Ag(011) experiment indicated that the bulk anisotropic susceptibility was potential independent. However, the evidence for this conclusion was not presented and the conclusion was drawn from experimental data that did not inherently isolate the bulk anisotropic susceptibility.

The first true spectral study reported by Richmond and coworkers was published in 1992 [71] and presented the SH response as a function of incident photon energy from a Ag(111) crystal at non-normal incidence. R. A. Bradley [72], one of Richmond's students, wrote a thesis which was a culmination of most of this work since 1990 and presented the SH response from the Ag(111) crystal as a function of applied potential and incident photon energy. Once again, the authors concluded that the spectral dependence of the SH response was due to the electronic states of the surface. It is this latest work by Richmond and coworkers which most resembles our efforts in the investigation of SHG from metals.

The main problems associated with all the work by Richmond and coworkers is the inadequate consideration of the linear optical coefficients to the SH response and the potentially complex SH response from systems that contain several susceptibili-

ties. Mostly, the latter problem is handled by rationalizing certain susceptibilities to be small and thus ignorable or by using inappropriate experimental results to justify setting susceptibilities to zero. At this point, valuable insight may be gained by a critique of Dr. Bradley's thesis with regards to this present work. Bradley's thesis does contain a good characterization of the SH response as a function of crystal orientation for Ag(111), Au(111) and Cu(111) at 1.17 eV incident photon energy. It is interesting to note that Bradley was unable to detect the surface reconstruction on the Au(111) crystal in UHV, a well known phenomena. However, Richmond and coworkers have recently observed this reconstruction with a different surface preparation technique [73]. Furthermore, Bradley's thesis contains a detailed characterization of the SH response from Ag(111) as a function of applied potential and incident photon energy in both the electrochemical environment and the UHV environment. The similarity between the spectral SH response in UHV and the electrochemical environment indicated that the SHG from the Ag(111) crystal was unaffected by the specific environment [72, 57]. This is not true for the other metals reported upon in Bradley's thesis.

The main conclusions drawn from this work involves the association of a "resonance at 3.82 eV" in the spectral SH response with the known surface states of Ag(111). The authors acknowledge the existence of a linear optical coefficient peak at this energy, and in fact measure it themselves. The spectral structure in the linear optical parameters is mainly due to the bulk interband transition projected on the surface. Surface states provide only a small effect on the linear optical property's spectral dependence. However, Bradley and coworkers ignore any spectral contribution from the linear optical parameters and conclude that the peak in the SH spectrum is due to an electronic transition between the surface state A near the bottom of

the band gap and the image potential surface state near the top of the band gap (the band structure of Ag(111) will be discussed later in this thesis, however to aid in understanding the present discussion, the reader should refer to Fig. 7.1 in the discussion chapter). Even if this transition were symmetry allowed, or other mechanisms allowed the transition to occur, the top surface state is inaccessible and the bottom surface state is unpopulated for positive potentials (Fig. 7.2). This means that the SH response should vanish at positive potentials, a result not observed in the experiments. The spectral SH response does have a potential dependence and a corresponding phase shift, which Bradley uses to correctly suggest that part of the spectral dependence is coming from the surface. The point is that the peak reported by Richmond and Bradley at 3.8 eV is more appropriately assigned to a bulk interband transition. The corresponding linear optical coefficients must be explicitly accounted for before any conclusions may be made regarding identification of a second order effect at the surface. This is especially the case since the so called "resonant peak" does not shift in energy with the applied potential, as would be expected for a transitions between a surface derived state and the projection of the bulk band edge at the surface. Also, if the transition originated from the lower surface state, the peak should disappear at positive charging. This is not observed in Bradley's data. Since we have performed experiments on Ag(111), we will comment further on Bradley's interpretations later in this document.

Our efforts have involved a careful evaluation of the SH response, including the spectral dependence and the corresponding changes induced by an applied electric field. In 1990 Guyot-Sionnest, Tadjeddine and Liebsch (GTL) [43] published a SHG paper using a density functional model to predict the SH response of the a_{RS} term as a function of incident photon energy and induced surface charge. We were ideally

suited to test this theory [13] since we had been doing spectral analysis from the Ag(111) crystal since 1989. By collecting the SHG intensity as a function of applied potential with different incident photon energies from 1.4 eV to 2.23 eV, we performed a differential nonlinear reflectance measurement. The experiments were carried out in an electrochemical sample chamber to modulate the Ag(111) surface charge of the SH isotropic contribution. While the GTL theory gave predictions for SH photon energies ranging from 0 eV to 4 eV, we were able to investigate the part of the theory of physical significance. This included photon energies well below any bulk or surface electronic transition to energies above the bulk interband transition. Ironically, even though GTL published SH intensity calculations for energies above the interband transition, the jellium approximation used in their density functional model prohibits predictions near to or above interband transition energies. This is because the theory does not properly account for the electronic structure of the material. The jellium approximation is only a "hydrodynamic" model and therefore, does not account for the heterogeneity in the electron concentration due to ion cores and the localized electrons, such as in the d-bands.

Since the GTL theory and our experimental results were not directly comparable (due to unknown scaling factors) we normalized the change with potential by comparison to the response at the potential of zero charge (PZC), for the entire experimental photon energy range. The theoretical results for the positively charged surface below the interband transition energy compared well with the experimental SH response. However, the negatively charged surface theory predictions were not good. The latter results were not completely unexpected, since the jellium model makes no allowance for the influence of the d bands which reduce the nonlinear polarizability of the surface [13].

One final detail from this isotropic data was observed at 3.4 eV. The negatively charged surface modulation had a sharp peak, which was tentatively assigned to a two photon resonance involving a crystal potential surface state and an image potential surface state [13].

With this same set of experimental data, the anisotropic response was also analyzed. It was observed that the anisotropic response for the surface with positive charged and with incident photon energies between 1.85 eV to 1.91 eV did not follow the expected C_{3v} phenomenological theory. However, a modified phenomenological theory using C_3 symmetry did fit the data. This indicated that, under these conditions, the surface appeared to have a different symmetry then an abruptly terminated (111) face. This surface reconstruction was reversible with applied potential. A signature feature (associated with C_{3v} going to C_3) was identified in the data. This parameter followed a power law with respect to a normalized interfacial potential. The narrow incident photon energy range under which the phase transformation could be observed was explained by a possible surface state resonance in the modified C_3 surface susceptibility ∂_{yyy}. Recently, these observations involving an ion induce reconstruction on the Ag(111) surface have been verified using STM, REM, and RHEED techniques [53].

This one experiment demonstrated SHG's ability to observe both isotropic and anisotropic effects from the inherent surface structure, and gave us insight into the electronic band structure at the surface and the bulk, and geometrical information about the surface. It should be noted that this was done without ultra-high vacuum constraints, which are required for so many other optical and non-optical probes [45]. However, even in this experiment, certain assumptions were made regarding the contribution from specific susceptibilities. Basically, these were the same as those

traditionally followed in theoretical developments [43]. The anisotropic surface susceptibilities were eliminated, in the isotropic analysis, by geometric considerations. However, the bulk isotropic susceptibility and isotropic surface susceptibilities like ∂_{zxx} were neglected.

Experimentally, obtaining information about the specific susceptibility contributions has proven to be difficult. Most experimental analyses of SHG data have made assumptions about specific symmetry allowed susceptibilities [43, 57, 13]. The prevailing wisdom, used by both experimentalist and theoreticians, is that the higher order bulk susceptibilities and some second order surface susceptibilities are either small and thus negligible, or zero. They base most of these assumptions on hand-waving arguments or poorly performed experiments [30]. The main problem is that due to the nonlinearity of SHG, even a very small contribution from a susceptibility may combine with other contributions in cross terms and result in a significant SH response. It was our goal to perform careful experiments which characterize many of those susceptibilities which are often ignored, and to determine quantitatively their specific contributions to the SH response. This will be the main emphasis of the thesis. Thus we will limit the remaining content of this thesis to results and discussions involving the systematic characterization of specific susceptibilities and contributions to the SH response that are normally ignored.

Chapter 3

PHENOMENOLOGICAL THEORY

In general the local optical response may be written in terms of a polarization, $\mathbf{P} = \chi\mathbf{E}$ [7], where χ is the susceptibility and $\mathbf{E}$ is the incident electric field. However, for nonlinear materials χ may vary with the electric field and the polarization then becomes a power expansion in terms of $\mathbf{E}$:

$$\mathbf{P} = \chi^{(1)}\mathbf{E} + \chi^{(2)} : \mathbf{EE} + \chi^{(3)} : \mathbf{EEE} + \ldots . \tag{3.1}$$

If we consider the nonlinear parts which represent a local SH response, then:

$$P_i^{(2\omega)} = \chi^s_{ijk} E_j^\omega E_k^\omega + \chi^s_{ijkl} E_j^\omega E_k^\omega E_l^0 + \ldots . \tag{3.2}$$

where the superscript "s" indicates a surface susceptibility. However, because the local second order bulk effects are symmetry forbidden for centrosymmetric materials (*ie.* $\chi_b^{(2)} = 0$), and the relatively small SH response from the surface, non-local bulk contributions must also be included in the SH response [8, 31]. Thus, the effective second order polarization becomes:

$$P_i^{(2\omega)} = \Gamma_{ijkl} E_j^\omega \nabla_k E_l^\omega + \chi^s_{ijk} E_j^\omega E_k^\omega + \chi^s_{ijkl} E_j^\omega E_k^\omega E_l^0 + \ldots . \tag{3.3}$$

Γ_{ijkl} is a fourth rank tensor which represents the non-local higher order multipole susceptibilities governing the SH response from the bulk. In this chapter we will present phenomenological calculations for the SH intensity, starting with this gener-

alized second order polarization. The calculations will follow the work done by Sipe *et al.* [8], and all these calculations are presented Sipe's paper except the four wave mixing contribution that we will present later. We will do this calculation for a SH response generated from a single plane wave incident on a cubic crystal face with (111), (011), and (001) orientations.

For experimental purposes, we will transform the usual crystal coordinate axes into the beam coordinate axes and will present our results in the latter coordinate system (Fig. 3). To do this, we consider a geometry such that the coordinate axis has the positive z-axis parallel to the outward surface normal, the s-axis perpendicular to the plane of incidence defined by the incident photon fields and parallel to the sample surface, and the k-axis parallel to both the plane of incidence and the sample surface.

We now define the incident and SH photon polarizations in the standard way such that the s-polarization is parallel to the positive s-axis and perpendicular to the plane of incidence, and the p-polarization is perpendicular to the wave vector in the plane of incidence. With this geometry we define the incident and SH fields with these two components and write the SH fields as (note the standard definition of 1,2,3 = x,y,z respectively):

$$E_s^{(2\omega)} = A_s i(2\omega/c)\hat{\mathbf{s}} \bullet \mathbf{P}^{2\omega} \tag{3.4}$$

$$E_p^{(2\omega)} = A_p i(2\omega/c)([\epsilon(2\omega)/\epsilon(\omega)]F_s\hat{\mathbf{z}} \bullet \mathbf{P}^{2\omega} - F_c\hat{\mathbf{k}} \bullet \mathbf{P}^{2\omega}) \tag{3.5}$$

where

$$\mathbf{P}^{2\omega} = \sum_i P_i^{2\omega}\hat{\mathbf{x}}_\mathbf{i};$$

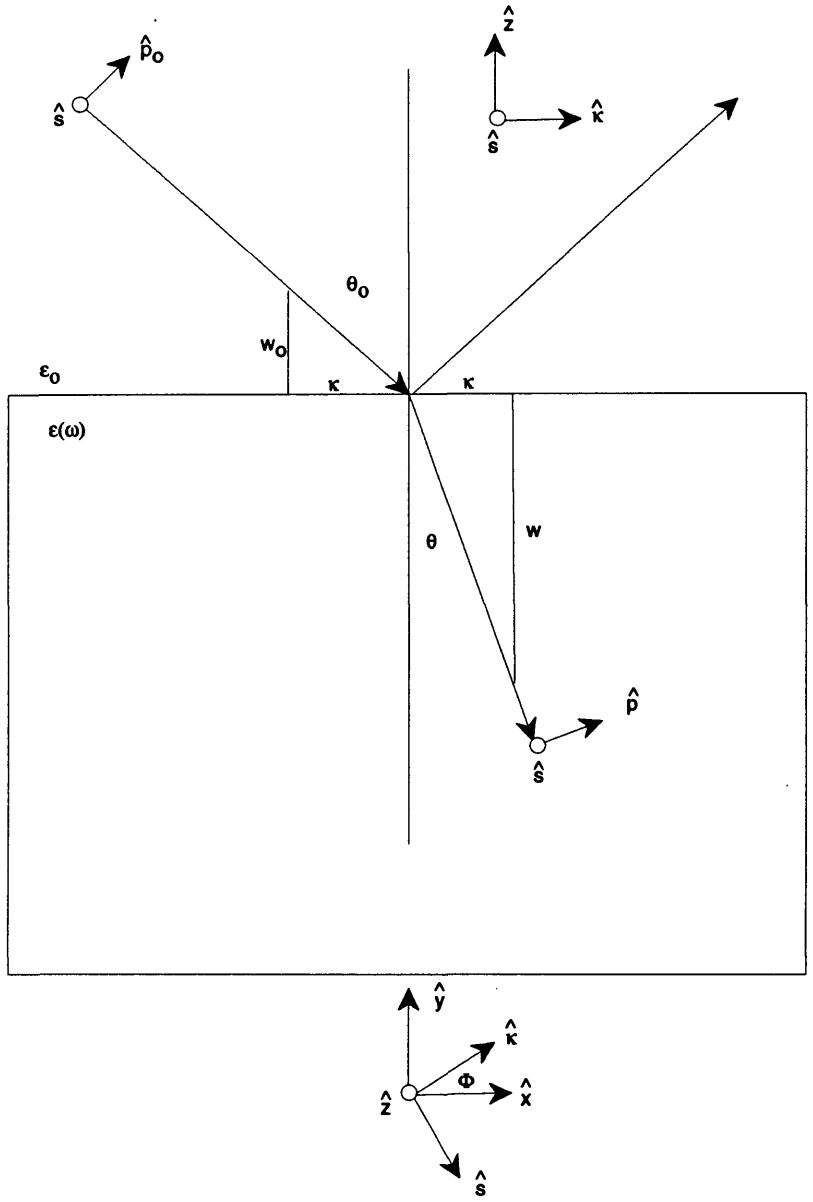

FIG. 3.1: The experimental fields geometric and unit vector designations and propagation directions as defined in the plane of the incident electric field.
Here the incident field is in a medium with dielectric constant ϵ_o and approaches the surface at an incident angle θ_o. The fields outside the crystal medium have polarizations $\hat{s}$ and $\hat{p}_o$ with component wave vectors w_o and κ. The crystal medium's dielectric constant is $\epsilon(\omega)$ with a field propagation angle θ. The fields in the crystal medium have polarizations $\hat{s}$ and $\hat{p}$ with component wave vectors w and κ. The surface normal is defined in the $\hat{z}$ direction. The beam coordinate axes is rotated by an angle ϕ with respect to the crystal coordinate axes about the $\hat{z}$ axis.

$$E_1 = f_c E_p \cos\phi + E_s \sin\phi;$$

$$E_2 = f_c E_p \sin\phi - E_s \cos\phi;$$

$$E_3 = f_s E_p;$$

and ϕ is the crystal orientation angle measured in the surface plane, generally between a well defined close packed plane and the plane of incidence of the light. The other terms are defined in Tables 3.1-3.5.

The generated SH fields (E_Ω) are then calculated in terms of the incident electric fields, which are transformed into beam coordinates. This calculation requires specific information about the interface symmetries and was done for the bulk and second order surface susceptibilities by Sipe *et al.* [8, 31]. Under the conditions of excitation and measurement appropriate to our experiment (s-polarized incoming light with a photon energy of $\hbar\omega$) the most general expression for the power density (S_Ω) of the reflected light at the second-harmonic frequency ($\hbar\Omega = 2\hbar\omega$) is [8]

$$S_\Omega = |F E_\Omega|^2 \tag{3.6}$$

The parameter F in Eq. 3.6 depends only upon the linear optical properties of the sample at ω and Ω and on the angle of incidence. In the following sections of this chapter we will discuss the various contributions to the SH response. We start with the bulk derived contributions, then the second order surface contributions, the dc field induced contributions, and finish with a section which presents the entire phenomenological theory.

3.1 Review of the Bulk-Derived SH Contribution

In the bulk of cubic symmetry crystals, using the standard crystal axes, the bulk derived second order polarization can be written as (suppressing the wavelength dependence designations on the incident electric fields) [8]:

$$P_i^{(2\omega)} = (\delta - \beta - 2\gamma)(\mathbf{E}\cdot\nabla)E_i + \beta E_i(\nabla\cdot\mathbf{E}) + \gamma\nabla_i(\mathbf{E}\cdot\mathbf{E}) + \zeta E_i\nabla_i E_i, \qquad (3.7)$$

where δ, β, γ and ζ are phenomenological constants. The first three terms are isotropic in nature and the last term is anisotropic with respect to the crystal orientation. For excitation of a homogeneous medium by a single transverse plane wave, the first two terms are identically zero. For the experiments reported here, only the last two terms may contribute to the SH response. The bulk derived second order polarization becomes:

$$P_i^{(2\omega)} = \gamma\nabla_i(\mathbf{E}\cdot\mathbf{E}) + \zeta E_i\nabla_i E_i, \qquad (3.8)$$

where γ and ζ are the bulk isotropic and bulk anisotropic susceptibilities respectively. The multipole contributions are generally much smaller then the dipole contributions. However, γ and ζ are integrated over the entire optical penetration depth of the incident light [8]. This potentially allows γ and ζ to contribute to the SH response with a similar magnitude as the surface dipole contribution.

3.2 Review of the Second Order Surface SH Contribution

At an interface between two dissimilar media, inversion symmetry is broken, resulting in a possible dipolar contribution [29] and a large electric field gradient due to the discontinuity in the normal component of the electric field [59]. These effects

are accounted for by an effective surface dipole polarization [8] given by:

$$P_i^{s(2\omega)} = \sum_{jk} \Delta_{ijk}^{(2)} E_j E_k \delta(z - z_o^+), \tag{3.9}$$

where the symmetry of $\Delta_{ijk}^{(2)}$ is determined by the crystal symmetry within the surface dipole sheet. C_{3v}, C_{2v}, and C_{4v} are the three main surface symmetries associated with the face centered cubic metals like crystalline silver. These symmetries correspond to the (111), (011), and (001) crystal planes respectively. The specific surface symmetries dictate the allowed second order susceptibilities, such that only the following susceptibilities are nonzero:

$$C_{3v}; \partial_{xxx} = -\partial_{xyy} = -\partial_{yyx}, \partial_{xxz} = \partial_{yyz}, \partial_{zxx} = \partial_{zyy}, \partial_{zzz};$$

$$C_{2v}; \partial_{xxz}, \partial_{yyz}, \partial_{zxx}, \partial_{zyy}, \partial_{zzz};$$

$$C_{4v}; \partial_{xxz} = \partial_{yyz}, \partial_{zxx} = \partial_{zyy}, \partial_{zzz}.$$

Using these susceptibilities with there associated incident electric fields, and then transforming to beam coordinates, gives the phenomenological equations which govern the SH response from the silver interfaces [8] (Tables 3.1-3.5).

3.3 dc Electric Field Contribution

We will use a formal four wave mixing approach to calculate the third order dc field contribution to the SH intensity [7]. Our contribution to this phenomenologi-

cal theory will be to calculate the specific SH fields generated from this third order contribution for the (111), (011), and the (001) crystal faces. Basically it is the same calculation we have discussed previously, but using an electrochemical system introduces a third static field into the experiment. For our purposes, we will assume that the induced dc field is wavelength independent, is perpendicular to the crystal surface, and assign it to the fourth frequency position in the third order susceptibility. The specific surface symmetries again dictate the allowed third order susceptibilities with the dc field orientation perpendicular to the surface, placing an additional constraint. Therefore the only allowed nonzero susceptibilities are:

$$C_{3v}; \chi_{yyyz} = -\chi_{yxxz} = -\chi_{xyxz} = -\chi_{xxyz}, \chi_{xxzz} = \chi_{yyzz}, \chi_{zxxz} = \chi_{zyyz}, \chi_{zzzz};$$

$$C_{2v}; \chi_{xxzz}, \chi_{yyzz}, \chi_{zxxz}, \chi_{zyyz}, \chi_{zzzz};$$

$$C_{4v}; \chi_{xxzz} = \chi_{yyzz}, \chi_{zxxz} = \chi_{zyyz}, \chi_{zzzz}.$$

We note here that the specific third order susceptibilities for C_{2v} and C_{4v} will enter the phenomenological equations in exactly the same way as their second order surface susceptibility counterparts, with an additional "z" in the fourth position of the subscript to designate the dc electric field contribution normal to the crystal surface. Thus this calculation shows that the second order susceptibilities for these two symmetries could be treated as if they had a linear dependence on the applied potential. However, while this is true for some of the susceptibilities for the C_{3v} symmetry surface, the dc field terms with the χ_{xxyz} susceptibility do enter independently. Again, with the appropriate incident fields for each susceptibility transformed to beam coordinates, the phenomenological equations governing the third order SH response may be derived (see Tables 3.1-3.5).

3.4 Complete Formalism

The specific symmetry associated with individual crystal faces will determine the nonzero susceptibilities and the final forms of Eqs. (3.4, 3.5). For this thesis we will consider the unreconstructed symmetries associated with a face centered cubic metal. Generally, the surface normal is perpendicular to one of three planes, the (111), (011), or (001) plane. The lattice then has the corresponding symmetry C_{3v}, C_{2v}, and C_{4v} respectively. The particular crystal symmetry places constraints on the allowable susceptibilities. By including only the symmetry-allowed susceptibilities and assuming the dc electric field is only modulated in the direction normal to the surface, we find that the SH field equations have the form:

$$\begin{aligned} E_s^{(2\omega)} &= (\zeta^{s1} + \partial^{s1} + \chi^{s1}) + (\zeta^{s2} + \partial^{s2} + \chi^{s2}) \sin M\phi \\ &+ (\zeta^{s3} + \partial^{s3} + \chi^{s3}) \cos M\phi + \zeta^{s4} \sin N\phi + \zeta^{s5} \cos N\phi \end{aligned} \tag{3.10}$$

$$\begin{aligned} E_p^{(2\omega)} &= (\gamma^{p} + \zeta^{p1} + \partial^{p1} + \chi^{p1}) + (\zeta^{p2} + \partial^{p2} + \chi^{p2}) \sin M\phi \\ &+ (\zeta^{p3} + \partial^{p3} + \chi^{p3}) \cos M\phi + \zeta^{p4} \sin N\phi + \zeta^{p5} \cos N\phi \end{aligned} \tag{3.11}$$

where the specific parameters for each symmetry are listed in Tables 3.1-3.5.

Table 3.1: Specific parameters for the SH fields phenomenological equations for the (001) face: M=2.

$$\zeta^{s1} = -A_s g_b 2\zeta f_s f_c E_s E_p$$

$$\zeta^{s2} = -A_s g_b \zeta f_s (f_c^2 E_p^2 - E_s^2)$$

$$\zeta^{s3} = A_s g_b 2\zeta f_s f_c E_s E_p$$

$$\partial^{s1} = A_s 2\partial_{xxz} f_s E_s E_p$$

$$\chi^{s1} = A_s 2\chi_{xxzz} f_s E_s E_p E^{dc}$$

$$\gamma^p = A_p \gamma F_s (E_s^2 + E_p^2)$$

$$\zeta^{p1} = A_p g_b \zeta f_s [F_c E_s^2 + (3F_c f_c^2 + 4 f_s f_c F_s) E_p^2]$$

$$\zeta^{p2} = A_p g_b \zeta 2 f_c f_s F_c E_s E_p$$

$$\zeta^{p3} = A_p g_b \zeta f_s F_c (f_c^2 E_p^2 - E_s^2)$$

$$\partial^{p1} = A_p [(\epsilon(2\omega)/2\epsilon_o(\omega)) F_s 2(\partial_{zxx}(f_c^2 E_p^2 + E_s^2) + \partial_{zzz} f_s^2 E_p^2) - 2\partial_{xxz} f_s f_c F_c E_p^2]$$

$$\chi^{p1} = A_p [(\epsilon(2\omega)/2\epsilon_o(\omega)) F_s 2(\chi_{zxxz}(f_c^2 E_p^2 + E_s^2) + \chi_{zzzz} f_s^2 E_p^2) - 2\chi_{xxzz} f_s f_c F_c E_p^2] E^{dc}$$

Table 3.2: Specific parameters for the SH fields phenomenological equations for the (011) face: M=2,N=4.

$$\zeta^{s1} = A_s g_b (1/2)\zeta f_s f_c E_s E_p$$

$$\zeta^{s2} = A_s g_b (1/2)\zeta f_s [(5f_c^2 - 2f_s^2)E_p^2 + E_s^2]$$

$$\zeta^{s3} = -A_s g_b 2\zeta f_s f_c E_s E_p$$

$$\zeta^{s4} = -A_s g_b (3/4)\zeta f_s (f_c^2 E_p^2 - E_s^2)$$

$$\zeta^{s5} = A_s g_b (3/2)\zeta f_s f_c E_s E_p$$

$$\partial^{s1} = A_s (\partial_{xxz} + \partial_{yyz}) f_s E_s E_p$$

$$\partial^{s2} = A_s (\partial_{xxz} - \partial_{yyz}) f_s f_c E_p^2$$

$$\partial^{s3} = -A_s (\partial_{xxz} - \partial_{yyz}) f_s E_s E_p$$

$$\chi^{s1} = A_s (\chi_{xxzz} + \chi_{yyzz}) f_s E_s E_p E^{dc}$$

$$\chi^{s2} = A_s (\chi_{xxzz} - \chi_{yyzz}) f_s f_c E_p^2 E^{dc}$$

$$\chi^{s3} = -A_s (\chi_{xxzz} - \chi_{yyzz}) f_s E_s E_p E^{dc}$$

$$\gamma^p = A_p \gamma F_s (E_s^2 + E_p^2)$$

$$\zeta^{p1} = A_p g_b \zeta [(F_s f_c + .75 f_s F_c) E_s^2 + (F_s f_c^3 + .25 f_s f_c^2 F_c + f_s^3 F_c) E_p^2]$$

$$\zeta^{p2} = A_p g_b \zeta (2f_c^2 F_s - 3 f_s f_c F_c - 2 f_s^2 F_s) E_s E_p$$

$$\zeta^{p3} = A_p g_b \zeta [(f_c^3 F_s + f_s f_c^2 F_c - 2 F_s f_s^2 f_c + f_s^3 F_c) E_p^2 + f_c F_s E_s^2]$$

$$\zeta^{p4} = A_p g_b (3/2)\zeta f_s f_c F_c E_s E_p$$

$$\zeta^{p5} = A_p g_b (3/4)\zeta f_s F_c (f_c^2 E_p^2 - E_s^2)$$

Table 3.3: Specific parameters for the SH fields phenomenological equations for the (011) face: M=2,N=4 (Continued).

$$\partial^{p1} = A_p[(\epsilon(2\omega)/2\epsilon_o(\omega))F_s[(\partial_{zxx} + \partial_{zyy})(f_c^2 E_p^2 + E_s^2) + 2\partial_{zzz} f_s^2 E_p^2] - (\partial_{xxz} + \partial_{yyz}) f_s f_c F_c E_p^2]$$

$$\partial^{p2} = A_p[(\epsilon(2\omega)/2\epsilon_o(\omega))F_s f_c 2(\partial_{zxx} - \partial_{zyy}) - (\partial_{xxz} - \partial_{yyz}) f_s F_c] E_s E_p$$

$$\partial^{p3} = A_p[[(\epsilon(2\omega)/2\epsilon_o(\omega))F_s f_c 2(\partial_{zxx} - \partial_{zyy}) - (\partial_{xxz} - \partial_{yyz}) f_s F_c f_c] E_p^2 - (\epsilon(2\omega)/2\epsilon_o(\omega))(\partial_{zxx} - \partial_{zyy}) F_s E_s^2]$$

$$\chi^{p1} = A_p[(\epsilon(2\omega)/2\epsilon_o(\omega))F_s[(\chi_{zxxz} + \chi_{zyyz})(f_c^2 E_p^2 + E_s^2) + 2\chi_{zzzz} f_s^2 E_p^2] - (\chi_{xxzz} + \chi_{yyzz}) f_s f_c F_c E_p^2] E^{dc}$$

$$\chi^{p2} = A_p[(\epsilon(2\omega)/2\epsilon_o(\omega))F_s f_c 2(\chi_{zxxz} - \chi_{zyyz}) - (\chi_{xxzz} - \chi_{yyzz}) f_s F_c] E_s E_p E^{dc}$$

$$\chi^{p3} = A_p[(\epsilon(2\omega)/2\epsilon_o(\omega))F_s(\chi_{zxxz} - \chi_{zyyz})(f_c^2 E_p^2 - E_s^2) - (\chi_{xxzz} - \chi_{yyzz}) f_s F_c f_c E_p^2] E^{dc}$$

Table 3.4: Specific parameters for the SH fields phenomenological equations for the (111) face: M=3.

$$\zeta^{s1} = A_s g_b \zeta (4/3) f_s f_c E_s E_p$$

$$\zeta^{s2} = A_s g_b \zeta f_c (8/9)^{1/2} [(f_c - 2f_s^2) E_p^2 - E_s^2]$$

$$\zeta^{s3} = -A_s g_b \zeta (32/9)^{1/2} (f_c^2 - f_s^2) E_s E_p$$

$$\partial^{s1} = A_s 2 \partial_{xxz} f_s E_s E_p$$

$$\partial^{s2} = A_s \partial_{xxx} (f_c^2 E_p^2 - E_s^2)$$

$$\partial^{s3} = -A_s 2 \partial_{xxx} f_c E_s E_p$$

$$\chi^{s1} = A_s 2 \chi_{xxzz} f_s E_s E_p E^{dc}$$

$$\chi^{s2} = -A_s 2 \chi_{xxyz} f_c E_s E_p E^{dc}$$

$$\chi^{s3} = -A_s \chi_{xxyz} (f_c^2 E_p^2 - E_s^2) E^{dc}$$

$$\gamma^p = A_p \gamma F_s (E_s^2 + E_p^2)$$

$$\zeta^{p1} = A_p g_b \zeta (2/3) [(f_s F_c + 2F_s f_c) E_s^2 + (2F_s f_c - f_s f_c^2 F_c - 4 f_s^2 f_c F_s + 2 f_s^3 F_c) E_p^2]$$

$$\zeta^{p2} = -A_p g_b \zeta (32/9)^{1/2} (f_c^2 F_c - f_s f_c F_s - f_s^2 F_c) E_s E_p$$

$$\zeta^{p3} = A_p g_b \zeta (8/9)^{1/2} [(2 f_c f_s^2 F_c + F_s f_c^2 f_s - f_c^3 F_c) E_p^2 + (f_c F_c + F_s f_s) E_s^2]$$

$$\partial^{p1} = A_p [(\epsilon(2\omega)/2\epsilon_o(\omega)) F_s 2 (\partial_{zxx} (f_c^2 E_p^2 + E_s^2) + \partial_{zzz} f_s^2 E_p^2) - 2 \partial_{xxz} f_s f_c F_c E_p^2]$$

$$\partial^{p2} = -A_p 2 \partial_{xxx} F_c f_c E_s E_p$$

$$\partial^{p3} = -A_p \partial_{xxx} F_c (f_c^2 E_p^2 - E_s^2)$$

$$\chi^{p1} = A_p [(\epsilon(2\omega)/2\epsilon_o(\omega)) F_s 2 (\chi_{zxxz} (f_c^2 E_p^2 + E_s^2) + \chi_{zzzz} f_s^2 E_p^2) - 2 \chi_{xxzz} f_s f_c F_c E_p^2] E^{dc}$$

$$\chi^{p2} = -A_p \chi_{xxyz} F_c (f_c^2 E_p^2 - E_s^2) E^{dc}$$

$$\chi^{p3} = A_p 2 \chi_{xxyz} F_c f_c E_s E_p E^{dc}$$

Table 3.5: Specific linear optical parameters for the SH fields phenomenological equations.

$A_s = i4\pi(2\omega/c)^2/(W_o + W);$

$A_p = i4\pi(2\omega/c)^2 N N_o/(W_o N^2 + W N_o^2);$

$g_b = (2n/16)(2\omega/c)/(2w + W);$

$F_s = 2\kappa/N(2\omega/c);$

$F_c = W/N(2\omega/c);$

$f_s = \kappa/n(\omega/c);$

$f_c = w/n(\omega/c);$

$n^2 = \epsilon(\omega);$

$N^2 = \epsilon(2\omega);$

$N_o^2 = \epsilon_o(2\omega);$

$W_o^2 = (2\omega/c)^2\epsilon_o(2\omega) - (2\kappa)^2;$

$W^2 = (2\omega/c)^2\epsilon(2\omega) - (2\kappa)^2;$

$w^2 + \kappa^2 = \omega^2\epsilon(\omega)/c;$

where γ is the multipole bulk isotropic susceptibility;
ζ is the multipole bulk anisotropic susceptibility;
∂ is the second order surface dipole susceptibility;
χ is the third order dipole susceptibility;
c is the speed of light;
ϵ and ϵ_o are the dielectric constants for the material and environment, respectively;
ω is the incident light frequency; and w and κ are geometrical constants.

Chapter 4

MICROSCOPIC THEORY REVIEW

The final theoretical discussion for this thesis involves the specific dependence of the susceptibilities on the physical material properties such as the electronic band structure and electron density profiles at the surface. Free electron models do exist [7, 23, 26]. However, even for a metal, the free electron assumptions are relatively poor and do not work at all for energies above which electronic band structure effects become important. We will only characterize how well the SH response is described by some microscopic theories. Our main purpose will be the experimental characterization of the susceptibilities. We will make no attempt at extending microscopic theories.

The macroscopic description of the SHG nonlinear effects described above needs a microscopic theory in order to provide a complete picture of the physical origins of the SH response. These microscopic considerations are specifically applicable to the nonlinear susceptibilities. Ideally, the generalized polarization is calculated by treating an interaction Hamiltonian between the fields and the material to second order. However, only for the jellium case, where the electrons are treated as if they were in the presence of a homogeneous positive background charge, have such calculations been done in detail. Jha and coworkers [28, 76, 77] used both classical and quantum mechanical calculations to derive a second order nonlinear response. Furthermore, Jha and Warke [28] showed that, except near interband transitions, the contributions from the bound electrons to the bulk nonlinear susceptibilities were governed by the dielectric constants $\epsilon(\omega)$ and $\epsilon(2\omega)$. Bower [78] generalized this earlier work of the

bulk nonlinear response to include effects from the surface or interface region and effects near resonant interband transitions such as surface states. This latter formulation was very general and difficult to apply to specific cases. The direct application of these first principles calculations to bulk properties is less difficult than to the surface susceptibilities. This is true because the bulk properties are better understood and because multipole expansions are valid. But even obtaining linear bulk property predictions is non-trivial.

The main benefits these jellium models provide is in the area of resonance predictions and sensitivity considerations. The main experimental prediction from the work of Rudnick and Stern is the predicted surface sensitivity of the surface current parallel to the surface. The longitudinal surface current, which is perpendicular to the sample's surface, is also predicted to be sensitive to surface modulations by the more recent hydrodynamic and density functional calculations. This is due to the longitudinal surface current's spatial orientation being well outside the sample in the exponentially decaying electron density tail where it is not screened by the electrons. The calculation of the longitudinal surface current required a complete non-local formulation, due to the abrupt boundary conditions at the surface. The parallel surface current could still be calculated using a local approximation. Rudnick and Stern used the random-phase approximation, and included the influence of the inversion symmetry breaking and the surface scattering effect to formulate a jellium model for these surface currents. The surface currents led to the two phenomenological parameters which have become known as a_{RS} and b_{RS}. a_{RS} is incorporated in the longitudinal surface current and b_{RS} in the surface current parallel to the sample surface. The calculations resulted in the following expressions for the second order surface

susceptibilities given in Eqs. 4.1 and 4.2 [45].

$$\partial_{zzz} = [a_{RS}e/(16m\pi\omega^2][\epsilon(\omega) - 1]/\epsilon^2(\omega) \tag{4.1}$$

$$\partial_{xzx} = [b_{RS}e/(16m\pi\omega^2][\epsilon(\omega) - 1]/\epsilon(\omega) \tag{4.2}$$

The a_{RS} and b_{RS} parameters were assumed to be of order unity, with -e being the electronic charge, m the electronic mass, and ϵ and ϵ_o being the dielectric functions of the metal and interface, respectively. The hydrodynamic model by Sipe and coworkers [26] found b_{RS} = -1 and a formal expression for a_{RS}, Eq. 4.3.

$$a_{RS} = -2(\omega_p^2 - \Omega^2)/(\omega_o^2 - \Omega^2) \tag{4.3}$$

ω_o is the effective plasma frequency and ω_p is the classical plasma frequency. This form of a_{RS} should be sensitive to the electronic structures of the surface and has resonance features when Ω^2 approaches ω_o^2.

The resonance predictions from the jellium models show up in the more conventional quantum mechanical formalism for the second order susceptibilities. The second order susceptibility may be written as [7, 25]:

$$\begin{aligned}\partial^2_{ijk}(\Omega;\omega,\omega) = (-Ne^3/\hbar^2) \sum_{a,b,c} \Big[& \frac{2\langle c|r_i|a\rangle\langle a|r_j|b\rangle\langle b|r_k|c\rangle}{(\Omega - \omega_{ac})(\omega - \omega_{ab})} \\ & + \frac{2\langle c|r_k|a\rangle\langle a|r_i|b\rangle\langle b|r_j|c\rangle}{(\Omega - \omega_{ca})(\omega - \omega_{bc})} \\ & + \frac{\langle c|r_j|a\rangle\langle a|r_i|b\rangle\langle b|r_k|c\rangle}{(\omega - \omega_{ba})(\omega - \omega_{ca})} \\ & + \frac{\langle c|r_k|a\rangle\langle a|r_i|b\rangle\langle b|r_j|c\rangle}{(\omega - \omega_{ca})(\omega - \omega_{ba})} \Big] f_a \end{aligned} \tag{4.4}$$

where r_i is the dipole operator and $|a\rangle$, $|b\rangle$ and $|c\rangle$ represent the electron band wavevec-

tors and f_a is the Fermi distribution factor for state $|a\rangle$. Ω and ω are the frequencies of the incident and second harmonic photons, respectively and ω_{ab} or ω_{bc} and ω_{ac} are the single photon and two photon absorption frequencies of the medium, respectively. This formalism is inherently sensitive to resonant conditions (when the denominator vanishes) and provides a useful tool in determining potential enhancement conditions. Similar expressions exist for the higher order susceptibilities, but the resonance conditions remain the same. The end result of these calculations is that a potential signal enhancement may occur any time the probe energies become equivalent to a fundamental electronic transition energy of the material. Explicit calculation of these terms also provides information on whether a transition is symmetry allowed.

Chapter 5

EXPERIMENTAL ARRANGEMENT

5.1 The Pulsed Nd:YAG and Dye Lasers

The experimental arrangement utilized a 10-Hz frequency-doubled Nd:yttrium-aluminum-garnet (Nd:YAG) pulsed laser to pump a dye laser which provides the polarized incident photons. This laser system provided incident photon energies between 1.17 eV and 2.33 eV. The incident laser spot size was approximately 0.5 cm^2 and a pulse energy of no greater then 5 mJ at the sample surface was used. This translates to about 1 MW of power. However, due to the relatively low SH conversion efficiency for silver (about 10^{-6}), less than 1 W of power or 5 nJ of SH energy was collected.

The pulsed Nd:YAG laser was a "Quantra-Ray DCA-2A" purchased in 1988. The main optical lasing cavity used a Nd:YAG rod as the lasing medium, which was pumped by two flashlamps contained in a water cooled elliptical cavity. The optical cavity also contained the Q-switch, which controlled the laser pulse, and the two reflective mirrors on either end. This arrangement resulted in laser pulses with energies around 300 mJ per pulse. Once the laser pulse left the main optical cavity, it passed through an identical Nd:YAG rod pumped by flashlamps, which acted as an amplifier. The amplified laser pulse may then reach energies of as much as 1 J per pulse. This initial laser pulse has a wavelength of 1064 nm and a pulse width of 8-9 ns. The final component of this laser is a temperature controlled second, third and fourth harmonic generator. The harmonic generator contained crystals which,

when placed in the optical path and aligned correctly, converts as much as 70% of the initial 1064 nm photons to 532 nm, 355 nm, and/or 266 nm photons, depending upon the crystal arrangement. For this experiment we used only the 1064 nm light as an incident light, or used the KDP crystal in the harmonic generator to provide the 532 nm photons, which were used to pump the dye laser.

The pulsed dye laser was a "Quantra-Ray PDL-2". The main lasing cavity used a cell with a dye containing methanol solution as the lasing medium. A grating was used at one end of the optical cavity to adjust the lasing wavelength, while the other end contains the usual reflecting mirror. A similar dye cell constituting the "preamp" was aligned in the optical path of the exiting dye laser pulse which amplifies the initial dye pulse. This preamp was used for the dyes which produce relatively weak intensity pulses. The main amplification came from a longitudinally pumped amplifying cell placed further down the optical path. The end result was a laser pulse that may be as much as 300 mJ per pulse. By using several different dyes, this dye laser produced laser pulses with wavelengths between 860 nm to 550 nm.

5.2 The Electrochemical System

The pulsed laser light is reflected from the electrochemically controlled Ag sample. The electrochemistry provided a dc field modulation to the sample surface and controlled the electrochemical interface. The electrochemical cell was made completely of teflon and used a quartz window. The sample was also mounted in teflon so that only the surface was in contact with the 0.01 M reagent grade electrolyte. Triple-distilled water or millipore deionized water was used for the electrolytic solvent. Zero grade nitrogen was used to purge and de-aerate the electrolyte.

The electrochemical cell used a Pd counter electrode and a saturated calomel

reference electrode (SCE) or a Ag Ag-Cl electrode to establish a reproducible reference potential with an arbitrary zero [61]. For silver in contact with an aqueous electrolyte, the surface is least perturbed at the potential of zero charge (PZC). Richmond et al [57] showed that the SH response for a well polished electrochemically controlled Ag surface at PZC is the same as the SH response of a similar surface exposed to ultra high vacuum. For a 0.01 M KPF_6 or a $NaClO_2$ solution, the PZC is -0.7 V or -0.72 V (SCE) for Ag(111) and -0.86 V or -0.89 V (SCE) for Ag(001), respectively [79]. The electrochemistry was controlled using a "Pine Instruments RDE-4" potentiostat and sweep generator.

5.3 Optical Alignment (Components and Detection)

The incident photons were guided by silver mirrors after leaving the lasers. The photon polarization from the laser was horizontal with respect to the laser. The polarization of the incident photons was controlled using a half wave plate in the laser beam and the correct alignment of the optics. A long pass filter was used immediately before the sample to filter out any SHG or photoluminescence in the incident photon light. A dichroic mirror and appropriate filters were used to separate the SH light from the fundamental. A polarizer was used to individually measure the SH electric field components parallel (p-polarization) and perpendicular (s-polarization) to the light's plane of incidence.

The SH light was then focused using a concave mirror and a cylindrical lens onto the incident slit of a "Kratos" monochromator. The monochromator allowed only the SH light to exit and be collected by the detector. A R212 Hamamatsu photomultiplier tube (PMT) was used as the detector. The incident photon energy was determined with a "Scientech" power and energy meter (Fig. 5.3).

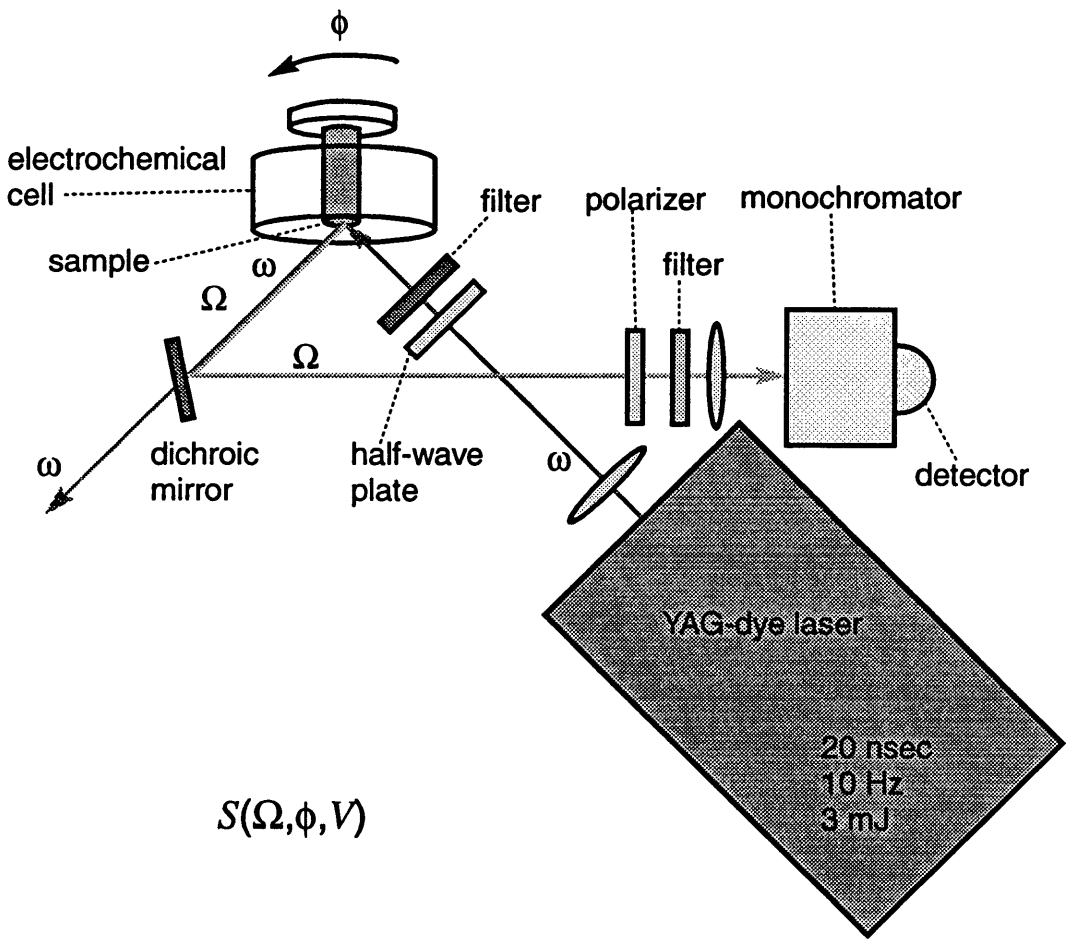

FIG. 5.1: Schematic of the optical components and alignment used in the SHG experiments.

5.4 Sample Preparation

The Ag crystals were generally mounted in a teflon shroud [60] by pressing powdered teflon around the sample and then annealing it at 380°C. The excess teflon was removed with a lathe.

The Ag surface was then mechanically polished. In order to remove large defects in the sample and achieve a flat surface, 600 and/or 1200 grit SiC was used. A polish table was then used with 1 micron, 0.3 micron and 0.05 micron alumina abrasive in sequence to remove the scratches. The sample was thoroughly rinsed in an ultrasound bath and scrubbed with a Q-tip swab to remove the previous polishing agents between each step.

The final polishing step (see Appendix A) utilized a chemical etch to remove the mechanically induced surface strain. For this process, two solutions were used. The Ag sample was dipped into a 21 g/l NaCN 30% hydrogen peroxide solution. A Q-tip cotton swab was then used to provide a uniform coverage of the solution. This solution was then removed using a 35 g/l NaCN water solution within 5-10 seconds of application. The latter solution was then applied with a cotton swab until the surface became specular. The sample was then thoroughly rinsed with high purity water. The sample was transported in a water shroud and immediately placed into an electrochemical cell after rinsing.

5.5 Computer Control and Data Acquisition

The SH photons were collected with the PMT and the signal was amplified 125 times with a "Stanford Research Systems Inc." (SRS) model SR440 DC-300 MHz Amplifier. A SRS gated integrator and box car averager model SR250 was used to accumulate the SH signal. Further filtering and amplification was done with the SRS

analog processor model SR235. The processed signal is transferred to the control program on the 286 "Hyundai" computer through a "Data Translation 2808". The computer control program was written and operated in the Asyst environment.

Chapter 6

RESULTS

6.1 Ag(001)

The bulk contributions to SHG can be separated into crystal orientation dependent factors (that depend upon linear optical properties) and "strength factors" (that should be the same for all crystal orientations). The latter quantities are conventionally identified as γ and ζ (Eq. 3.8). What one learns about these two parameters from experiments performed on a given crystal face can, with care, be carried over to other orientations of the same material. This concept also applies to free electron contributions influencing ∂_{zxx}, although on a given face, there may also be crystal-potential derived contributions to ∂_{zxx} related to surface states.

An estimate of the size of ζ has been published by Richmond *et al.* [30], based upon experiments on Ag(110) using a single incoming photon energy (1.17 eV). They found, through an optical configuration involving only s-polarized light, that SHG associated with ζ was below their detection limit. This result justified the usual practice of setting ζ equal to zero [52]. However, recently we have become involved with spectral measurements of optical SHG where questions about the size of ζ, as well as of γ and ∂_{zxx}, must be re-addressed.

Under the conditions of excitation and measurement appropriate to our experiment (Ag(001), s-polarized incoming light with a photon energy of $\hbar\omega$), the most general expression for the power density (S_Ω) of the reflected light at the second-harmonic frequency ($\hbar\Omega = 2\hbar\omega$) is given by Eq.(3.6). The corresponding SH electric

fields are then given by:

$$E_{\Omega,s\to s} = E_\omega^2 \, [b \, \zeta \, \sin(4\phi)], \tag{6.1}$$

for s-polarized outgoing light, and

$$E_{\Omega,s\to p} = E_\omega^2 \, [a_1 \, \partial_{zxx} + a_2 \, \gamma + a_3 \, \zeta \, \sin^2(2\phi)], \tag{6.2}$$

for p-polarized outgoing light. Here $\hat{z}$ is parallel to [001] with $\hat{x}$ and $\hat{y}$ along [100] and [010], respectively. The crystal orientation about [001] is specified by ϕ, the angle between [100] and the projection of the incoming wave vector on the surface plane (Fig. 3). The parameters a_n and b in Eqs. 6.1 and 6.2 depend only upon the linear optical properties of the sample at ω and Ω and the angle of incidence. Of the nonlinear susceptibilities in Eqs. 6.1 and 6.2, only ∂_{zxx} would be expected to change with V_a (the externally applied potential), since the others are bulk derived and are, therefore, beyond the range of the interfacial field.

For each set of conditions we recorded the second harmonic reflectance as a function of the orientation of the sample about its surface normal (sample rotation experiment, $S_\Omega(\phi)$). This allowed us to make qualitative statements about the relative influences of the various terms found in Eqs. 6.1 and 6.2. In most cases this simple analysis was sufficient to lead to important conclusions regarding surface versus bulk effects.

Figs. 6.1 and 6.2 were both obtained with the detection system set for only s-polarized light. The appropriate harmonic field expression is Eq. 6.1, where only ζ can contribute. Under these conditions $S_\Omega(\phi)$ must demonstrate a periodicity of 45° with no offset. The magnitude of the variation is a measure of $|\zeta|^2$. Figure 6.1 compares two excitation energies, 1.75 eV and 2.03 eV, on an uncharged surface, while Fig. 6.2

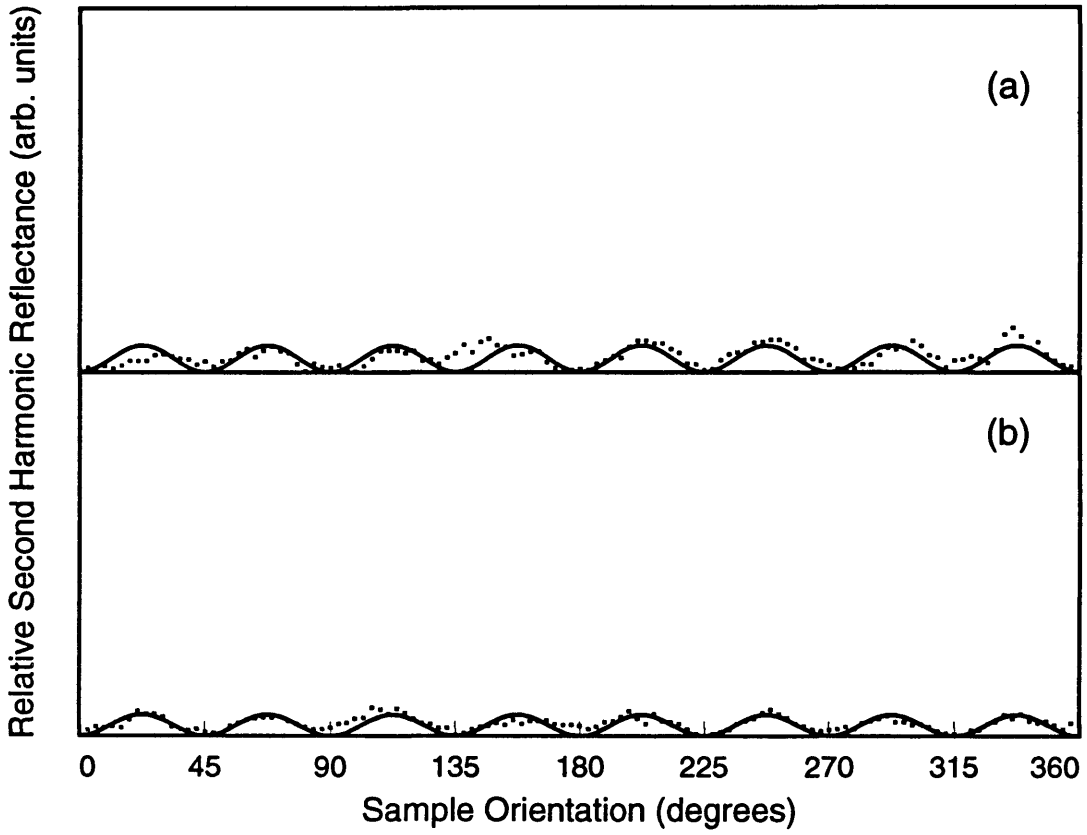

FIG. 6.1: Demonstration of the photon energy independence of ζ. Sample rotation experiment. (dotted) - experimental data, (solid) - phenomenological fit. Uncharged surface. (a): Incoming light; s-polarized, 1.75 eV. Outgoing light; s-polarized, 3.50 eV. (b): Incoming light; s-polarized 2.03 eV. Outgoing light; s-polarized, 4.06 eV. Similar behavior was observed throughout the entire spectral range of incoming light that we measured, 1.17 eV to 2.03 eV.

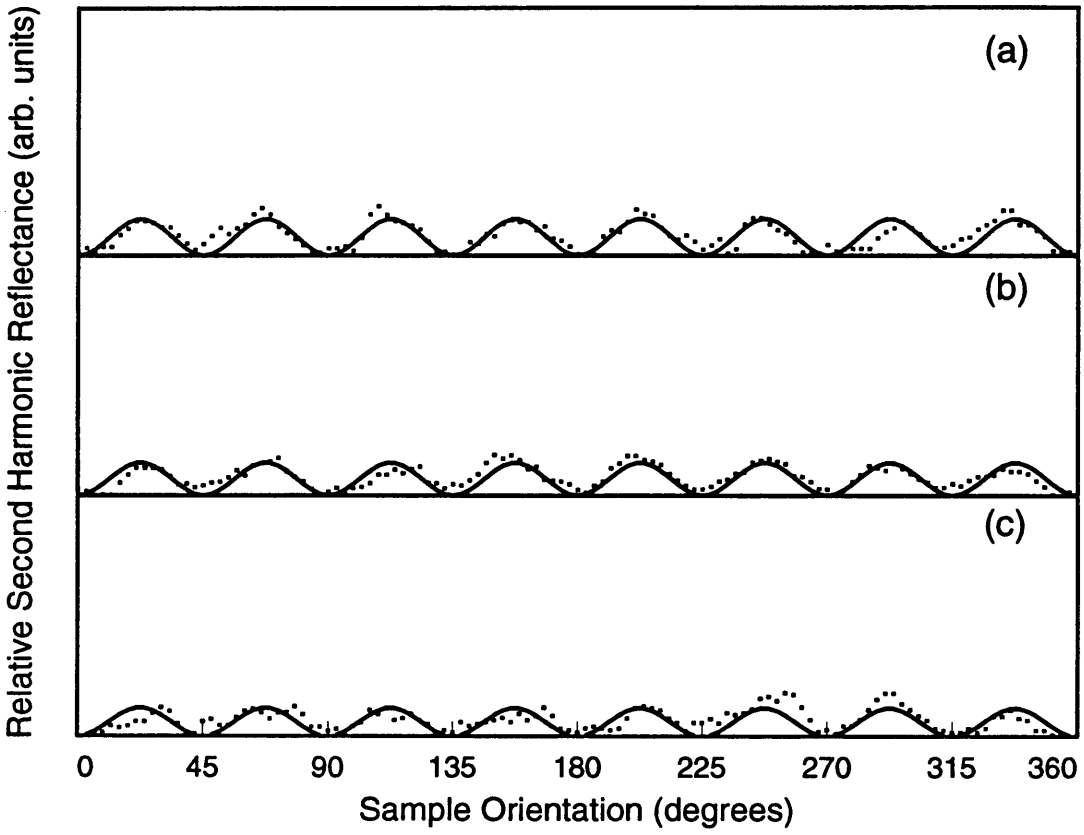

FIG. 6.2: Demonstration of the surface charge independence of ζ. Sample rotation experiment. (dotted) - experimental data, (solid) - phenomenological fit. Incoming light: s-polarized, 1.97 eV. Outgoing light: s-polarized, 3.94 eV. (a): Positively charged surface (V_a = 0 V vs SCE). (b): Uncharged surface (V_a = -0.89 V vs SCE). (c): Negatively charged surface (V_a = -1.2 V vs SCE). Similar behavior was observed throughout the entire range of the interfacial charge that we measured, from negative (where V_a = -1.20 V vs SCE) to positive (where V_a = 0 V vs SCE).

shows results obtained with and without a surface charge ($V_a = -0.89$ V). What we have displayed here is typical of what we observed over the entire spectral range (between 1.17 eV and 2.03 eV) and at all values of interfacial charge (controlled by V_a variations between -1.2 V and 0 V) that we studied. This means that ζ does not change significantly with $\hbar\omega$ or V_a. The data demonstrate an 8-peaked sinusoidal pattern as a function of ϕ. Although we have not explicitly calibrated the size of this variation, we can say that, based upon our experience with SHG from Ag, Figs. 6.1 and 6.2 contain a very weak effect, primarily due to the relatively small linear optical parameters associated with ζ. Yet, even under these unfavorable conditions the SH response governed by ζ is obviously not zero. Therefore, ζ cannot be discarded in any detailed analysis, particularly under conditions where it might lead to cross terms (as we will see below).

Fig. 6.3 shows the normalized SH magnitude as a function of SH photon energy for the s-polarized SH response. The data points corresponding to the different $a_3\,\zeta$ values were obtained by fitting the sample rotation experiments using the appropriate phenomenological equations. The known linear optical parameters in a_3 were then plotted on the same graph and fit to the data using a multiplying factor. The linear optical parameters accounted completely for the relatively small spectral dependence observed in the data. Furthermore, the data show no significant dependence on the applied potential. Thus we again conclude that ζ is independent of incident photon energy and applied potential. This result is very significant, since ζ should be a constant in all SH experiments using silver crystals, regardless of crystal face or experimental conditions at the surface. Future experiments will now be able to compare the linear optical parameters from the different SH terms and determine the significance, if any, of a contribution from the ζ term.

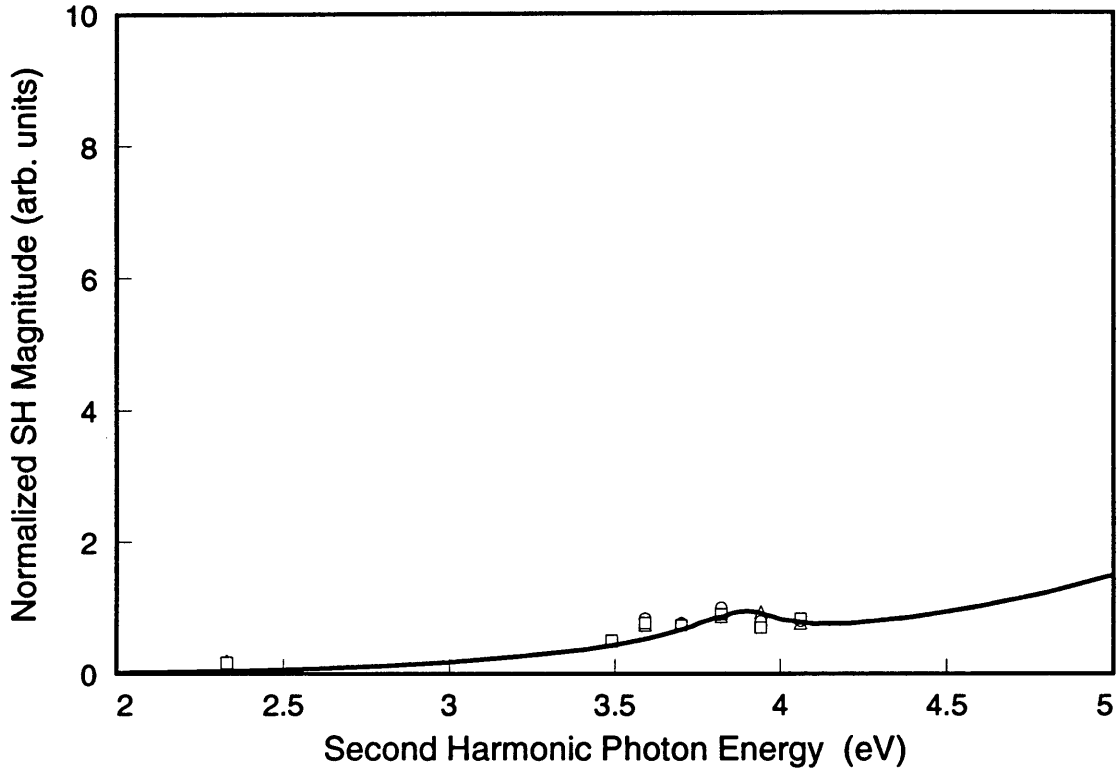

FIG. 6.3: Measurement of the absolute magnitude of ζ.
The normalized SH magnitude of the s-polarized SH response as a function of SH photon energy. Incoming light: s-polarized. (circles): Uncharged surface ($V_a = -0.89$ V vs SCE). (triangles): Positively charged surface ($V_a = 0$ V vs SCE). (squares): Negatively charged surface ($V_a = -1.2$ V vs SCE). (line): The linear optical parameters associated with ζ given by the phenomenological equations, multiplied by a factor of 1500 to 2000. These data indicate that ζ is truly independent of incident photon energy and applied potential. All incident photon energy dependence is determined by the linear optical properties for SH contributions governed by ζ.

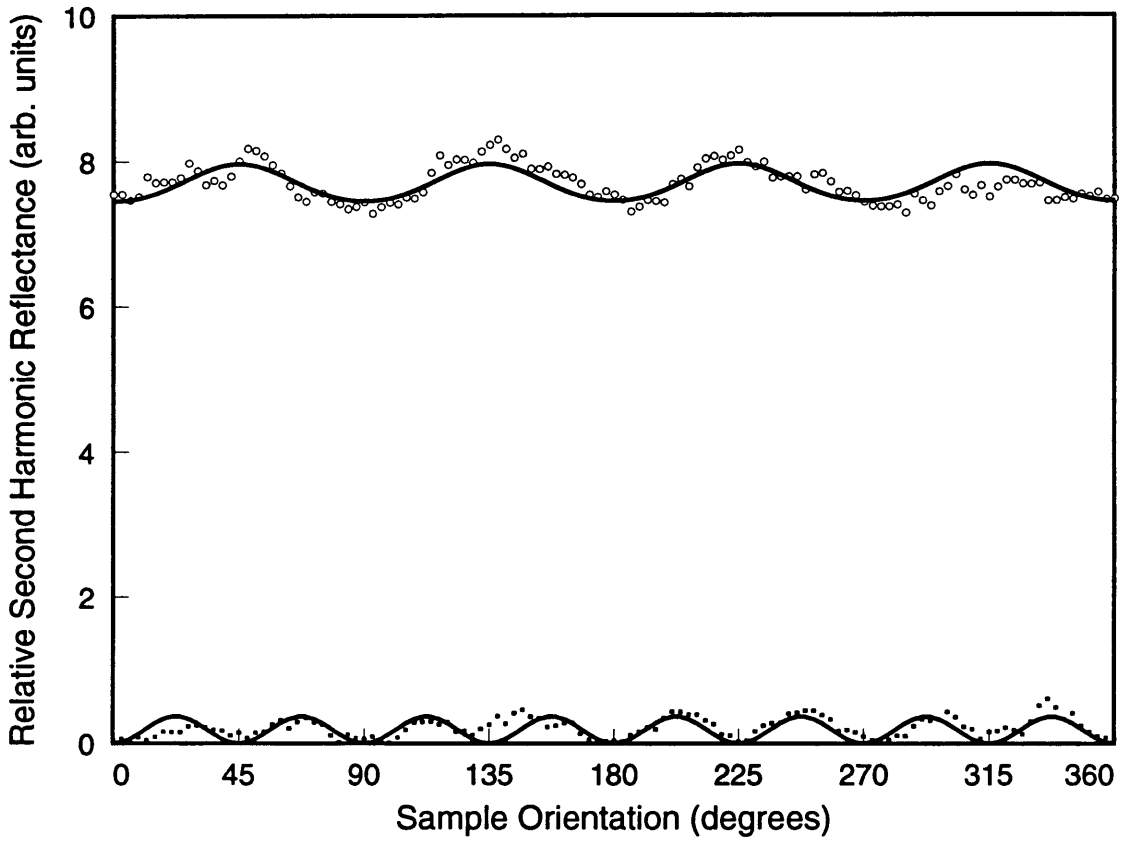

FIG. 6.4: Qualitative comparison of the relative magnitudes of $a_3\zeta$ and $(a_1\partial_{zxx}+a_2\gamma)$ from Ag(001).
Sample rotation experiment. Incoming light: s-polarized, 1.75 eV. Outgoing light: (dotted); s-polarized or (circles); p-polarized, 3.50 eV. Uncharged surface. Here, $(a_1\partial_{zxx}+a_2\gamma)$ contributes only to the p-polarized data. Similar behavior was observed throughout the spectral range of incoming light from 1.17 eV to 2.03 eV.

With this information about ζ it is now possible to systematically explore the other susceptibilities. First, we present the results obtained from an uncharged surface. Fig. 6.4 shows data from the sample rotation experiment with the detection set for either s-polarized or p-polarized light. What we see here is a comparison between conditions appropriate to Eqs. 6.1 or 6.2, respectively. Fig. 6.4 shows that the p-polarized SH response is approximately an order of magnitude larger then the s-polarized SH response. By fitting the curves using Eqs. 6.1 and 6.2 we extracted the isotropic and anisotropic contributions from each set of data. The SH response is separated into the part which changes intensity as the crystal is rotated about its surface normal (the anisotropic part) and the part which remains the same as the crystal is rotated (the isotropic part). This division is more appropriately made in the SH fields where the isotropic components are easily identified by not having any sinusoidal dependence, while the anisotropic components do. The anisotropic contributions in the SH fields of the two curves were found to be approximately the same. This was expected since the SH response governed by ζ should not change appreciably from s- to p- polarization. This is because the linear optical parameters do not change appreciably for the s- and p- polarized response. The periodicity does become more well-defined with p-polarization, displaying a 90° cycle. This is fully consistent with Eqs. 3.6 and 6.2, where we see that $S_\Omega(\phi)$ should be proportional to $\sin^4(2\phi)$. Thus the entire isotropic p-polarized SH response is attributable to the other susceptibilities ∂_{zxx} and γ. This trend was maintained at all excitation energies (from 1.17 eV to 2.03 eV) and for the different surface charging conditions.

Under conditions of positive surface charge ($V_a = 0$ V and $V_a = -0.5$ V) or negative surface charge ($V_a = -1.2$ V) the SH intensity decreased and increased respectively. This phenomenon is displayed in Fig. 6.5, 6.6 and 6.7, where $S_\Omega(\phi)$

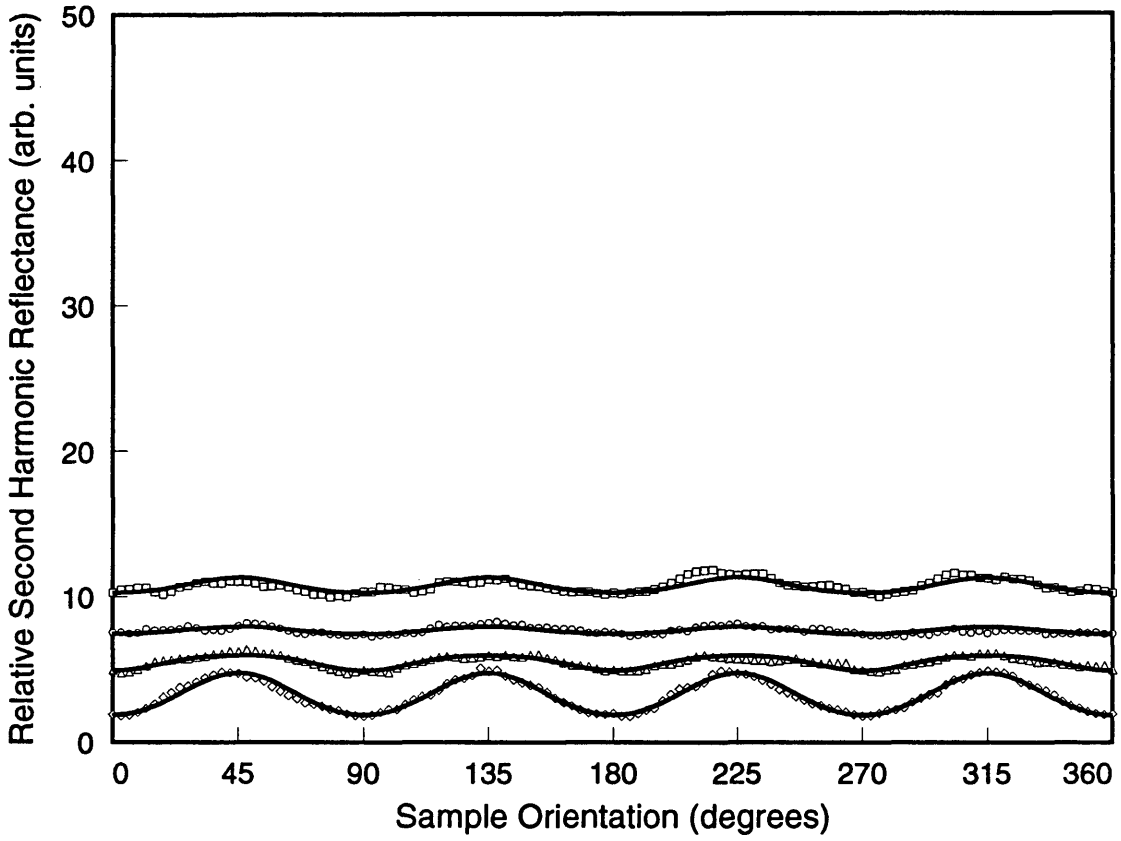

FIG. 6.5: Demonstration that $(a_1\ \partial_{zxx} + a_2\ \gamma)$, or a higher order term with the same symmetry, depends upon the interfacial potential at 1.75 eV on Ag(001).
Sample rotation experiment. Incoming light: s-polarized, 1.75 eV. Outgoing light: p-polarized, 3.50 eV. (circles): Uncharged surface ($V_a = -0.89$ V vs SCE). (triangles): Positively charged surface ($V_a = 0$ V vs SCE). (diamonds): Positively charged surface ($V_a = -0.5$ V vs SCE). (squares): Negatively charged surface ($V_a = -1.2$ V vs SCE).

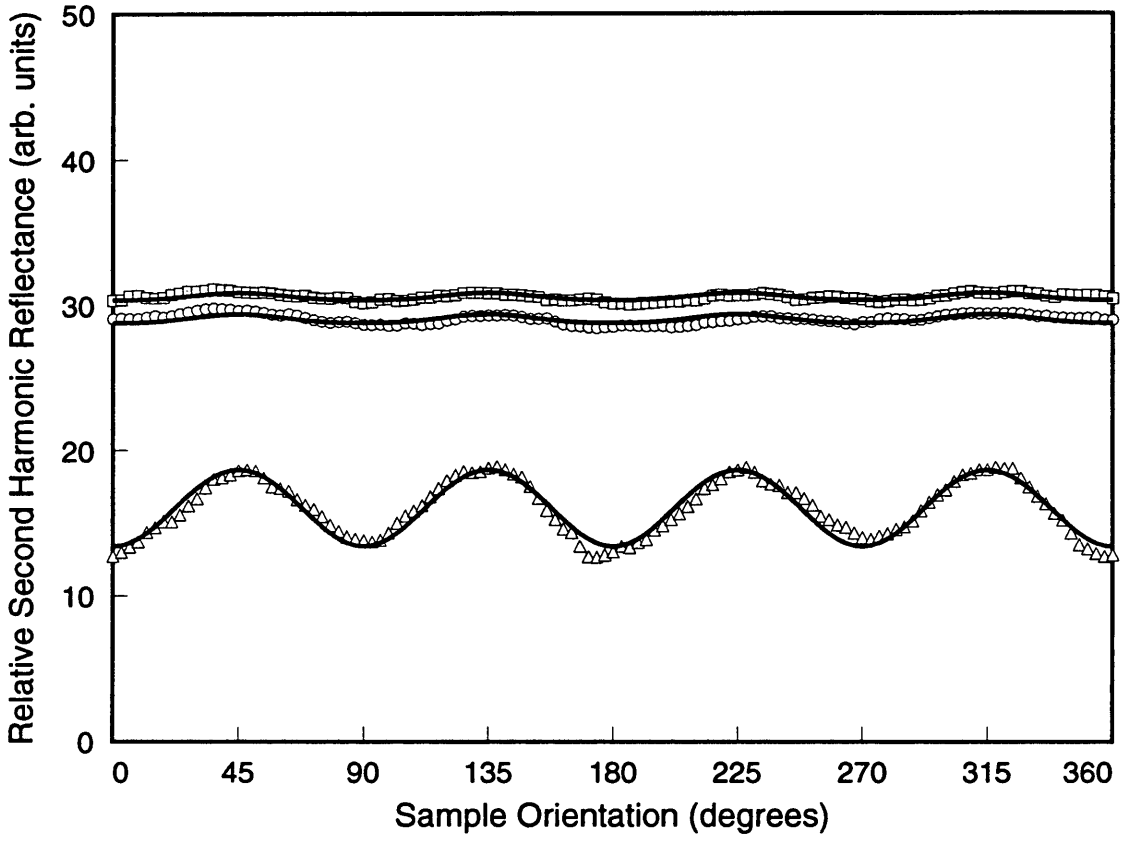

FIG. 6.6: Demonstration that $(a_1\ \partial_{zxx} + a_2\ \gamma)$, or a higher order term with the same symmetry, depends upon the interfacial potential at 1.91 eV on Ag(001).
Sample rotation experiment. Incoming light: s-polarized, 1.91 eV. Outgoing light: p-polarized, 3.82 eV. (circles): Uncharged surface ($V_a = -0.89$ V vs SCE). (triangles): Positively charged surface ($V_a = 0$ V vs SCE). (squares): Negatively charged surface ($V_a = -1.2$ V vs SCE).

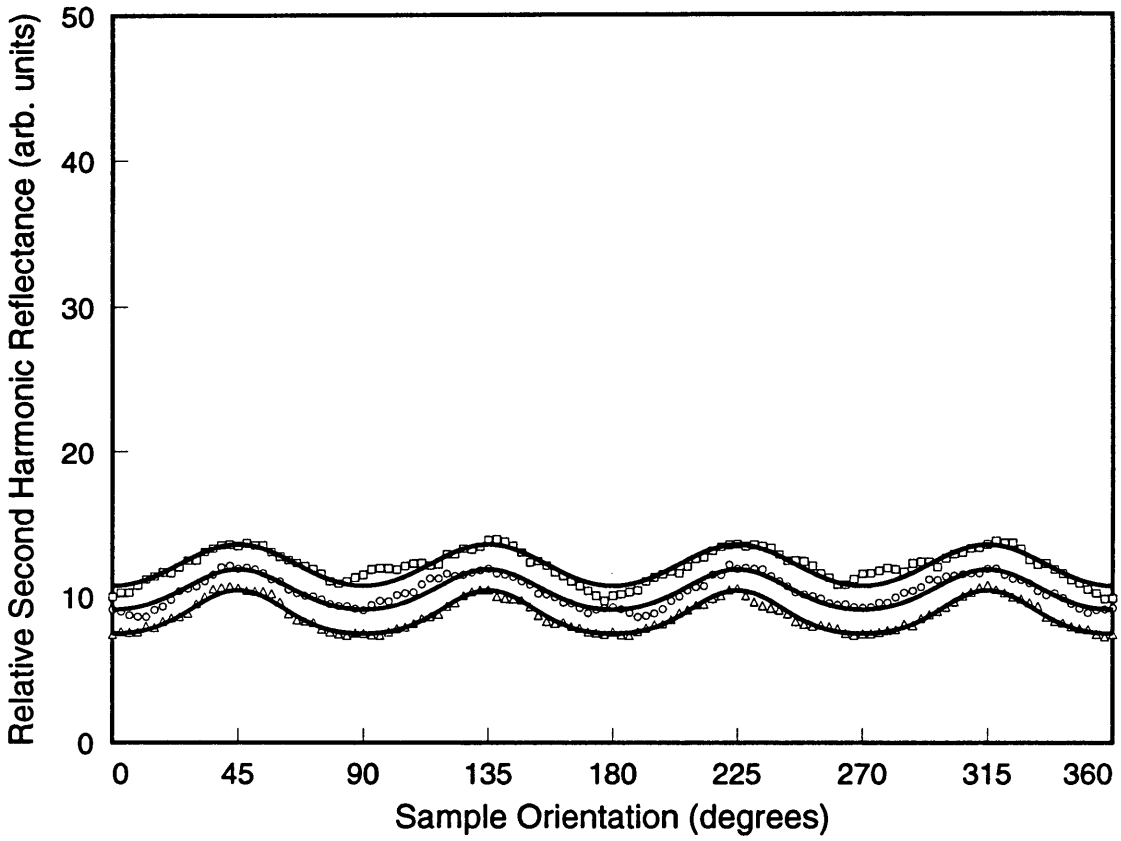

FIG. 6.7: Demonstration that $(a_1\ \partial_{zxx} + a_2\ \gamma)$, or a higher order term with the same symmetry, depends upon the interfacial potential at 1.97 eV on Ag(001).
Sample rotation experiment. Incoming light: s-polarized, 1.97 eV. Outgoing light: p-polarized, 3.94 eV. (circles): Uncharged surface ($V_a = -0.89$ V vs SCE). (triangles): Positively charged surface ($V_a = 0$ V vs SCE). (squares): Negatively charged surface ($V_a = -1.2$ V vs SCE).

shows an amplitude variation with a 90° periodicity, as well as a significant constant contribution for each of the surface charging conditions. The appropriate harmonic field expression is Eq. 6.2. The behavior seen in Fig. 6.5, 6.6 and 6.7 can be explained by expanding Eq. 6.2 using Eq. 3.6.

$$S_\Omega(\phi) \propto |a_1\,\partial_{zxx} + a_2\gamma|^2 + 2|a_1\,\partial_{zxx} + a_2\gamma||a_3\zeta|\cos(\delta)\sin^2(2\phi) + |a_3\zeta|^2\sin^4(2\phi) \quad (6.3)$$

Here δ, in the second term is the relative phase between $a_3\,\zeta$ and $(a_1\,\partial_{zxx} + a_2\,\gamma)$. The data from Figs. 6.5, 6.6 and 6.7 indicates that at least one part of $a_1\,\partial_{zxx} + a_2\,\gamma$ is potential dependent at all the incident photon energies used in these experiments.

Fig. 6.8 shows the results from fitting the isotropic part of the crystal orientation data at the different incident photon energies and the different applied potentials. We found that the spectral dependence of the data could be satisfactorily accounted for by using the linear optical properties associated with γ. A constant multiplying factor was used to fit the positively charged data ($V_a = 0$ V vs SCE) and another multiplying factor 25% larger was used to fit the PZC data ($V_a = -.89$ V vs SCE). The difference in the multiplying factors is needed to account for the applied potential dependence of the SH response. However, within the resolution of these data we were unable to find a correlation between the spectral dependence and the applied potential dependence.

One final calibration is shown in Fig. 6.9. The previous results indicated that the spectral dependence of the s-polarized and p-polarized SH response from the Ag(001) crystal is completely accounted for by the linear optical properties. Thus the ratio of the isotropic to anisotropic SH response should also have the spectral dependence accounted for by the appropriate linear optical properties with a corresponding multiplying factor reflecting the ratio of the previous multiplying factors. The multiplying factors used in Fig. 6.9 were 0.1 and 0.13 for the different applied potentials, which

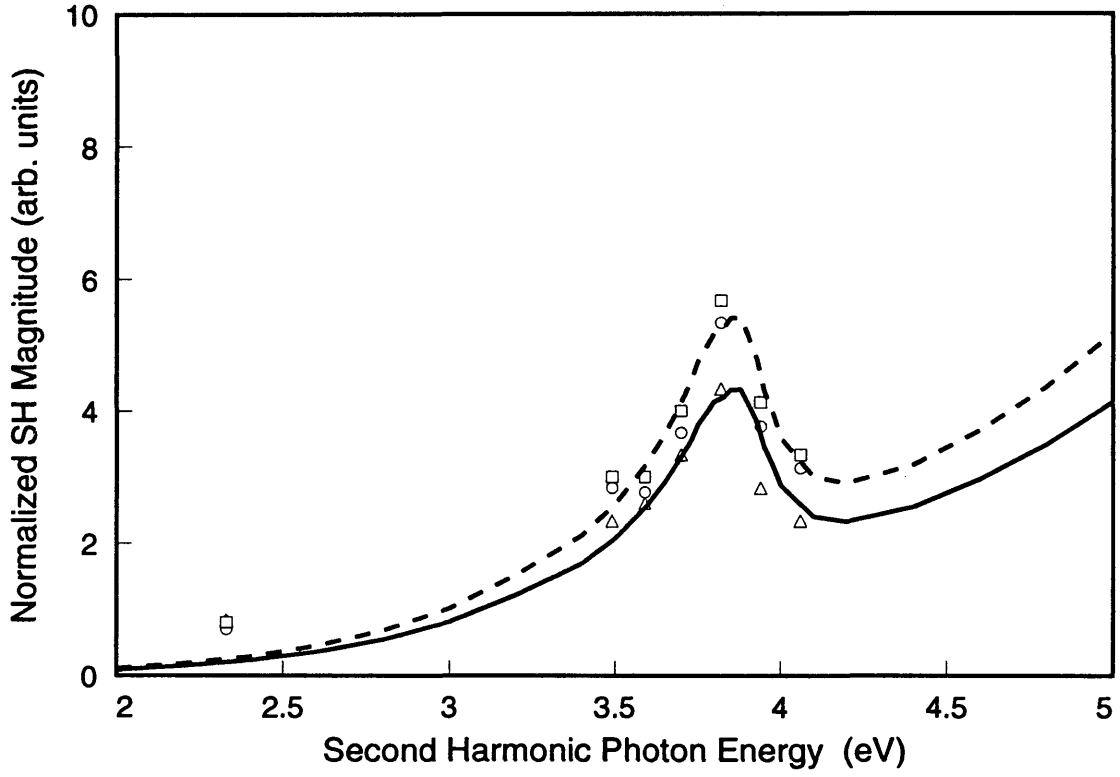

FIG. 6.8: Normalized SH magnitude of $(a_1\ \partial_{zxx} + a_2\ \gamma)$ from Ag(001). The normalized SH magnitude of the isotropic p-polarized SH response as a function of SH photon energy. Incoming light: s-polarized. (circles): Uncharged surface ($V_a = -0.89$ V vs SCE). (triangles): Positively charged surface ($V_a = 0$ V vs SCE). (squares): Negatively charged surface ($V_a = -1.2$ V vs SCE). (line): The linear optical parameters "a_2" given by the phenomenological equations, multiplied by a factor of 200. (dashed line): The linear optical parameters "a_2" given by the phenomenological equations, multiplied by a factor of 250. All incident photon energy dependence is determined by the linear optical properties.

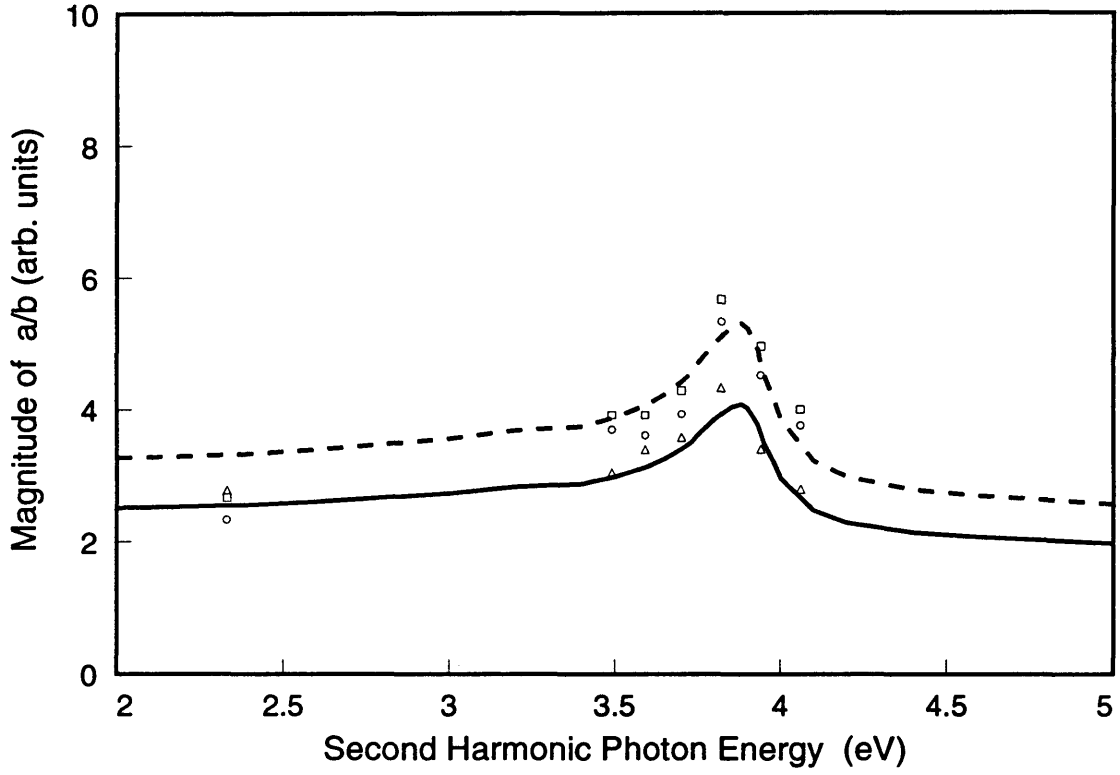

FIG. 6.9: Magnitude of $(a_1\,\partial_{zxx} + a_2\,\gamma)/(a_3\,\zeta)$ from Ag(001).
The magnitude of the isotropic to anisotropic ratio of the SH response as a function of SH photon energy. Incoming light: s-polarized. (circles): Uncharged surface ($V_a = -0.89$ V vs SCE). (triangles): Positively charged surface ($V_a = 0$ V vs SCE). (squares): Negatively charged surface ($V_a = -1.2$ V vs SCE). (line): The linear optical parameters given by the phenomenological equations, multiplied by a factor of 0.1. (dashed line): The linear optical parameters given by the phenomenological equations, multiplied by a factor of 0.13. All incident photon energy dependence is determined by the linear optical properties.

is completely consistent with the previous results. However, unlike the previous fitting factors which are not applicable for other SH experiments, these latter values of ratios are generally applicable since they do not contain details explicit only to these experiments. Thus the ratio of these susceptibilities $[\gamma + (\epsilon(\Omega)/\epsilon_o)\partial_{zxx}]$ should be between 0.1 and 0.13 for all crystal faces of Ag in the free electron approximation.

6.2 Normal Incidence SHG from Ag(111)

In general, 7 nonlinear susceptibilities govern the SH response from the Ag(111) face. Of these, two of them are the crystal orientation independent bulk derive susceptibilities ζ and γ. The results reported from the Ag(001) experiments should still be applicable for the Ag(111) face. Unfortunately, separating any one of the 7 nonlinear susceptibilities is experimentally intractable. However, like the Ag(001) experiment, certain geometries and polarization conditions limit the number of allowed contributions. In general, the magnitude of the s-polarized SH response is governed only by the bulk anisotropic susceptibility ζ, the second order surface susceptibility ∂_{xxx} and the third order surface susceptibility χ_{xxyz} (Table 3.4). We have included the explicit contribution of the third order susceptibility, since this has the potential of supplying an anisotropic contribution that is significantly different then the applicable second order susceptibilities for this configuration. In general this is not the case. We can further decrease the number of linear optical parameter contributions by doing the experiments at normal incidence.

Under the conditions of excitation and measurement appropriate to our experiment (Ag(111), s-polarized incoming light at normal incidence with a photon energy

of $\hbar\omega$) the corresponding SH electric fields are:

$$E_{\Omega,s\to s} = E_\omega^2 \left[(a_{1s}\,\partial_{xxx} + b_{1s}\,\zeta)\,\sin(3\phi) + a_{1s}\,\chi_{xxyz}\,E^{dc}\,\cos(3\phi)\right], \tag{6.4}$$

for s-polarized outgoing light, and

$$E_{\Omega,s\to p} = E_\omega^2 \left[(a_{1p}\,\partial_{xxx} + b_{1p}\,\zeta)\,\cos(3\phi) + a_{1p}\,\chi_{xxyz}\,E^{dc}\,\sin(3\phi)\right], \tag{6.5}$$

for p-polarized outgoing light. Here $\hat{z}$ is parallel to [111] with $\hat{x}$ along $[2\bar{1}\bar{1}]$. For non-normal incidence angles the crystal orientation about [111] is specified by ϕ, the angle between $2\bar{1}\bar{1}]$ and the projection of the incoming wave vector on the surface plane. However, for normal incidence, polarization vectors have to be used to describe ϕ. We will define the crystal orientation about [111] to be specified by ϕ, the angle between $[2\bar{1}\bar{1}]$ and the polarization vector $\hat{e}_1$, which is parallel to the surface and for non-normal incidence would be associated with the projection of the p-polarized incident wave vector. We also define the polarization vector $\hat{e}_2$, which is perpendicular to $\hat{e}_1$ but still parallel to the surface. The polarization of the incident light in these experiments is parallel to $\hat{e}_2$. In these normal incident experiments we will refer to an incident or SH light polarized parallel to $\hat{e}_2$ as being s-polarized, in order to minimize confusion and maintain a consistent notation. The parameters a_1 and b_1 in Eqs. 6.4 and 6.5 depend only upon the linear optical properties of the sample at ω and Ω and the angle of incidence.

For each set of conditions we recorded the second harmonic reflectance as a function of the sample orientation about its surface normal (sample rotation experiment, $S_\Omega(\phi)$). By analyzing these data we were able to make quantitative statements about the relative influences of the various terms found in Eqs. 6.4 and 6.5. From this we

were able to formulate several conclusions about the specific contributions from each susceptibility.

The Ag(111) sample rotation experiments shown in Figs. 6.10 and 6.11 indicate that the SH response at normal incidence has both an applied potential and incident photon energy dependence. Perhaps the most surprising effect contained in the data of Figs. 6.10 and 6.11 is the isotropic contribution apparent in all the SH data. This is not explicitly predicted from Eq. 6.4. The isotropic contribution was not due to any systematic error since it demonstrates a large potential dependence. This means that the isotropic contribution is sensitive to the electronic conditions at the surface.

The data in Figs. 6.10 and 6.11 may be completely fit using Eq. 6.4. However, the $\chi_{xxyz}E^{dc}$ component is an integral part of that fitting process, and requires that the PZC data have no isotropic contribution since E^{dc} is zero at the PZC by definition. So unless the dc applied field is not zero at the PZC then an anomalous source must be contributing to the SH response. Furthermore, since any isotropic contribution from Eq. 6.4 would require an unprecedented match between ∂_{xxx} and χ_{xxyz} so that $\partial_{xxx}^2 \sin^2(3\phi) + \chi_{xxyz}^2 (E^{dc})^2 \cos^2(3\phi) = \partial_{xxx}^2(\text{ a + b } \sin^2(3\phi))$, it is unlikely that χ_{xxyz} contributes at all to the SH response in this experiment.

The isotropic contribution in Figs. 6.10 and 6.11 must be accounted for with the addition of an isotropic term, such that Eq. 6.4 becomes:

$$E_{\Omega,s\to s} = E_\omega^2 \left[(a_{1s}\, \partial_{xxx} + b_{1s}\, \zeta)\, \sin(3\phi) + a_2\right], \tag{6.6}$$

for s-polarized outgoing light. If the above situation were true where E^{dc} was not zero at PZC, and χ_{xxyz}^2 did contribute to the SH response, then a_2 would reduce back to:

$$a_2 = a_{1s}\, \chi_{xxyz}\, E^{dc}\, \cos(3\phi) = x a_{1s}\, \partial_{xxx}\, \sin(3\phi) \tag{6.7}$$

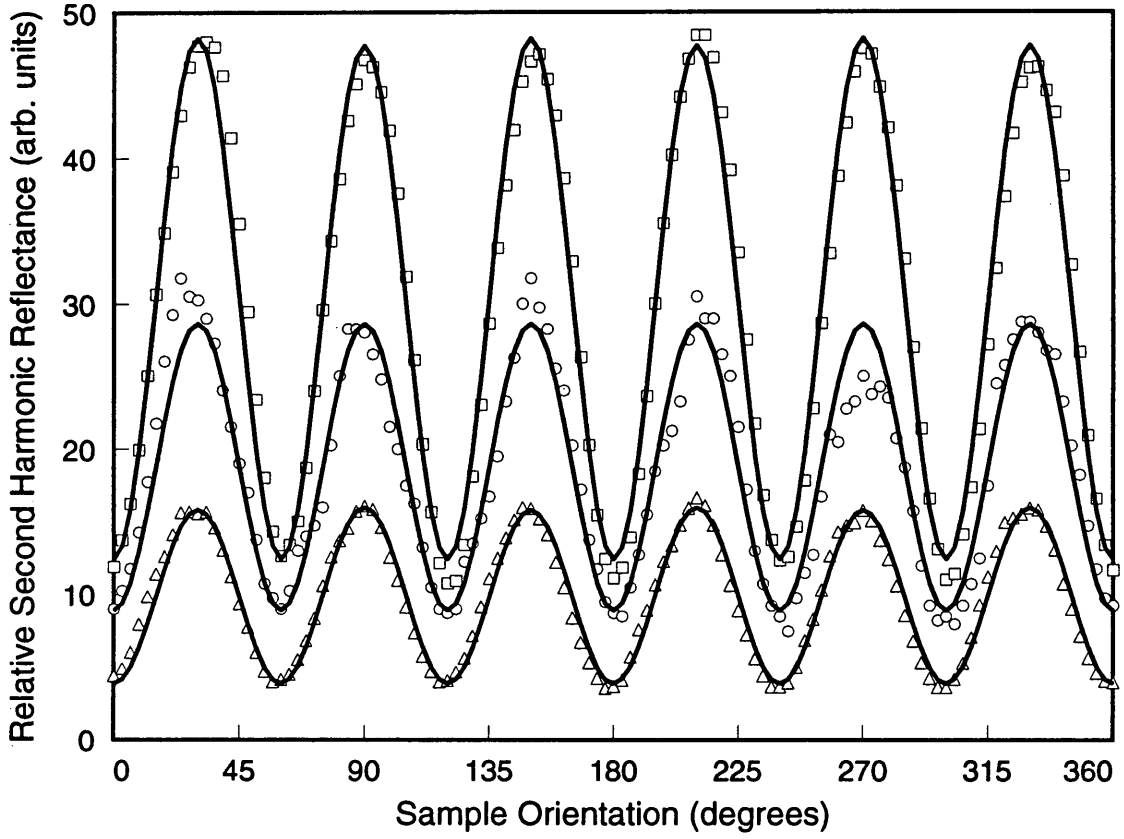

FIG. 6.10: Demonstration of the photon energy dependence of the Ag(111) SH response.
Sample rotation experiment. (symbols) - experimental data, (solid) - phenomenological fit. Uncharged surface. (triangles): Incoming light; s-polarized, 1.61 eV. Outgoing light; s-polarized, 3.22 eV. (circles): Incoming light; s-polarized 2.18 eV. Outgoing light; s-polarized, 4.35 eV. (squares): Incoming light; s-polarized 1.89 eV. Outgoing light; s-polarized, 3.76 eV. Similar behavior was observed throughout the entire spectral range of incoming light that we measured, 1.17 eV to 2.25 eV.

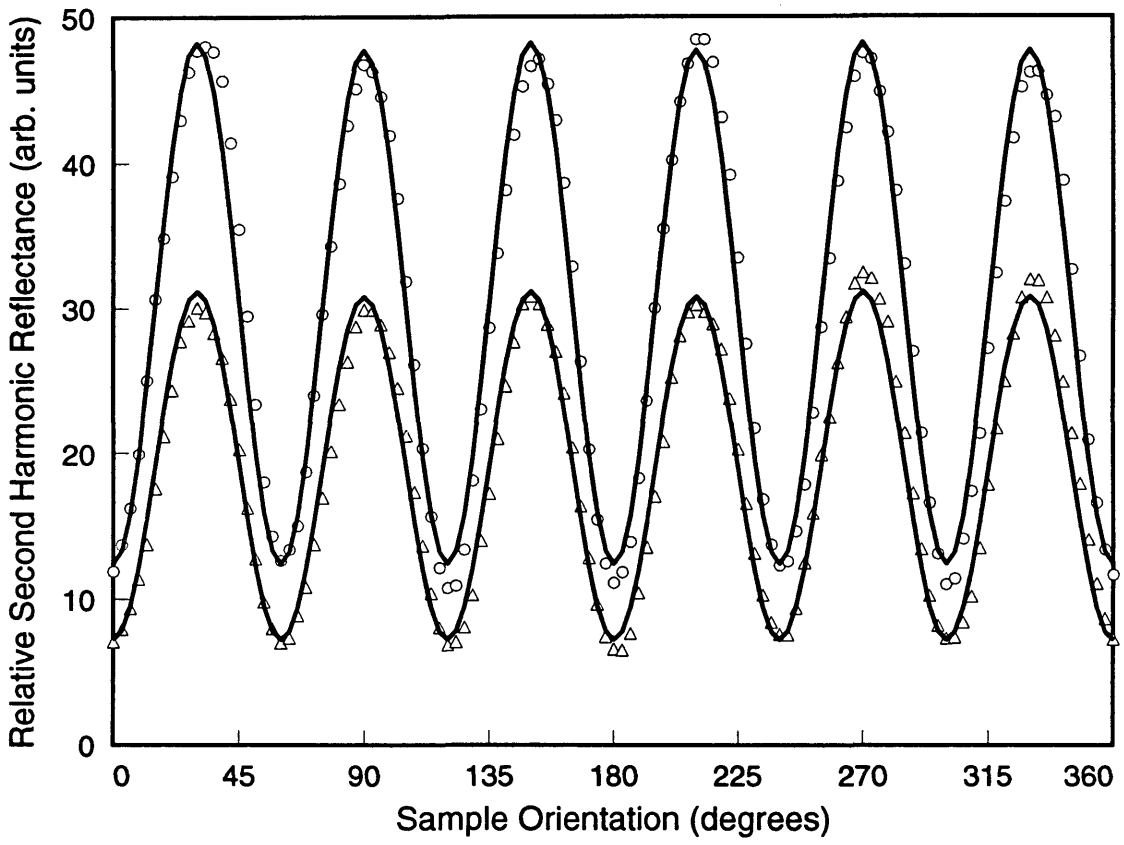

FIG. 6.11: Demonstration of the surface charge dependence of the Ag(111) SH response.
Sample rotation experiment. (symbols) - experimental data, (solid) - phenomenological fit. Incoming light: s-polarized, 1.89 eV. Outgoing light: s-polarized, 3.76 eV. (triangles): Positively charged surface (V_a = 0 V vs SCE). (circles): Uncharged surface (V_a = −0.89 V vs SCE). Similar behavior was observed throughout the entire range of the interfacial charge that we measured, from negative (where V_a = −1.20 V vs SCE) to positive (where V_a = 0 V vs SCE).

and no generality would be lost (x is a fraction between zero and 1).

We fit the sample rotation data using Eq. 6.6. The results are shown in Figs. 6.12, 6.13 and 6.14 and demonstrate that the SH response is potential dependent with a peak around 3.76 eV. This peak is not fit by the linear optical parameters. Fits by the linear optical parameters are shown in Fig. 6.12, 6.13 and 6.14 that do adequately fit the SH response on either side of the peak and does account for the potential dependence there. In Fig. 6.12 and 6.14 comparisons between the linear optical parameter fits, which include and neglect the bulk anisotropic contributions, and the data can be made. The best fits are obtained when the linear optical parameters of ζ are multiplied by the previously measured value and included with the other contributions. By changing the multiplying factor in front of a_1 (which represents changing E^{dc}) we were able to account for the potential dependence on either side of the peak.

The peaks in Fig. 6.12, 6.13 and 6.14 are not accounted for by the linear optical properties and therefore must be intrinsic to the susceptibility ∂_{xxx} (Fig. 6.12 and 6.13) and a_2 (Fig. 6.14). Furthermore, since Fig. 6.12 and 6.13 show potential dependence, ∂_{xxx} must be inherently dependent upon the applied potential. The contributions from the known linear optical parameters and the fitted potential dependence outside the peak region were removed from the data. This resulted in a peak (Fig. 6.15) which must be due entirely to an enhancement in the nonlinear susceptibility $\partial_x xx$. The enhancment in $\partial_x xx$ begins around 3.5 eV and ends around 4.0 eV with a maximum at 3.76 eV and still displays potential dependence (Fig. 6.15). The similarity between the two spectra in Fig. 6.12 and 6.13 and Fig. 6.14 indicate that similar processes are governing both ∂_{xxx} and a_2.

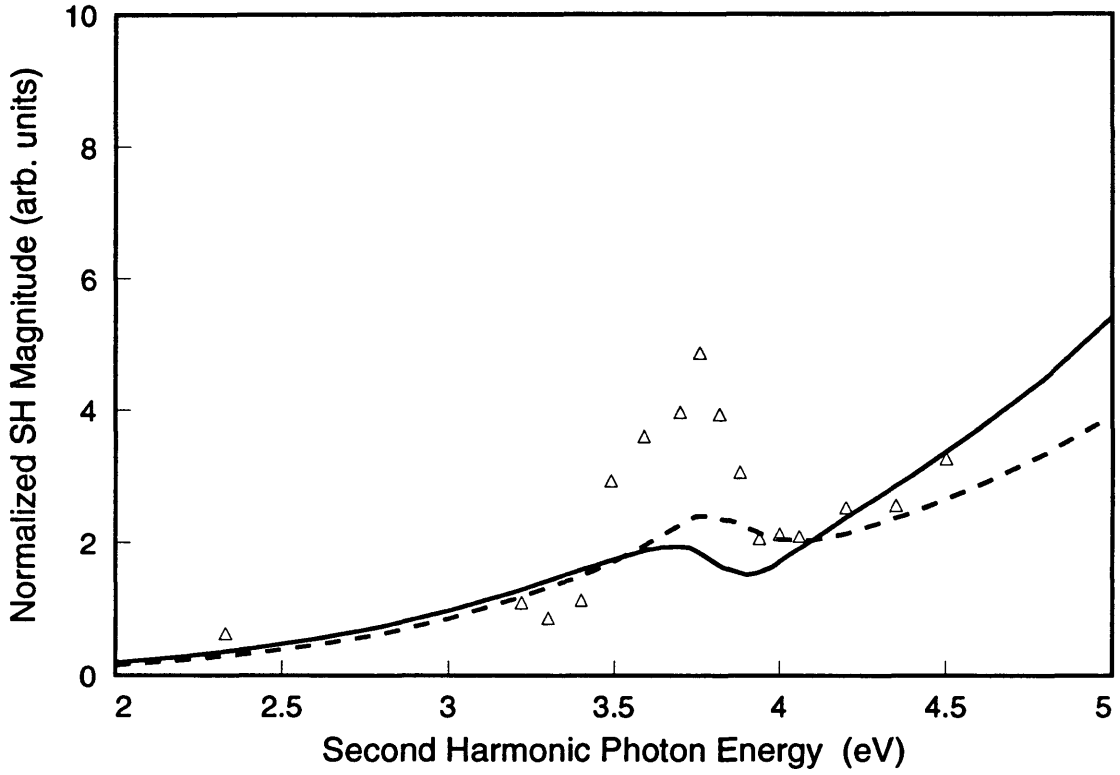

FIG. 6.12: Measured a_1 ∂_{xxx} values as a function of SH photon energy from Ag(111) at $V_a = 0$ V vs SCE.
(triangles): Positively charged surface ($V_a = 0$ V vs SCE). (line): phenomenological equation fit using 190 a_1 - 1500 b. (dashed line): phenomenological equation fit using 55 a_1.

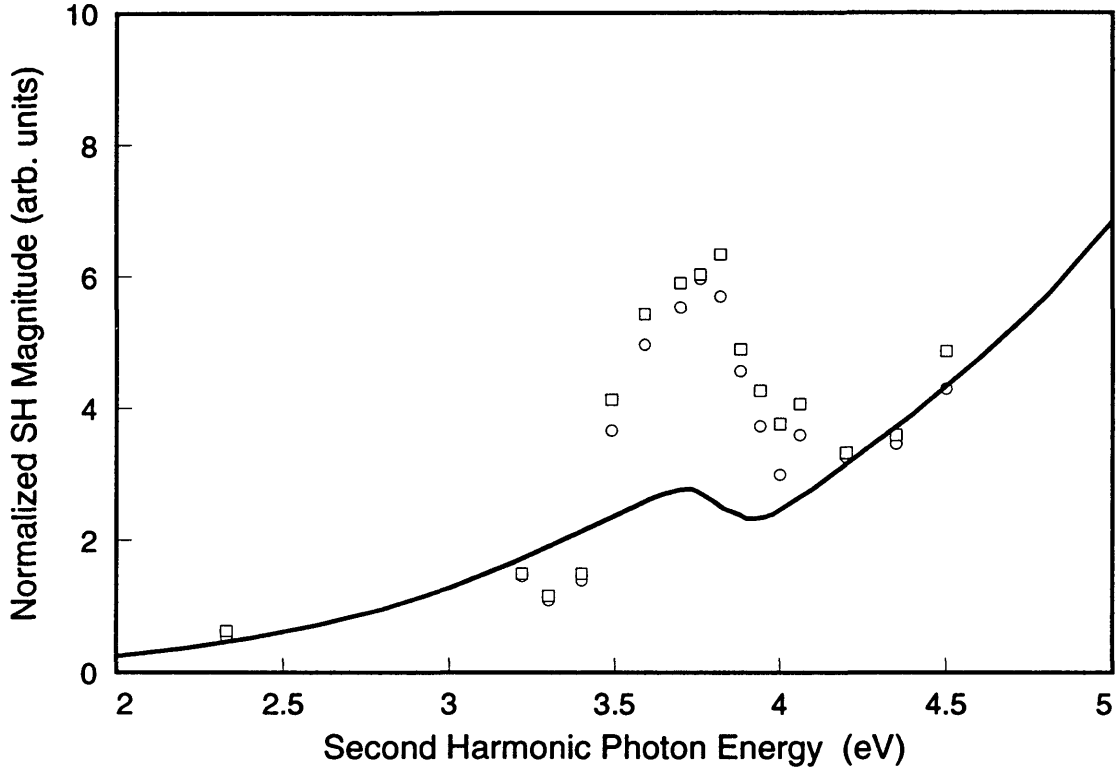

FIG. 6.13: Measured a_1 ∂_{xxx} values as a function of SH photon energy from Ag(111) at $V_a = -0.89$ V vs SCE and $V_a = -1.2$ V vs SCE.
(circles): PZC surface ($V_a = -0.89$ V vs SCE). (squares): Negatively charged surface ($V_a = -1.2$ V vs SCE). (line): phenomenological equation fit using 230 a_1 - 1500 b.

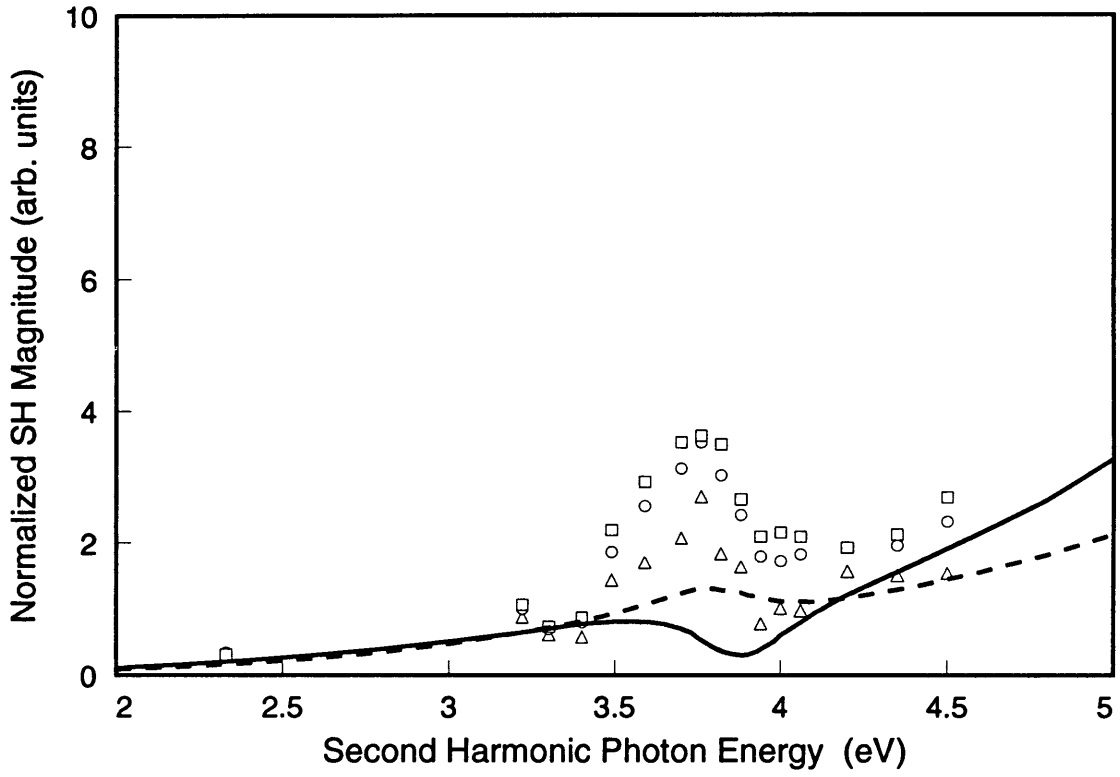

FIG. 6.14: Measured a_2 values as a function of SH photon energy from Ag(111). (circles): PZC surface (V_a = −0.89 V vs SCE). (triangles): Positively charged surface (V_a = 0 V vs SCE). (squares): Negatively charged surface (V_a = −1.2 V vs SCE). (line): phenomenological equation fit using 160 a_1 - 1500 b. (dashed line): phenomenological equation fit using 35 a_1.

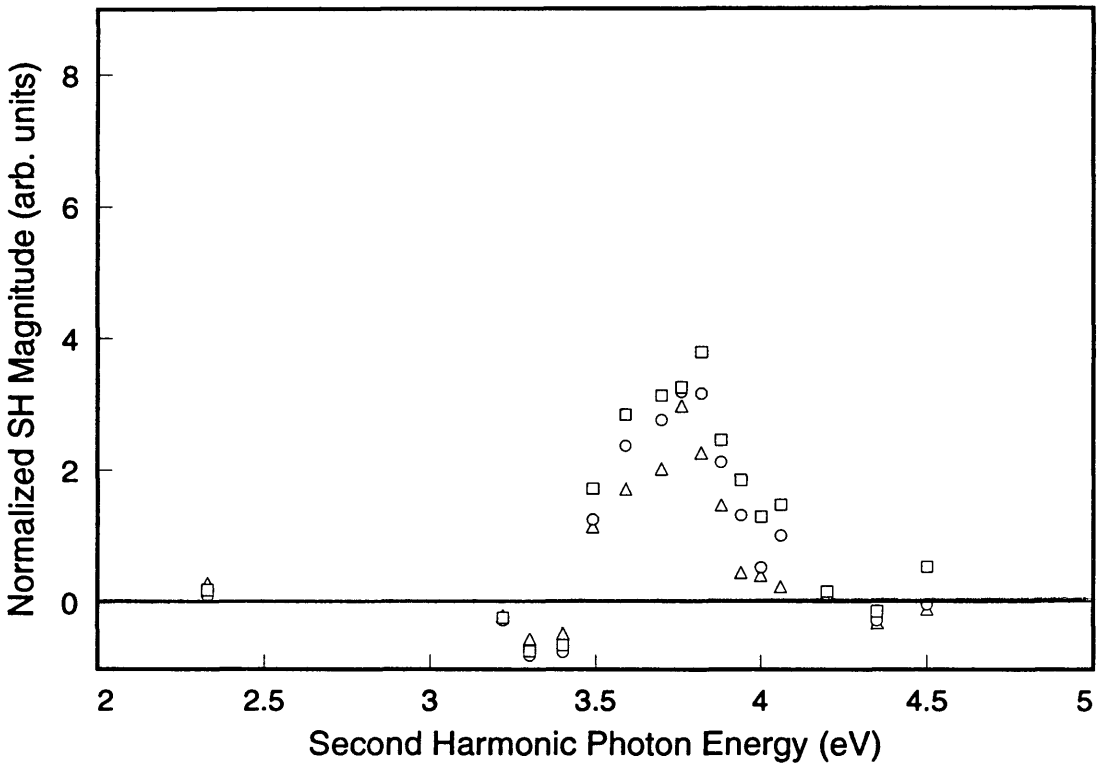

FIG. 6.15: Measured ∂_{xxx} values as a function of SH photon energy and applied potential from Ag(111)
(triangles): Positively charged surface ($V_a = -0$ V vs SCE). (circles): PZC surface ($V_a = -0.89$ V vs SCE). (squares): Negatively charged surface ($V_a = -1.2$ V vs SCE). The contribution from the known linear optical parameters and the applied potential contributions outside the peak region were systematically removed. This data indicates that ∂_{xxx} has an enhancement which produces a peak in the SH response with a maximum around 3.76 eV.

6.3 Surface Defect-Induced SHG

Recently, a surge in literature publications has sparked interest in the SHG from vicinal surfaces [85, 80, 82, 83, 81, 84]. The vicinal surfaces are cut at small angles from the standard crystal surface planes. This induces a stepped surface and ultimately modifies the defect density on the surface. By increasing the vicinal angle, the surface defect density increases. In our Ag(111) experiment described above, we found an unexpected isotropic SH contribution that may be due to surface defects. This necessitated further investigation of surface defect-induced SHG.

Most of the literature attributes the additional SH response from vicinal surfaces to a decrease in the symmetry at the surface [80]. The interpretation from most of the experimental data in the literature is complicated by the presence of the normally allowed SH contributions. To get a better understanding of the processes involved in the step induced or defect induced SHG, we chose to do an experiment with no intrinsic SH response. A SH response is not allowed from the (011) and (001) faces at normal incidence. Therefore, a SH response at normal incidence from the C_{4v} or C_{2v} symmetry second order surface susceptibilities and the multipole bulk susceptibilities is not expected from a vicinal surface.

Under the conditions of excitation and measurement appropriate to our experiment (Ag(001), s-polarized incoming light at normal incidence with a photon energy of $\hbar\omega$) the associated SH fields for C_1 symmetry is then

$$E_{\Omega,s\to s} = E^2_{\omega,s}\,[d_{2s}\,\cos(\phi) + d_{3s}\,\cos(3\phi) + d_{4s}\,\sin(\phi) + d_{5s}\,\sin(3\phi)], \tag{6.8}$$

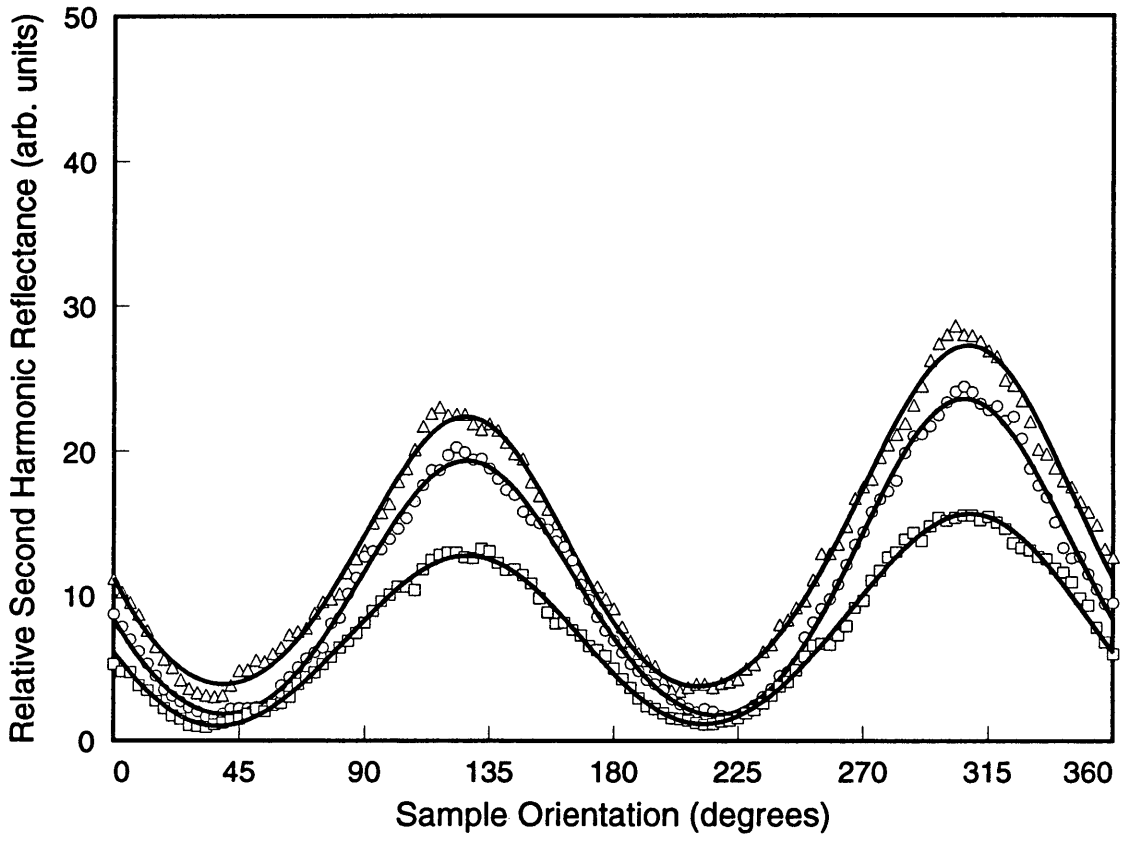

FIG. 6.16: Demonstration of the potential dependence of the defect induced normal incidence SHG from a 7° vicinal Ag(001) at 1.85 eV.
Sample rotation Experiment. Incident light: s-polarized, 1.85 eV, normal incidence. Outgoing light: s-polarized, 3.7 eV. (circles): PZC surface ($V_a = -0.89$ V vs SCE). (triangles): Positively charged surface ($V_a = 0$ V vs SCE). (squares): Negatively charged surface ($V_a = -1.2$ V vs SCE). (line): fits using the phenomenological equations.

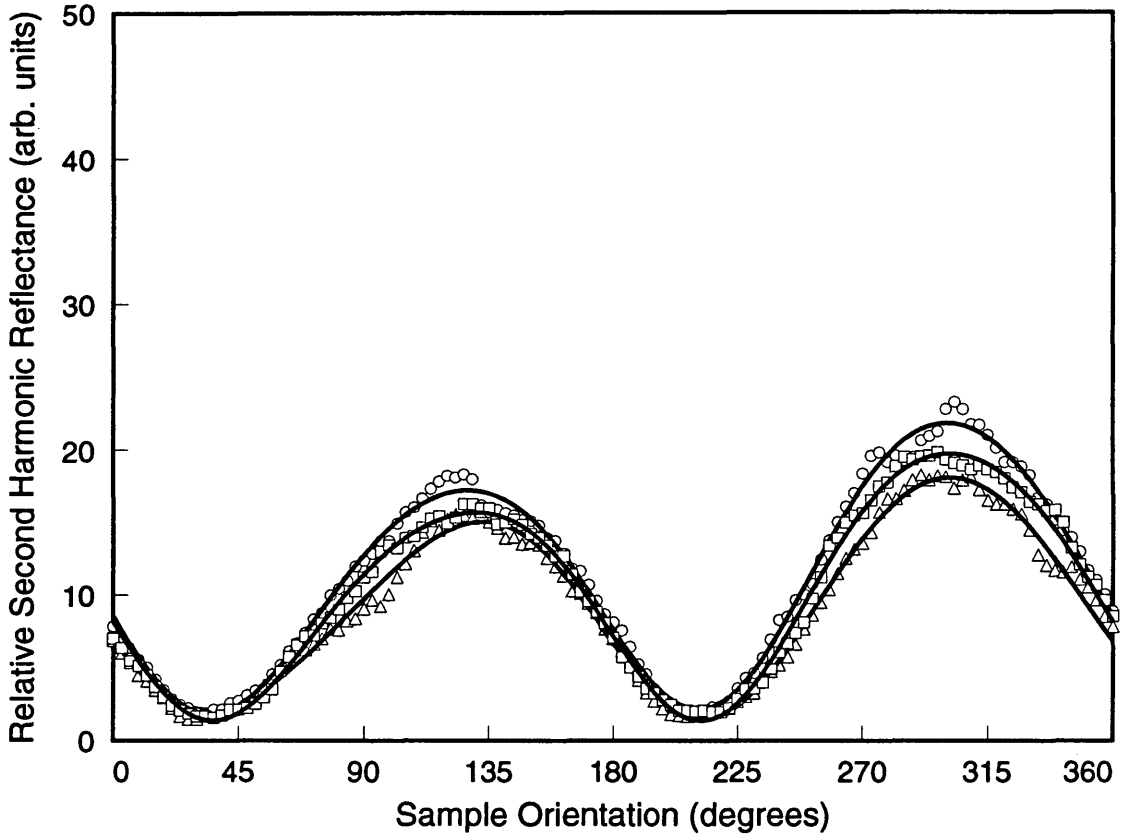

FIG. 6.17: Demonstration of the potential dependence of the defect induced normal incidence SHG from a 7° vicinal Ag(001) at 1.8 eV.
Sample rotation Experiment. Incident light: s-polarized, 1.8 eV, normal incidence. Outgoing light: s-polarized, 3.59 eV. (circles): PZC surface ($V_a = -0.89$ V vs SCE). (triangles): Positively charged surface ($V_a = 0$ V vs SCE). (squares): Negatively charged surface ($V_a = -1.2$ V vs SCE). (line): fits using the phenomenological equations.

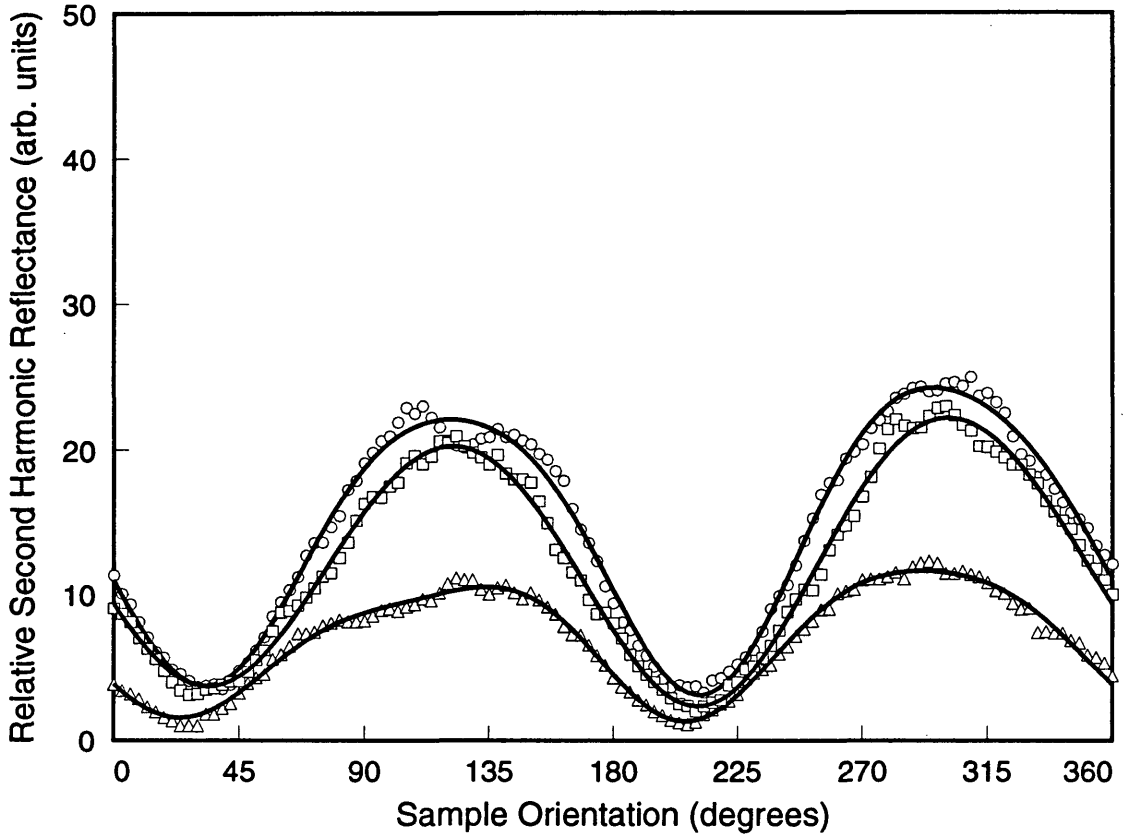

FIG. 6.18: Demonstration of the potential dependence of the defect induced normal incidence SHG from a 7° vicinal Ag(001) at 1.75 eV.
Sample rotation Experiment. Incident light: s-polarized, 1.75 eV, normal incidence. Outgoing light: s-polarized, 3.49 eV. (circles): PZC surface ($V_a = -0.89$ V vs SCE). (triangles): Positively charged surface ($V_a = 0$ V vs SCE). (squares): Negatively charged surface ($V_a = -1.2$ V vs SCE). (line): fits using the phenomenological equations.

for s-polarized outgoing light, and

$$E_{\Omega,s\to p} = E^2_{\omega,s}\, d_{2p}\, \cos(\phi) + d_{3p}\, \cos(3\phi) + d_{4p}\, \sin(\phi) + d_{5p}\, \sin(3\phi)], \qquad (6.9)$$

for p-polarized outgoing light. Here $\hat{z}$ is parallel to the vicinal [001] with $\hat{x}$ along [210] . The crystal orientation about the vicinal (001) surface is specified by ϕ, the angle between [210] and the incident polarization vector $\hat{e}_1$. The "d" parameters in Eqs. 6.8 and 6.9 depend upon the linear optical properties of the sample at ω and Ω, the angle of incidence and second order nonlinear susceptibilities. It should be noted that C_1 symmetry is so general, that just about any sinusoidal curve may be fit with this symmetry, and therefore little information may be gained from the fit. However, if we look at the data in Figs. 6.16, 6.17, and 6.16, we find an anomalous difference in the two peak heights. This cannot be accounted for with Eqs. 6.8 and 6.9. Therefore, we were forced to include an anomalous isotropic contribution to Eqs. 6.8 and 6.9, such that:

$$E_{\Omega,s\to s} = E^2_{\omega}\, [d_{1s} + d_{2s}\, \cos(\phi) + d_{3s}\, \cos(3\phi) + d_{4s}\, \sin(\phi) + d_{5s}\, \sin(3\phi)], \qquad (6.10)$$

for s-polarized outgoing light, and

$$E_{\Omega,s\to p} = E^2_{\omega}\, [d_{1p} + d_{2p}\, \cos(\phi) + d_{3p}\, \cos(3\phi) + d_{4p}\, \sin(\phi) + d_{5p}\, \sin(3\phi)], \qquad (6.11)$$

for p-polarized outgoing light. For each set of conditions we recorded the second harmonic reflectance as a function of the sample orientation about its surface normal (sample rotation experiment, $S_\Omega(\phi)$). This allowed us to make qualitative statements

about the relative influences of the various terms found in Eqs. 6.10 and 6.11.

The SH response from a vicinally cut Ag(001) surface (miscut 7^o along the [210] direction) is shown in Figs. 6.16, 6.17, and 6.16. The SH response is relatively large and on the order of the normal SH response from Ag(001) (Fig. 6.6) or Ag(111) (Fig. 6.11). This SH response demonstrates a relatively large potential dependence and an incident photon energy dependence. This is demonstrated by comparing the SH response from the positively charged surface. At 1.75 eV this SH response is the smallest of the three potentials and at 1.85 eV this SH response is the largest. The SH data in Fig. 6.16, 6.17, and 6.16 were fit using C_1 symmetry with an additional isotropic term. C_1 is the most general symmetry and was expected given our alignment choice along the [210] direction. These trends shown in Figs. 6.16, 6.17, and 6.16 were present at a vicinal angle of 3.5^o, and the normal incident SH response was undetectable for the Ag(001) surface as expected.

Chapter 7

DISCUSSION

7.1 Ag(001)

The study of silver has concentrated on the (111) and (011) faces since these have the largest number of susceptibilities and thus the greatest potential for a SH response [10, 12, 13, 30, 43]. Due to the number and the interrelationship between the susceptibilities, the problem of determining each susceptibility's specific contributions to the SH response for an arbitrary experimental arrangement is in general intractable. Sipe [8] has discussed this point in detail. This has led to unsubstantiated assumptions about susceptibilities, such as the anisotropic and isotropic bulk susceptibilities, that have permeated the literature [12, 30, 43, 23]. For specific geometries and crystal orientations, the SH contributions by these susceptibilities may be determined directly by experimentation. For s-polarized incident photons, the bulk anisotropic susceptibility is determined by the s-polarized SH field from the Ag(001) surface [8]. The generated SH fields in terms of the incident electric fields transformed into beam coordinates are:

$$E_{\Omega,s-in,s-out}(\phi,2\omega,V) = A_s E_s^2[\zeta 2 g_b F_c f_s \sin(4\phi)] \tag{7.1}$$

$$E_{\Omega,s,p}(\phi,2\omega,V) = A_p E_p^2[(\epsilon(2\omega)/\epsilon_o(\omega))F_s(\partial_{zxx} + \chi_{zxxz}E^{dc}) + F_s\gamma + 2g_b F_c f_s \zeta \sin^2(2\phi)]. \tag{7.2}$$

where ϕ is the angle between the [100] crystal direction and the projection of the incident wave vector on the surface plane [56]; ϵ and ϵ_o are the dielectric functions

for the material and outside environment respectively; and F, f, A, and g are linear optical coefficients as described by Sipe [8] (Table 3.5). The only difference between this notation and Sipe's is that we include the $i\Omega$ in the A term. These experimental arrangements allow the SH response from the bulk anisotropic (ζ), the bulk isotropic (γ), the second order surface (∂_{zxx}), and the third order surface (χ_{zxxz}) susceptibilities to be determined.

The data in Figs. 6.1 and 6.2 show that, under a wide range of conditions, the SH response governed by ζ is relatively small but not zero. As stated above, this is mainly due to the specific linear optical parameters involved. Fig. 6.3 indicates that the SH response governed by ζ is independent of applied potential and the spectral characteristics are governed by the linear optical parameters. The lack of potential dependence was expected since ζ is a bulk derived susceptibility that should not be effected by surface modulation. However, the lack of spectral dependence is somewhat surprising after consideration of the electronic properties of Ag. The onset of direct interband transitions occurs at 3.85 eV. This energy is within the range of the second harmonic energies which were explored in our experiment. We had expected that ζ might have been resonantly enhanced for $\hbar\Omega > 3.85$ eV. This is apparently not the case. One final point about neglecting susceptibilities is demonstrated in Fig. 6.5. Here ζ must be non-zero from Eq. 6.3, since ζ is required in order to observed the 90° periodicity. This latter point emphasizes the potential for cross terms providing a significant SH response.

The other bulk-related susceptibility is γ. What we need to know is how γ changes as the excitation energy increases. Early models of the nonlinear optical

properties of a free electron gas provide an analytical expression for γ [26].

$$\gamma = \frac{|e|(1-\epsilon_\Omega)}{32\pi m\omega^2} \tag{7.3}$$

where m and $-|e|$ are the electron mass and charge, and ϵ_Ω is the linear dielectric function of the metal at the harmonic energy. Provided $\hbar\Omega < 3.87$ eV the spectral variation of γ should be small. Beyond that point, at higher harmonic energies, a better model that includes the effects of bulk interband transitions is needed. It should be noted that when Eq. 7.3 is used for γ, the SH response from this term is several orders of magnitude smaller than other contributions which are experimentally observed. This would indicate that a γ term described by the free electron model would be below the detection abilities of most experimental arrangements used today.

The surface susceptibility, ∂_{zxx}, has traditionally been ignored because it was thought unlikely that two optical fields parallel to the surface could couple to a second harmonic field perpendicular to the surface. The mechanism would have to involve the gradient in electron density in the $\hat{z}$-direction. There is no clear guidance in the literature about how to handle this term. However, some theoretical progress is being made by Schaich and Mendoza [74] using a dipolium model, and hopefully the experimental work presented in this thesis will assist in these endeavors.

It is an interesting fact, pointed out by Sipe [8], that for all three of the standard crystal faces, γ and ∂_{zxx} appear jointly, with the form:

$$A[(\epsilon(2\omega)/\epsilon_o(\omega))(\partial_{zxx} + \chi_{zxxz}E^{dc}) + \gamma]. \tag{7.4}$$

We have also explicitly included the third order surface contribution χ_{zxxz} in order to emphasis the inherent potential dependence. Unlike γ, both χ_{zxxz} or ∂_{zxx} should be

different for the different crystal faces. However, the phenomenological form of Eq. 7.4 remains the same and ultimately the processes involving the field geometries are similar (ie. two fields parallel to the surface combine to give one field perpendicular to the surface). Later in this thesis we will investigate several possible interpretations for the possible individual contributions of the three nonlinear susceptibilities described in Eq. 7.4. However, certain general observations may be made governing the form presented in Eq. 7.4, which we will discuss now. With the appropriate care, these general observations will be applicable to other configurations involving Ag(001) and hopefully other faces including Ag(111) and Ag(011).

Figs. 6.6, 6.7 and 6.8 all indicate that the SH response governed by the parameters in Eq. 7.4 have potential and spectral dependence. However, the spectral dependence is completely accounted for by the linear optical parameters in "A" of Eq. 7.4. The potential dependence is accounted for by varying the multiplying factor representing the susceptibilities by 25%. This result is very important and unexpected. It means that the rest of the terms in Eq. 7.4 [ie.$(\epsilon(2\omega)/\epsilon_o(\omega))(\partial_{zxx} + \chi_{zxxz}E^{dc}) + \gamma$] have no spectral dependence. This is very surprising given the the explicit appearance of the dielectric function for Ag ($\epsilon(2\omega)$) in both Eq. 7.4 associated with ∂_{zxx} and in the free electron model for γ (Eq. 7.3).

There are two distinct explanations for the above observations. The potential dependence of the data would at first indicate that the SH contribution is from the surface and thus governed by the second order and third order surface susceptibilities ∂_{zxx} and χ_{zxxz}, respectively. However, this requires that ∂_{zxx} and χ_{zxxz} contain the inverse of the Ag dielectric constant ($1/\epsilon(2\omega)$). We have no ability at this time to know whether this is possible or not. Thus the first interpretation requires ∂_{zxx} and χ_{zxxz} to have the exact inverse spectral dependence of the Ag dielectric function, γ

to be a constant or negligible, with the potential dependence governed by the explicit contribution of E^{dc} given in Eq. 7.4.

The other interpretation requires ∂_{zxx} and χ_{zxxz} to be negligible so that any of their possible spectral dependence is not present in the SH response, and requires γ to be independent of incident photon energy but influenced by the surface modulation of the applied electric field. This latter condition is possible, as elaborated on by Rudnick and Stern [23]. The possibility is due to the Friedel oscillations of the electron density profile extending into the bulk of the material and being modulated by an applied electric field at the surface. However, if this were the case, and γ were sensitive to these Friedel oscillations, we would have to wonder why ζ was not. The next problem with this interpretation results from the requirement that γ be independent of the incident photon energy, in direct contradiction to the free electron model.

Of course, a combination of these two interpretations is also possible, with varying degrees of contributions from each. The final conclusion drawn from the experimental results of Ag(001) with s-polarized incident light is that the entire spectral behavior is governed completely by the linear optical parameters. One final test of this statement is shown in Fig. 6.9, in which the ratio of the isotropic to anisotropic data is plotted as a function of SH photon energy. By taking this ratio, three nonlinear optical coefficients contribute to the SH response in the ratio $[[(\epsilon(2\omega)/\epsilon_o(\omega))\partial_{zxx}+\gamma]/\zeta]$. The results once again confirm the lack of spectral dependence of this susceptibility ratio and, since ζ is known to be a constant, the numerator must also be independent of incident photon energy. Furthermore, this ratio of nonlinear susceptibilities has the value of 0.13 for the PZC surface and 0.1 for the 0 V vs SCE surface condition.

The Rudnick and Stern [23] parameters a_{rs} and b_{rs} contain the two susceptibilities ∂_{zzz} and ∂_{xzx}, respectively. Both these susceptibilities have received extensive

theoretical attention, and are thus the best candidates for the experiments performed in this thesis. Unfortunately, it is experimentally impossible to isolate ∂_{zzz} and ∂_{xzx} from other potential susceptibility contributions. However, with the results described in this thesis, it is now possible to try and explicitly determine the spectral and potential dependence of each of these susceptibilities. This will be an arduous task, which is outside the realm of this thesis. However, given the results from this thesis, the most prudent approach would be to first investigate the SH response from the Ag(001) crystal using p-polarized incident light. The experiment will have to be performed as a function of incident photon energy, applied potential, and also incident angle. Given the results from this thesis concerning the SH response from Ag(001), and the work performed by Richmond and coworkers on Ag(111) [73], it is probably a reasonable guess that ∂_{zzz}, ∂_{xzx} and ∂_{xxz} will, to first order, prove to be independent of incident photon energy.

It should be noted that the lack of incident photon energy dependence for the nonlinear susceptibilities observed in these experiments, does not indicate that the nonlinear surface susceptibilities are insensitive to the surface electronic structure. The primary point, is that the spectral dependence of the SH response is overwhelmingly governed by the linear optical parameters. A nonlinear differential reflectance experiment, similar to the one we performed for our previous publication [13], may be used to obtain the nonlinear surface susceptibilities spectral dependencies.

7.2 Ag(111)

Initially, the primary goal for investigating the normal incident SH response from Ag(111) was to test the third order dc field contribution predicted by the phenomenological theory presented in this thesis (Table 3.4). For the s-polarized incident light

experiments performed in this thesis, our calculations predicted a dc field dependent cosine contribution in conjunction with the expected sine function contribution. The primary evidence for this cosine contribution would have been an anomalous effect on the charged surfaces. The anomalous effect would have to vanish at the PZC. This was not observed. Therefore, we conclude that the contribution to the SH response governed by the third order susceptibility χ_{xxyz} is too small to be detected under these experimental conditions. This type of contribution may have been an alternative explanation for the ion induced surface reconstruction interpretation we found for the Ag(111) surface in $NaSO_2$ [12]. Furthermore, under different experimental conditions, this third order term may still contribute to the SH response and should be considered in future experiments where appropriate. It should be noted that an anomalous isotropic contribution to the SH response from the Ag(111) surface is not sufficient to adequately explain the data presented in the ion-induced reconstruction paper by Furtak [12] as was implied by statements made in Bradley's thesis [72]. This would have been the end of the story from these Ag(111) experiments, except for the presence of an anomalous isotropic SH response (Figs. 6.11 and 6.10). An anomalous effect of this type would be overlooked with non-normal incidence experiments involving p-polarized SH light [12, 13, 10] or experiments involving s-polarized SH light that do not measure rotational anisotropy [71, 72].

The extremely good fit of the data in Figs. 6.11 and 6.10 to a sine function indicate that, short of a fortuitous reduction of a susceptibility associated with a $\cos(3\phi)$, an anomalous isotropic contribution is required. Under these experimental conditions, even a reduction of symmetry to the most general C_1 symmetry will not account for this anomalous isotropic contribution. The final conclusion, is that this anomalous effect cannot be accounted for by the general phenomenological theory

developed in this thesis and by Sipe [8]. We will investigate the ramifications of this statement in the next section of this chapter.

The careful investigation of the anomalous isotropic SH response from Ag(111) also resulted in a quantitative characterization of the anisotropic SH response governed by the nonlinear second order surface susceptibility ∂_{xxx}. Figs. 6.12 and 6.13 show that the normal incidence SH response is dependent upon both the applied potential and the incident photon energy and has a resonant peak at 3.76 eV. The spectral dependence of the SH response for the SH energies above (greater than 4.0 eV) and below (less than 3.5 eV) the resonant peak is completely accounted for by the linear optical properties. The best fits include the contributions from the bulk anisotropic susceptibility and uses the experimentally derived results for ζ from the Ag(001) experiments. The potential dependence on either side of the peak is accounted for by changing the multiplying factor in front of the linear optical properties associated with ∂_{xxx}. This represents the effects from a dc field dependence of ∂_{xxx}.

The peak in the SH response shown in Fig. 6.15 can only be explained by a resonance in ∂_{xxx}. The resonance has a maximum at 3.76 eV and begins and ends at 3.5 eV and 4.0 eV respectively. This energy region covers several intrinsic material properties of Ag, including: the bulk interband transition energy (3.84 eV) [88], the surface plasmon energy (3.4-3.6 eV) [86], the bulk plasmon energy (3.8 eV) [86], the image potential surface state transition (3.9 eV) [90], the transition from the surface state A to the top of the bulk band (3.84 eV) and possibly the transition energy between two surface states (3.9 eV).

The surface plasmon energy is usually associated with a roughened surface and is not applicable to the smooth surface experiment discussed here [86]. The bulk plasmon is associated only with incident light polarizations perpendicular to the sur-

face, and is therefore not applicable for these experiments. The applied potential to the electrode directly represents the electrochemical potential of the electrons in the electrode [87]. Changing the applied potential of the electrode by 1 V causes a corresponding change of the Fermi level of 1 eV. A change to positively charged surfaces increases the Fermi level with respect to the vacuum level, and a negatively charged surface decreases the Fermi level with respect to the vacuum level [86, 87]. In general, the Fermi level for Ag (E_F) is 4.46 eV below the vacuum level. Thus a positively charged surface with an applied potential of 0.89 V from the PZC will have a Fermi level 4.549 eV below the vacuum level and a negatively charged surface with an applied potential of 0.31 V from the PZC will have a Fermi level 4.429 eV below the vacuum level. These two values represent the applied potentials used in these experiments.

In general, the electron band structure of the bulk is projected onto the surface in roughly the same proportions. Thus the relative energies from the Fermi level for the upper and lower bulk band edge remains 3.84 eV and -0.4 eV, respectively. Similarly, the bulk band edges feel the full effect of the applied potentials and move in direct relation to the Fermi energy when a surface charge is applied. Thus a bulk interband transition would not shift in energy with applied potential. Surface states are an intrinsic part of the two dimensional band structure of the surface (Fig. 7.1). Their electronic wavefunctions are localized at the surface and decay rapidly in both directions normal to the surface. This strong surface localization means that only a fraction of the surface state extends into the electrochemical double layer and is affected by the applied potential. The end result is that the surface states shift less with applied potential than the projected bulk states. For the positively charged surfaces observed in this thesis we would expect to see a transition from an occupied

surface state to an unoccupied bulk band edge shift to lower energies by as much as 0.089 eV (Fig. 7.2) and for negatively charged surfaces (Fig. 7.3), we would expect to see this surface state transition shift to higher energies by as much as 0.031 eV. This would be a total shift of over 0.1 eV in the SH spectrum, which is well within the spectral resolution of our experiment. There is also an expectation that the surface states should shift by different amounts depending on the type.

There are two surface states associated with the bulk band gap from a Ag(111) surface. An image potential (IP) surface state (SS), exist between 3.84 eV and 3.9 eV above the Fermi level at PZC. A crystal derived surface state (usually referred to as A) is located from -0.1 eV to 0.4 eV about the Fermi level at PZC. A transition using surface state A would thus become depopulated as the surface charge became more positive (Fig. 7.2), and would become more populated as the surface charge became more negative (Fig. 7.3). This would result in a smaller SH response for positive surface charges and a larger SH response for negative surface charges. The data shown in Fig. 6.15 are in tentative agreement with the above observations as far as relative SH intensity. However, no spectral shift of the peak centered at 3.76 eV with applied potential is observed. Furthermore, a transition should not be seen from surface state A at all when it moves above the Fermi level (for applied potentials anywhere from -1.3 V to -0.79 V SCE depending on the exact position of the A surface state). Thus if the SH response from Ag(111) where due to a transition starting from surface state A, the peak should vanish for our positively charged surface experiments. This is not observed in any of the data.

Our experimental data are also in qualitative agreement with the results found by Bradley [72]. Bradley found a peak in the s-polarized SH response from Ag(111) with a maximum at 3.82 eV. Bradley's data is fit better at the peak by the linear

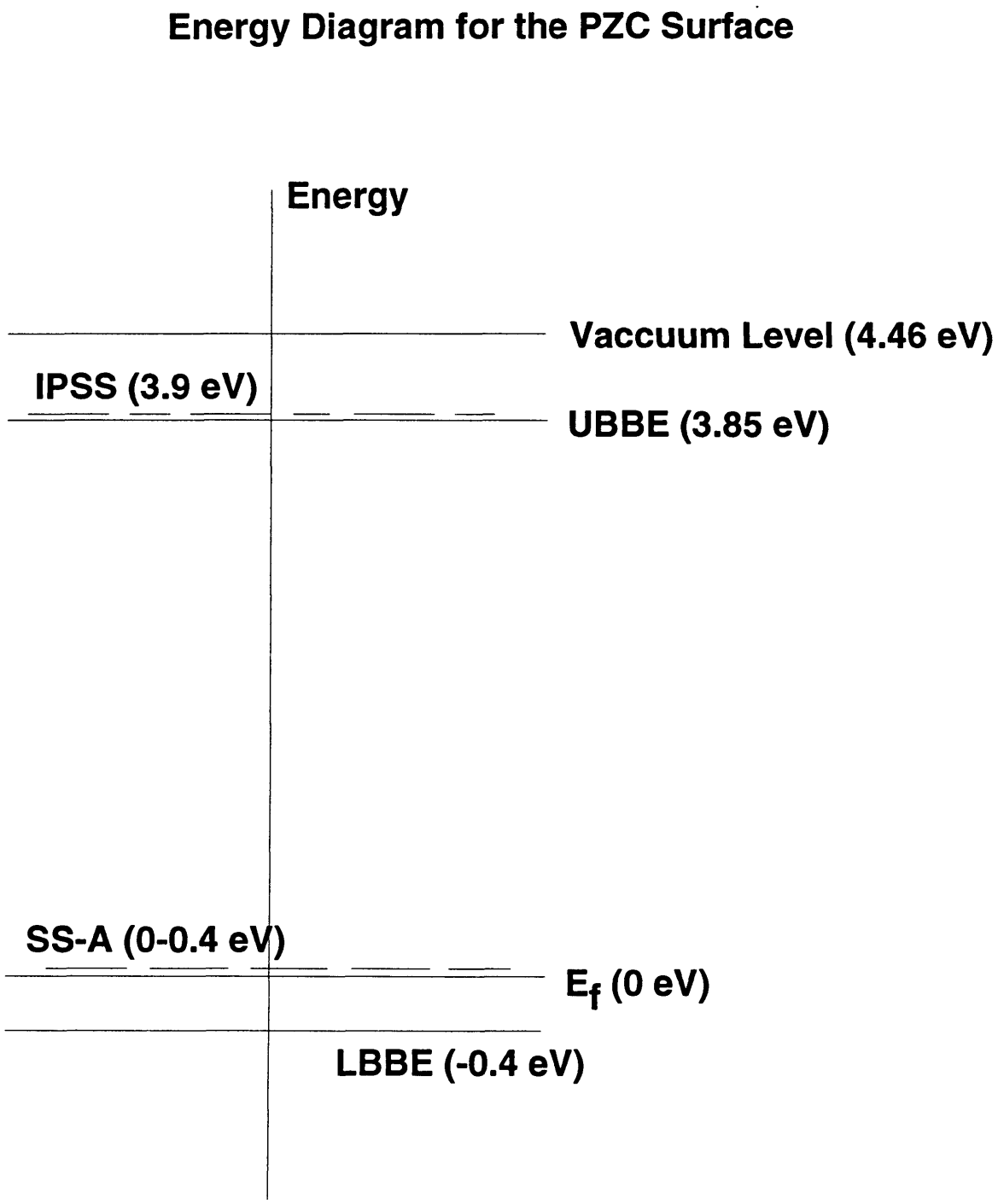

FIG. 7.1: The zone center electronic band structure at the surface of Ag(111) held at the PZC.
The energy levels are all referenced to the Fermi level (E_f). IPSS and SS-A are the image potential and the "A" surface states, respectively. UBBE and LBBE are the upper and lower bulk band edges projected onto the surface, respectively.

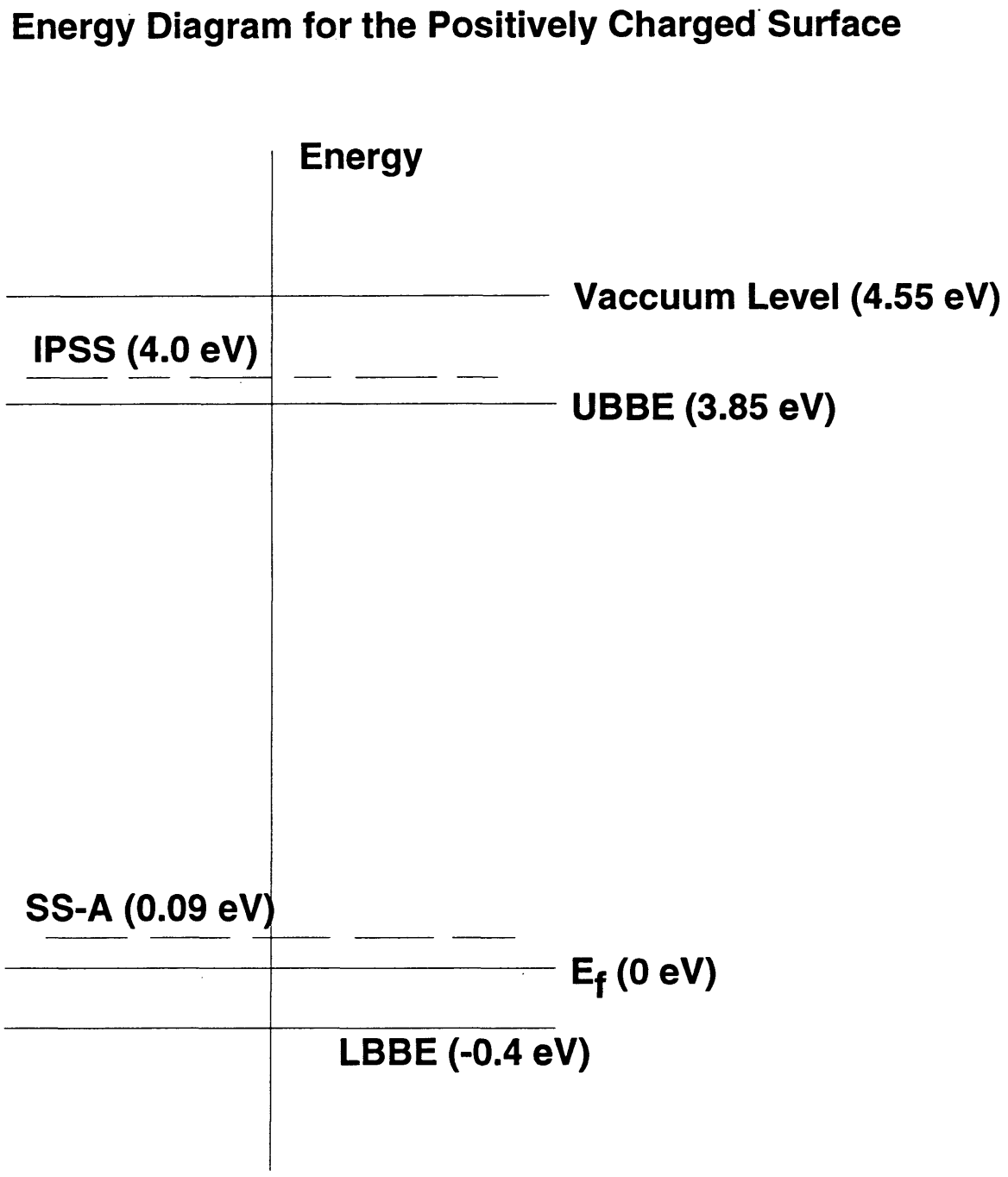

FIG. 7.2: The zone center electronic band structure at the surface of Ag(111) held at 0 V vs SCE.
The energy levels are all referenced to the Fermi level (E_f). IPSS and SS-A are the image potential and the "A" surface states, respectively. UBBE and LBBE are the upper and lower bulk band edges projected onto the surface, respectively.

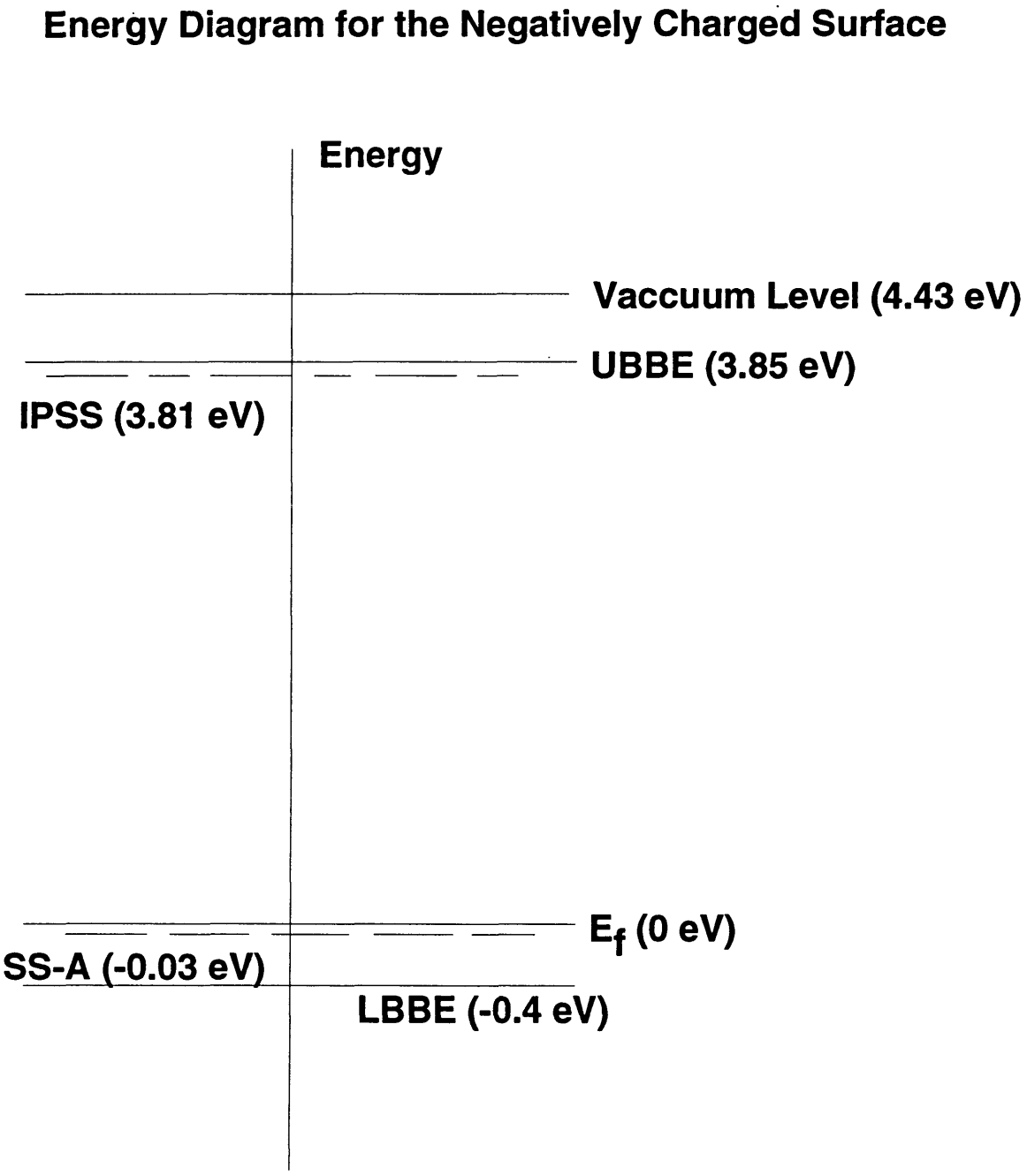

FIG. 7.3: The zone center electronic band structure at the surface of Ag(111) held at -1.2 V vs SCE.
The energy levels are all referenced to the Fermi level (E_f). IPSS and SS-A are the image potential and the "A" surface states, respectively. UBBE and LBBE are the upper and lower bulk band edges projected onto the surface, respectively.

optical properties then the data in Fig. 6.15. This is due to the proportionately larger contribution from more linear optical parameters and nonlinear susceptibilities in Bradley's non-normal incidence experiment. Bradley and coworkers, assigned the peak to the transition between the two surfaces states, even though they admit the peak does not shift with applied potential and acknowledge that the transition is symmetry forbidden at the zone center. The lack of a measurable shift in the peak with applied potential implies that either the peak is not due to transitions involving a surface state, or that the transition is between two surface states that do not move with applied potential relative to one another.

Given the overwhelming evidence for the observed spectral shifts with applied potential between bulk band edges and surface states, it is unlikely that the resonant peak is due to a transition between the A surface state and the top of the bulk band edge. The image potential surface state is inaccessible to probing for positively charged surfaces and the A surface state is unpopulated. This and the fact that a transition between surface state A and the IPSS is symmetry forbidden at the zone center leads us to the conclusion that the resonant peak is not due to any transitions involving surface states.

Basically, this leaves only a transition between the bulk bands. However, this transition is normally associated with 3.85 eV and usually has experimental results that are more localized around this energy, then the data presented in Fig. 6.15. Also the large potential dependence associated with this peak would not be explained by a transition between the lower and upper bulk band edges, since they move in approximately the same manner with applied potential. The only conclusion that may be drawn from this lengthy discussion which has considered and rejected all the known effects that could have produced a SHG peak, is that we have a completely

unknown effect that has not been reported before and is not expected with the present theoretical models available. However, ∂_{xxx} has never been theoretically calculated. It may be that the single electron excitations, such as surface states, do not adequately account for the observed SH response since their contribution would be largest where the incident photon energy or SH photon energy is equal to the separation of the states. However, using an electron gas approach where structure is added to the free electron system, a collective electron response may have a resonance at 3.76 eV and adequately account for the observed SH response.

To summarize, we have discovered a previously unpredicted peak in the second order surface susceptibility ∂_{xxx}. This peak was found by monitoring the normal incidence SH response from an Ag(111) crystal. The linear optical parameters and known bulk anisotropic susceptibility account for the spectral dependence for incident photon energies outside the peak region. The peak itself extends from approximately 3.5 eV to 3.9 eV with a maximum at 3.76 eV. This peak displays potential dependence, such that the peak increases in magnitude with negative surface charging and decreases with positive surface charging. The most likely and simplest explanation for the potential dependence would involve increasing the electron density outside the surface for a negatively charged surface and decreasing the electron density outside the surface for a positively charged surface. Thus the magnitude of the SH response at the peak would simply be related to the magnitude of the electron density profile outside the crystal surface. The spectral character of the peak must be explained with a theory that includes electron density profiles and gradients parallel to the surface. The data indicate that a new transition energy around 3.76 eV will be found to account for the peak. It is necessary for these states not to have the potential dependence associated with the bulk bands projected onto the surface, as described

above. This indicates that these electronic transition states will probably be localized in the surface or at least in the crystal, but with different symmetry and energy dependence then the A surface state or the image potential surface state. It should be noted that the SH response reported by Bradley [73] is in qualitative agreement with our observations made here, and require a similar explanation.

7.3 Defect-Induced SHG

Figs. 6.16, 6.17 and 6.18 show the normal incidence SH response from a vicinally cut Ag(001) surface. The Ag(001) crystal at normal incidence has no SH response from any of the symmetry allowed second order, third order, or bulk susceptibilities. This is due to the linear optical parameters, f_s and F_s, both going to zero at normal incidence. These parameters are still too small for the vicinal surface to allow any contribution from the C_{4v} symmetry allowed susceptibilities. Thus, the SH response observed from the vicinal Ag(001) surface is only a result of the incident electric field interactions with the induced steps (ie. induced defects). We cannot be observing any SH response from the bulk or the terraced surfaces.

The vicinal surface was cut along a direction approximately 30^o from the [100] crystal direction at an angle of approximately 7^o from the [001] crystal direction. The incident and SH light was polarized perpendicular to this misorientation direction, or parallel to the induced step faces, for $\phi = 0$ (Figs. 6.16, 6.17 and 6.18). With this polarization the data have two maxima and two minima which is consistent with C_1 symmetry. The vicinal Ag(001) surface should have no mirror planes and should be characterized by a C_1 symmetry. This is the most general symmetry a surface may have and we would expect a SH field to be governed by Eq. 6.8. However, the two peaks in Figs. 6.16, 6.17 and 6.18 have different peak heights. This peak height

difference is another example of data that cannot be explained by the conventional surface symmetry arguments. Even C_1 symmetry cannot account for this effect. The peak height difference is only accounted for by an isotropic contribution to the SH field equations. Thus the SH field equation which would govern the entire SH response in Figs. 6.16, 6.17 and 6.18 is given by Eq. 6.10. The difference in the peak heights of the SH response indicates that a cross term has a significant contribution. This would manifest itself in a relative phase between d_{1s} and other d_s terms that was not 90^o.

The only possible source for the SH response in this experiment is the steps. Previous publications assumed the vicinal surfaces simply decreased the surface symmetries at the steps and thus allowed more nonlinear surface susceptibilities to contribute to the SH response. Our results indicate that the anisotropic SH response here is governed by this type of symmetry reduction. However, the anomalous isotropic contribution cannot be accounted for by a simple symmetry reduction mechanism. Comparison of our results to those of Verheijen [80] and Richmond [85], indicate that the anisotropic SH responses are very similar. Therefore, the increased defects in the step faces due to our choice of vicinal direction does not seem to be a large contributing factor to the SH response. However, our experimental results are in direct contradiction to conclusions made by Richmond *et al.* [85] regarding observed potential dependence. Richmond [85] concluded, from the s-polarized SH response they observed from a vicinal Ag(111) surface using s-polarized incident photons, that the step induced SH response did not change with applied potential. However, as stated above and clearly evident in Figs. 6.16, 6.17 and 6.18 the step induced SH response does change with applied potential. Part of the problem with Richmond's experiment, is that it required analysis of the SH response to separate the SH contributions

from the steps and the normal SH contributions from the smooth surface plateaus and the bulk. This type of analysis is inherently inaccurate. Thus, our experiment has the advantage of measuring the step induce SH response directly, which allows even relatively small changes due to applied potential and incident photon modulations to be observed. This has allowed us for the first time, to observe the incident photon dependence of the step induced SH response which indicates that the steps are intricately tied to the inherent electron density of the surface.

The anomalous isotropic SH response observed here in the normal incident Ag(001) experiment is very similar to the anomalous isotropic SH response observed from the normal incident Ag(111) experiment. The fact that the induced step defects result in a relatively large two fold anisotropic SH response would imply that the Ag(111) anomalous effect was not due to crystal misorientation or a stepped surface. However, the most likely explanation lies with surface defects for both anomalies. Even the most perfect and best surfaces have some inherent defects. The process involved with this anomalous isotropic signal cannot be characterized by a change in surface symmetry or gradients perpendicular to the surface. Furthermore the experimental conditions used here, preclude any contribution due to an increased number of allowed susceptibilities from loss of surface symmetry. This is seen in the anisotropic SH response from the normal incident Ag(111) experiment and the normal incident vicinal Ag(001) experiment. In both cases, effects from an overall decrease in the surface symmetry where not observed.

The anomalous isotropic SH responses must be due to a SHG source contained in the surface and excited by an incident polarization in the surface plane. The spectral characterization from the normal incident Ag(111) experiment, Fig. 6.14, shows that this anomalous SH response does depend upon the incident photon energy

and the applied potential in an analogous way to ∂_{xxx}. The same mechanism which is required to explain the characteristics of ∂_{xxx} may ultimately also explain the anomalous isotropic SH response.

As an initial effort to explain the anomalous isotropic effect, we considered the contribution from the isotropic multipole terms at the surface. For this we followed the phenomenological description followed by Sipe [8] and chapter 3 of this thesis for the bulk derived multipole terms. If the surface could no longer be considered homogeneous, then the effective surface polarization would have to include:

$$P_{i,pit}^{(2\omega)} = D(\mathbf{E}\cdot\nabla)E_i + BE_i(\nabla\cdot\mathbf{E}), \tag{7.5}$$

where D and B are multipole isotropic phenomenological constants.

However, our first order derivations indicate that the optical field gradients in the surface plane will not account for the effect. This is due to the corresponding SH fields having a form of:

$$E_{\Omega,s-in,s-out}(\phi,2\omega,V) = B_s E_s E_p f_s f_c B, \tag{7.6}$$

$$E_{\Omega,s,p}(\phi,2\omega,V) = B_p E_p^2 f_s f_c B[F_s f_s - F_c f_c]. \tag{7.7}$$

which vanish at normal incidence. Both D and B result in the same forms for the SH fields, and $B_{s,p}$ depends upon linear optical parameters. The answer must lie in the electron density distribution parallel to the surface plane or in effects which require a complicated interaction between the optical fields and the electron density profile. Rudnick and Stern [23] did note that the second order surface susceptibility ∂_{xzx} should be very sensitive to the overall surface quality and ultimately the surface electron gradients. This should be even more so for ∂_{xxx} If the exposed surface of

a defect were characterized by a different surface structure, then the overall surface, and these defect surfaces did contribute specularly to the normal SH response, then perhaps the geometric requirements governing Eq. 7.6 could be relaxed. An example of a geometric defect which could specularly contribute to the SH response, would be a pit in the surface that was shaped more or less in the form of a corner cube. Thus even though all of the exposed surfaces in the pit would individually reflect light in a different direction then the required detection direction, all the pit surfaces combined may reflect the SH light in the appropriate direction. The extra phenomenological contribution would then come from Eq. 7.6, such that the geometric constants like f_s and E_p would be dictated by the pit surface, rather than the crystal surface.

One final observation may be made from the anisotropic SH response from the vicinal Ag(001) surface. The positively charged surface, provides a SH response that increases relative to the PZC and negatively charged surface data as the incident photon energy changes from 3.5 eV to 3.7 eV. Once again, this is an indication that the SH response is sensitive to the electron density profile at the step.

Chapter 8

CONCLUSION

We conducted SHG experiments from Ag(001) and Ag(111) crystals in an electrochemical environment. The specific contributions to the SH response of the higher order bulk and surface susceptibilities, such as ∂_{xxx}, as a function of incident photon energy and interfacial potential were determined. The Ag(001) data indicate that the bulk anisotropic susceptibility and the sum of the bulk isotropic susceptibility and the second order surface susceptibility ($\epsilon(\Omega)\partial_{zxx}/\epsilon_o+\gamma$) are, to first order, independent of incident photon energy. Furthermore, ζ is independent of applied potential. The sum $\epsilon(\Omega)\partial_{zxx}/\epsilon_o + \gamma$ does have a potential dependence, and the ratio of susceptibilities $[(\epsilon(\Omega)\partial_{zxx}/\epsilon_o + \gamma)/\zeta]$ has a value between 0.1 and 0.13 depending on the applied potential. While the individual contributions of either γ or ∂_{zxx} may still be in question, since these two terms always appear together in the phenomenological equations, as a pair, they may not be ignored. This is also the case with any SH contribution involving ζ. The realization of the importance of this isotropic contribution and the necessity for including the anisotropic SH contribution from the bulk may require reinterpretation of several previous SH experiments [10, 43, 13].

The normal incident SH response from Ag(111) displayed a previously unknown resonant peak with a maximum at 3.76 eV which is associated with the second order surface susceptibility ∂_{xxx}. This peak cannot be explained by any of the known microscopic mechanisms usually employed to explain this type of phenomena. The peak is potential dependent but does not shift with applied potential. ∂_{xxx} is potential dependent throughout the entire spectral range, but is relatively constant for incident

photon energies above and below the resonant peak. The best explanation for the resonance is that ∂_{xxx} is sensitive to the electron density profile parallel to the Ag surface; this electron density has properties not yet accurately characterized.

Furthermore, the normal incident SH response from Ag(111) had an anomalous isotropic contribution that had similar spectral and applied potential dependencies as ∂_{xxx}. This anomalous isotropic SH response was also observed on the vicinal Ag(001) surface. This effect cannot be explained by a reduction in surface symmetry, as was the case for the relatively large anisotropic SH response from the vicinal Ag(001) surface. The only explanation for the anomalous isotropic SH response from either surface is the inherent defects associated with any real surface. The defects produce gradients and modulations in the electron density profile of the surface which ultimately contribute to the SH response.

The final experiment we performed for this thesis involved the SH response from a vicinal Ag(001) surface. This SH response was completely governed by the expected phenomenological equations which used C_1 symmetry (except for the anomalous isotropic contribution). The relatively large SH response and the symmetry lowering at the steps were consistent with previously published results. However, this experiment had the advantage of not having any other SH contributions, so that the SH response from the steps could be measured directly. This removed the analysis required in other experiments for separating the SH response from competing effects, and thus the possibility for error. Thus our experiment was able to detect for the first time the potential and incident photon dependence of the SH response from the steps using light polarized parallel to the surface plane. The processes governing the SH response from the steps are contained in the present phenomenological theory, unlike the processes governing the anomalous isotropic SH response, which lie outside the

present phenomenological theory.

Throughout this thesis we have obtained significant information from experimental configurations and geometries not commonly used. The results indicate that as much information, if not more, may be obtained from experiments which isolate specific SH contributions, rather than trying to evaluate the SH response from several susceptibilities. The fact that several of the higher order nonlinear susceptibilities contribute significantly to the SH response further complicates matters. These experiments indicate that future experiments should be done with experimental configurations where all the SH contributions are known and well characterized. In fact the vicinal Ag(001) experiment indicates that a great deal of information may be obtained by using an experimental configuration where no other contributions are present.

Appendix A

CHEMICAL AND ELECTROCHEMICAL POLISHING TECHNIQUES FOR SILVER SURFACES

The sample preparation breaks down into three distinct areas. The first is sample mounting and handling procedures. The second involves the mechanical cleaning and polishing processes. The third, and the area we will discuss here, involves the final surface polish of the sample surface to remove the strained layers induced by the mechanical polish. While the first two parts follow a very standard and successful set of procedures, which we have previously discussed in this thesis, the latter part is very tenuous and the results depend sensitively on minute changes in procedure. The final surface preparation techniques fall into one of two categories, chemical and electrochemical surface polishes. Sometimes, the solutions will utilize similar chemical reactions in either method, and simply drive or control these reactions using electrochemical methods or let them follow thermodynamically defined controls with the chemical methods. However, there is a far greater number of solutions used for chemical polishes then electrochemical polishes.

Ultimately, this final surface polishing is an attempt to remove the strained atoms at the surface which are presumable at a higher thermodynamic energy then the unstrained surface atoms. This involves a precarious balance of thermodynamically controlled chemical potentials, where the chemical polish will energetically etch the strained atoms and leave the unstrained atoms untouched. Ultimately, this is a highly dynamic process, that is dependent upon contact time, temperature, chemical composition and chemical concentration. The surface polish is deemed a failure, if

scratches and thus induced strain remains on the surface, or unstrained atoms are removed from the surface, most commonly resulting in pits. Ultimately, by the strictest enforcement of this definition, all surfaces polishes are a failure, since some remnants of scratches always remain, and some pits are always formed. Thus, experimentally, the surface polish is judged by the relative number of defects on the surface, with the minimum number being the desired result. Fortunately, in most experiments, these so called good surfaces are sufficient. However, as we have shown in this thesis, the presence of defects will ultimately affect experimental results, and thus there presence must be incorporated into any comprehensive interpretation involving the surface.

We will first discuss the chemical polishing technique we found to be most successful and ultimately used. The main problem in our experiments, which for the most part was unique to us, involved obtaining a good specular surface uniformly over the entire sample area. This was due to our use of crystals with surfaces areas of approximately 1 cm^2. By far the best surface polish resulted from the cyanide procedure described above and in more detail here. This cyanide process used two solutions. The Ag sample is dipped into a 21 g/l NaCN 30% hydrogen peroxide solution. A Q-tip cotton swab is then used to provide a uniform coverage of the solution. This first cyanide solution is absolutely required to initiate the removal of the strained surface atoms. However, this first step also induces the formation of pits. The contact time is the most critical component in this step and usually a minimum contact time to obtain a good specular surface is warranted. Times between 5 and 10 seconds have been found to be best. This solution is then removed using a 35 g/l NaCN water solution. The latter solution was then applied with a cotton swab until the surface became specular. This usually requires constant swabbing for 3 to 5 minutes. The sample is then thoroughly rinsed with high purity water. The sample is transported

in a water shroud and immediately placed into an electrochemical cell after rinsing. The crystal is usually rinsed with half a liter of triple distilled water and a clean cotton swab is used during this rinsing to dislodge any remaining contaminants from the surface. An additional cleaning using concentrated perchloric acid is sometimes incorporated to ensure the removal of all contamination. This involves soaking the sample in perchloric acid from 1 to 20 minutes.

It is imperative that the initial surface etch be strong enough to remove strain hardened layers from the sample surface. These layers form when the sample is mechanically polished and the surface atoms are moved to defective areas of the surface, effectively filling in the nonuniformities. Thus large scratches may be present but are undetected due to the presence of surface atoms filling in the defects. This was especially prevalent with some of the other chemical polishes which required chemical rubbing on Microcloth pads. If large defects are present after the cyanide chemical etch, repolishing the crystal starting with the 0.05 micron mechanical polish is advisable. It should be noted that once pits are formed, further polishing with the chemical etch will only increase the size of the pit. Thus polishing techniques that claim to remove pits are simply filling the pits with other surface atoms or contamination.

The final surface after the cyanide polish will be highly specular under normal light. A good surface will not have the appearance of grain boundaries or waviness. These type of observable defects are actually indications of a large number of surface pits. These pits may be observed under a bright light source (such as a flashlight). Even good surfaces though, will show defects under this type of illumination and under the correct orientation to the eye. These defects include very fine scratches and small pits. However, unlike the big surface defects which are visible under normal light and

most orientations, these fine defects are often very hard to detect and focus on due to their relatively small size and limited number. In fact, it is very difficult to find these defects from a good surface using a microscope. The location and focusing on a defect is hampered by the specular surface of the good sample.

Several of these chemical polishing techniques were tried and evaluated by V. Hallmark in an unpublished document. Of these, two solutions were rated the best for polishing the Ag(111) and Ag(001) surfaces, and we tried these polishes. The first chemical polish involved a CrO_3 solution in conjunction with Hydrochloric acid for the Ag(111) surface (100 ml sat CrO_3 to 5 ml 10% HCl). The other involves a Nitric acid and CrO_3 for the Ag(001) surface (10 ml HNO_3, 50 ml HCl, and 60 ml H_2O). Since this is an unpublished document, we will reproduce the technical procedure, here, for completeness.

1) After completing the mechanical polishing steps, dilute the HNO_3-CrO_3 (25% HNO_3, 75% sat CrO_3) polish with an equal amount of water on a Microcloth pad.

2) Rub the crystal in a circular motion on the pad for 3-4 sec.

3) Rinse on another Microcloth pad that has a solution of water and Buehler sonicating detergent on it. Then rinse with a stream of water, then ethanol and dry with nitrogen gas.

4) Repeat steps 2) and 3)

5) On a third Microcloth pad, dilute the CrO_3-HCl polish with an equal amount of water.

6) Polish the crystal in a circular motion for 3-4 seconds.

7) Rinse and check for scratches under a microscope at a magnification of 200X.

8) Repeat steps 6) and 7) until all scratches are removed and very few pits remain.

9) If necessary, alternate between the two chemical polishes, or go back to the alumina step and repeat the entire procedure.

This procedure was considered the best polish of those tried for the Ag(111) surface. The best polish for the Ag(001) surface substitutes 25% HNO_3, 75% sat CrO_3 for the CrO_3-HCl solution in step 5. The other chemicals used in step 5) used different combinations of CrO_3, HCl, Ammonium Persulphate, Iodine and water. We did not try these other polishes and will not comment on them further, except to say that Hallmark considered them to produce surfaces of poorer quality then the ones discussed in the above procedure.

The Hallmark polishes we tried performed reasonably well. However, surface contamination was a constant problem and scratches induced from the Microcloth pads collecting residuals from polishing deterred the surface quality. As with all the polishes involving CrO_3, a white residual that may be silver oxide or some other chemical by product is formed that adheres to the surface and becomes difficult to move. This results in a non-uniform surface polish on our relatively large crystals which is due to excess polishing in regions where this residue is removed. Similar problems were observed with a revised chemical etch which was published by Hamelin [91]. Since this is published, we will not reproduce it here. The procedure involves different concentrations of CrO_3 and HCl then Hallmark's process, but remains approximately the same in all other regards.

The last chemical surface polish we tried involved a surface polish described by Furtak [92]. This involves simply dipping the crystal surface in a NH_4OH : H_2O_2 (5 : 3 by volume) solution for 1 to 15 sec. This method removes all surface strain. Unfortunately, it also removes a great deal of the higher energy surface atoms as well, resulting in a preferential pitting of the surface that is very non-specular. This polish

may be useful in determining bulk contributions, but is not useful for SHG studies of surfaces.

We tried two different electrochemical surface polishes as well. The first surface polish used NH_4OH and will be referred to as the NH_4OH electropolish. The second used NaCN and will be referred to as the NaCN electropolish. We will begin with the NH_4OH electropolish.

Two solutions were prepared for the NH_4OH electropolish. The first solution combined 32 ml of high purity water, with 4 g $(NH_4)_2SO_4$, 3.4 $K_4P_2O_7X3H_2O$, and 10 ml of 25% NH_4OH. The second solution combined 32 ml of high purity water, with 1.46 g $AgNO_3$, 0.88 g $K_4P_2O_7X3H_2O$, and 8 ml of 25% NH_4OH. These two solutions were then combined together and diluted 3 times with high purity water. This formed the basic solution which was held in a sealed container for future use. 4 to 5 ml of this basic solution was combined with 0.5 ml of 25% NH_4OH and 25-30 ml high purity water. This constituted the working solution. 50 ml of the working solution was used in an electrochemical cell, which used a ring of Pt wire and the silver sample surface as the two electrodes. The two electrodes were connected in a circuit with a variable resistor and a power supply. The silver sample was connected to the positive output of the power supply with the variable resistor between them. The power supply was initially set to provide 10 V at 0.1 A. The resistor was set so that the current between the silver sample and the Pt wire without the electrolyte solution is approximately 2 mA. The sample was shaken or the electrolyte stirred during the electropolishing procedure, to ensure a uniform polish. The silver sample and the Pt loop were placed in the electrolyte with the circuit open. The circuit was then closed for 4-5 seconds and then switched off for 5-10 seconds. This procedure was repeated 25-50 times while slowly increasing the current to 3-4 mA. During this procedure, the

Ag surface became matted, and could not be removed from the solution. Observation of the sample was made through the side of the glass container. Continuing the on off procedure the current was slowly decreased to 1-2 mA. If the surface did not become specular, the entire procedure was repeated once more. This procedure had similar problems to the chemical polishes. The sample developed a large amount of pitting similar to the NH_4OH : H_2O_2 (5 : 3 by volume) polish and surface uniformity was very difficult to control. It did remove all of the scratches and strained surface atoms, but we could never achieve a satisfactory specular surface.

The final surface polish we will discuss here, involved NaCN and was outlined by Larkin *et al.* [93] and Koos [94]. The solution used 41 g/l NaCN, 44g/l $AgNO_3$ and 38 g/l K_2CO_3. The solution was purged with zero grade nitrogen in order to remove oxygen from the process and thus minimize the whitish film that often formed with electrochemical polishes. The sample was used as a working electrode in the electrochemical cell and was surrounded at a distance by a ring of silver wire that was used as the counter electrode. The geometry and orientation of the electrodes was important in maintaining a homogeneous current flux at the electrode surface. The SCE reference electrode was held as close as possible to the working electrode surface to obtain an accurate current measurement. The sample was held in a horizontal position in order to form a stable and homogeneous concentration gradient of soluble species at the surface. The bias potential of +0.20 V vs SCE was applied prior to immersion of the electrode into the polishing bath. A brown film soon appeared at the electrode surface. After two minutes of polishing the electrode was quickly removed and rinsed with water. It was then immersed in a 0.1 M NaF bath and potentiostated at -1.7 V for several minutes to remove oxidized species from the surface. This procedure was repeated three times. In the final polishing sequence,

the electrode was removed from the polishing bath after the viscous, brown film became homogeneous in appearance [94].

The main problem with the NaCN electropolish was a relatively large amount of pitting and surface waviness associated with current density variations across the surface. The latter is a problem specific to our larger crystal surfaces and was never adequately solved. We tried a variety of geometric configurations and even used a Copper metal beaker as the counter electrode in an attempt to decrease and homogenize the current density across the samples surface. Again, the electropolish is a balance between removing the strained surface atoms without removing unstrained surface atoms. Next to the cyanide chemical polish we have adopted for these experiments, we were able to adapt the NaCN electropolish such that the surfaces obtained were almost as good as the chemical polish surfaces. In fact, the electrochemical polish did not leave the small scratches that the chemical polishes often did, due to mechanical agitation. However, we were never able to keep the surface from obtaining a slight degree of waviness. The major change we applied was to continually stir the electrolytic solution during etching and to only keep the sample in the electropolish solution for the minimum amount of time to remove the strained atoms. The optimal time was found to be between 3-10 minutes.

REFERENCES

[1] N.W. Ashcroft and N. D. Mermin, *Solid State Physics*, (Saunders College, PA, 1976).

[2] A. Zangwill, *Physics at Surfaces* (Cambridge Univ. Press, 1988).

[3] T. F. Heinz, M. M. T. Loy, and W. A. Thompson, *Phys. Rev. Lett.* **54**, 63 (1985).

[4] T. F. Heinz, C. K. Chen, D. Ricard and Y. R. Shen, *Phys. Rev. Lett.* **48**, 478 (1982).

[5] X. Gao, A. Hamelin, and M. J. Weaver, *Phys. Rev.* **44**,10983 (1991).

[6] B. M. Ocko, J. Wang, A. Davenport, and H Isaacs, *Phys. Rev. Lett.* **65**, 1466 (1990).

[7] N. Bloembergen, *Nonlinear Optics* (Addison-Wesley Publ., 1965).

[8] J. E. Sipe, D. J. Moss, and H. M. van Driel, *Phys. Rev. B* **35**,1129 (1987).

[9] J. Goodisman, Electrochemistry: *Theoretical Foundations* (John Wiley and Sons, New York 1987).

[10] G. L. Richmond, J. M. Robinson, and V. L. Shannon, *Prog. Surf. Sci.* **28**, 1 (1988).

[11] M. L. Lynch and R. M. Corn, *J. Electroanal. Chem.* **318**, 379 (1991).

[12] Y. Tang, L. J. Simpson, and T. E. Furtak, *Phys. Rev. Lett.* **67**, 2814 (1991).

[13] T. E. Furtak Y. Tang, and L. J. Simpson, *Phys. Rev. B* **46**, 1719 (1992).

[14] E. D. Palik, *Handbook of Optical Constants of Solids*, (Academic Press, New york, 1985).

[15] P. A. Franken, A. E. Hill, C. W. Peters, and G. Weinreich, *Phys. Rev. Lett.* **7**, 118 (1961).

[16] R. W. Terhune, P. D. Maker, and C. M. Savage, *Phys. Rev. Lett.* **8**, 404 (1962).

[17] F. Brown, R. E. Parks, and A. M. Sleeper, *Phys. Rev. Lett.* **14**, 1029 (1965), F. Brown and R. E. Parks, *Phys, Rev. Lett.* **16**, 507 (1966), F. Brown and M. Matsuoka, *Phys. Rev.* **185**, 985 (1969).

[18] N. Bloembergen, R. K. Chang, and C. H. Lee, *Phys. Rev. Lett.* **16**, 986 (1966).

[19] H. Sonnenberg and H Heffner, *J. Opt. Soc. Am.* **58**, 209 (1968).

[20] G. V. Krivoshchekov and V. I. Stroganov, *Sov. Phys. Solid State* **9**, 2856 (1968).

[21] N. Bloembergen and R. K. Chang, *Phys. of Quant. Elect., edited by P. L. Kelley* (McGraw Hill, New York, 1966).

[22] C. C. Wang and A. N. Duminski, *Phys. Rev. Lett.* **20**, 668 (1968).

[23] J. Rudnick and E. A. Stern, *Phys. Rev. B* **4**,4272 (1971).

[24] C. C. Wang, *Phys. Rev.* **178**, 1457 (1969).

[25] Y. R. Shen, *Principles of Nonlinear Optics*, (Wiley, New York, 1984).

[26] J. E. Sipe and G. I. Stegeman, *Surface Polaritons, edited by V. M. Agronovich* (North-Holland, Amsterdam, 1982).

[27] J. M. Chen, J. R. Bower, C. S. Wang and C. H. Lee, *Opt. Comm.* **9**, 132 (1973).

[28] S. S. Jha and C. S. Warke, *Phys. Rev.* **153**, 751 (1967).

[29] N. Bloembergen, R. K. Chang, S. S. Jha, and C. H. Lee, *Phys. Rev.* **174**, 813 (1968).

[30] D. A. Koos, V. L. Shannon, and G. L. Richmond, *J. Phys. Chem.* **94**, 2091 (1990).

[31] V. Mizrahi and J. E. Sipe, *J. Opt. Soc. Am. B* **5**, 660 (1988).

[32] J. E. Sipe, V. C. Y. So, M. Fukui, and G. I. Stegeman, *Phys. Rev. B* **21**, 1389 (1980).

[33] J. E. Sipe, *Phys. Rev. B* **22**, 1589 (1980).

[34] M. Corvi and W. L. Schaich, *Phys. Rev. B* **33**, 3688 (1988).

[35] M. Weber and A. Liebsch, *Phys. Rev. B* **35**, 7411 (1987).

[36] M. G. Weber and A. Liebsch, *Phys. Rev. B* **36**, 6411 (1987).

[37] W. L. Schaich and A. Liebsch, *Phys. Rev. B* **37**, 6187 (1988).

[38] A. Liebsch, *Phys. Rev. Lett.* **61**, 1233 (1988).

[39] A. Liebsch and W. L. Schaich, *Phys. Rev. B* **40**, 5401 (1989).

[40] A. Liebsch, *Phys. Rev. B* **40**, 3421 (1989).

[41] A. Liebsch, *Appl. Phys. A* **49**, 677 (1989).

[42] P. G. Dzhavakhidze, A. A. Kornyshev, A. Liebsch M. Urbakh, *Phys. Rev. B* **45**, 9339 (1992).

[43] P. Guyot-Sionnest, A. Tadjeddine, and A. Liebsch, *Phys. Rev. Lett.* **64**, 1678 (1990).

[44] P. Guyot-Sionnest and A. Tadjeddine, *J. Chem. Phys.* **92**, 734 (1990).

[45] T. F. Heinz, *Nonlinear Electromagnetic Phenomena at Surfaces*, edited by H. Pometer and G. Stegeman. (1992).

[46] J. Miragliotta and T. E. Furtak, *Phys. Rev. B* **37**, 1028 (1988).

[47] J. Miragliotta and T. E. Furtak, *Surface and Interface Analysis* **14**, 53 (1989).

[48] H. J. Simon, D. E. Mitchell and J. G. Watson, *Phys. Rev. Lett.* **33**, 1531 (1974). H. J. Simon, R. E. Benner and J. G. Rako, *Opt. Comm.* **23**, 245 (1977).

[49] A. Chizmeshya and E. Zaremba, *Phys. Rev. B* **37**, 2805 (1988).

[50] R. K. Chang and T. E. Furtak, *Surface Enhanced Raman Scattering* (Plenum, New York, 1982).

[51] L. E. Urbach, K. L. Percival, J. M. Hicks, E. W. Plummer, and H.-L. Dai, *Phys. Rev. B* **45**, 3769 (1992).

[52] R. Murphy, M. Yeganea, K. J. Song, and E. W. Plummer, *Phys. Rev. Lett.* **63**, 318 (1980).

[53] X. Bao, J. V. Barth, G. Lehmpfuhl, R. Schuster, Y. Uchida, R. Schlogl and G. Ertl, *Surface Science* **284**, 14 (1993).

[54] R. M. Corn, M. Romagnoli, M. D. Levenson, and M. R. Philpott, *Chem. Phys. Lett.* **106**, 30 (1984), M. L. Lynch and R. M . Corn, *J. Electroanal. Chem.* **318**, 379 (1991), M. L. Lynch and R. M. Corn, *J. Phys. Chem.* **94**, 4382 (1990).

[55] C. K. Chen, A. R. B. de Castro, and Y. R. Shen, *Phys. Rev. Lett.* **46**, 145 (1981).

[56] E. A. Wood, *Crystal Orientation Manual*, (Columbia Univ. Press, 1963).

[57] R. A. Bradley, S. Arekat, R. Georgiadis, J. M. Robinson, S. D. Kevan and G. L. Richmond, *Chem. Phys. Lett.* **168**, 468 (1990).

[58] C. Kittel, *Intro. to Solid State Physics*, (John Wiley and Sons, 1976).

[59] P. Guyot-Sionnest, W. Chen, and Y. R. Shen, *Phys. Rev. B* **33**, 8254 (1986).

[60] Z. Nagy and J. Mchardy, *J. Electrochem. Soc.*, 1222 (1971).

[61] J. Bockris and A. Reddy, *Modern Electochemistry.* (Plenum, Newyork, 1973).

[62] D. M. Kolb and C. Franke, *Appl. Phys.* **A49**, 379 (1989).

[63] D. M. Kolb, W. Boeck, K.-M. Ho, and S. H. Liu, *Phys. Rev. Lett.* **47**, 1921 (1981).

[64] A Friedrich, C Shannon, and B Pettinger, *Surf. Sci.* **251**, 587 (1991).

[65] A Friedrich, B Pettinger, D. M. Kolb, G. Lupke, R. Steinhoff and G. Marowsky, *Chem. Phys. Lett.* **163**, 123 (1989).

[66] F. Ercolessi, E. Tosatti and M. Parrinello, *Phys. Rev. Lett.* **57**, 719 (1986).

[67] G. L. Richmond, *Chem. Phys. Lett.* **110**, 571 (1984).

[68] R. Georgiadis, G. A. Neff and G. L. Richmond, *J. Chem. Phys.* **92**, 4623 (1990).

[69] R. Georgiadis and G. L. Richmond, *J. Phys. Chem.* **95**, 2895 (1991).

[70] D. A. Koos, V. L. Shannon, and G. L. Richmond, *Phys. Rev. B* **47**, 4730 (1993).

[71] R. A. Bradley, R. Georgiadis, S. D. Kevan and G. L. Richmond, *J. Vac. Technol. A* **10(5)**, 2996 (1992).

[72] R. A. Bradley, *Thesis (Ph. D)*, University of Oregan, (1992).

[73] R. A. Bradley, *1993 APS March Meeting*, Seattle, (1993).

[74] W. L. Schaich and B. S. Mendoza, *Phys. Rev. B* **45**, 14279 (1992).

[75] C. H. Lee, R. K. Chang, and N. Bloembergen, *Phys. Rev. Lett.* **18**, 167 (1967).

[76] S. S. Jha, *Phys. Rev.* **140**, A2020 (1965).

[77] S. S. Jha, *Phys. Rev. Lett.* **15**, 412 (1965).

[78] J. R. Bower, *Phys. Rev. B* **14**, 2427 (1976).

[79] A Hamelin, T. Vitanov, E Sevastyanov, and A. Popov, *J. Electroanal. Chem.* **145**, 225 (1983).

[80] M. A. Verheijen, C. W. van Hasselt and Th. Rasing, *Surface Science* **251**, 467 (1991).

[81] C. W. van Hasselt, M. A. Verheijen and Th. Rasing, *Phys. Rev. B* **42**, 9263 (1990).

[82] R. W. J. Hollering and M. Barmentlo, *Optics Comm.* **88**, 141 (1992).

[83] R. W. J. Hollering, D. Dijkkamp and H. B. Elswijk, *Surface Science* **243**, 121 (1991).

[84] S. Janz, D. J. Bottomley and H. M. van Driel, *Phys. Rev. Lett.* **66**, 1201 (1991).

[85] K. A. Friedrich and G. L. Richmond, *Ber. Bunsenges. Phys. Chem.* **97**, 386 (1993).

[86] D. M. Kolb and C. Franke, *Appl. Phys. A* **49**, 379 (1989).

[87] D. M. Kolb, *Europhysics Journal* **C5**, 167 (1977).

[88] RB. Reihl, K. H. Frank and A. Otto, *Z. Phys. B* **62**, 473 (1986).

[89] K. Giesen *et al.*, *Physica Scripta* **35**, 578 (1986).

[90] A. Goldmann, V. Dose and G. Borstel, *Phys. Rev. B* **32**, 1971 (1985).

[91] A. Hamelin, S. Morin, J. Richer, and J. Lipkowski, *J. Electroanal. Chem.* **285**, 249 (1990).

[92] T. F. Furtak and J. K. Sass, *Surface Science* **78**, 591 (1978).

[93] Larkin *et al.*, *J. Electroanal. Chem.* **138**, 401 (1982).

[94] D. Koos *Personal Communication* (1990).